11

THE UNIVERSITY OF CALIFORNIA
LET THERE BE LIGHT
1868

MARINE PHYSICAL LABORATORY

SCRIPPS INSTITUTION OF OCEANOGRAPHY

San Diego, California 92152

High Resolution Beamforming on Large Aperture Vertical Line Arrays: Processing Synthetic Data

Jean-Marie Q.D. Tran and William S. Hodgkiss

MPL TECHNICAL MEMORANDUM 419

MPL-U-8/90
September 1990

UNCLASSIFIED
SECURITY CLASSIFICATION OF THIS PAGE

REPORT DOCUMENTATION PAGE

Form Approved
OMB No. 0704-0188

1a. REPORT SECURITY CLASSIFICATION
UNCLASSIFIED

1b. RESTRICTIVE MARKINGS

2a. SECURITY CLASSIFICATION AUTHORITY

2b. DECLASSIFICATION / DOWNGRADING SCHEDULE

3. DISTRIBUTION / AVAILABILITY OF REPORT
Approved for public release; distribution unlimited.

4. PERFORMING ORGANIZATION REPORT NUMBER(S)
MPL Technical Memorandum 419 [MPL-U-8/90]

5. MONITORING ORGANIZATION REPORT NUMBER(S)

6a. NAME OF PERFORMING ORGANIZATION
University of California, San Diego

6b. OFFICE SYMBOL *(If applicable)*
MPL

7a. NAME OF MONITORING ORGANIZATION
Office of Naval Research
Department of the Navy

6c. ADDRESS *(City, State, and ZIP Code)*
Marine Physical Laboratory
Scripps Institution of Oceanography
San Diego, California 92152

7b. ADDRESS *(City, State, and ZIP Code)*
800 North Quincy Street
Arlington, VA 22217-5000

8a. NAME OF FUNDING / SPONSORING ORGANIZATION
Office of Naval Research

8b. OFFICE SYMBOL *(If applicable)*
ONR

9. PROCUREMENT INSTRUMENT IDENTIFICATION NUMBER
N00014-89-K-0038

8c. ADDRESS *(City, State, and ZIP Code)*
800 North Quincy Street
Arlington, VA 22217-5000

10. SOURCE OF FUNDING NUMBERS

PROGRAM ELEMENT NO.	PROJECT NO.	TASK NO	WORK UNIT ACCESSION NO

11. TITLE *(Include Security Classification)*
HIGH RESOLUTION BEAMFORMING ON LARGE APERTURE VERTICAL LINE ARRAYS: PROCESSING SYNTHETIC DATA

12. PERSONAL AUTHOR(S)
Jean-Marie Q.D. Tran and William S. Hodgkiss

13a. TYPE OF REPORT
technical memorandum

13b. TIME COVERED
FROM ________ TO ______

14. DATE OF REPORT *(Year, Month, Day)*
September 1990

15. PAGE COUNT
93

16. SUPPLEMENTARY NOTATION

17. COSATI CODES

FIELD	GROUP	SUB-GROUP

18. SUBJECT TERMS *(Continue on reverse if necessary and identify by block number)*
large aperture vertical line arrays, beamforming, coherent processing, subaperture processing

19. ABSTRACT *(Continue on reverse if necessary and identify by block number)*

This technical memorandum studies the beamforming of large aperture line arrays deployed vertically in the water column. The work concentrates on the use of high resolution techniques. Two processing strategies are envisioned: full aperture coherent processing which offers in theory the best processing gain, and subaperture processing which consists in extracting subapertures from the array and recombining the angular spectra estimated from these subarrays. The conventional beamformer, the Minimum Variance Distortionless Response (MVDR) processor, the MUltiple SIgnal Classification (MUSIC) algorithm and the Minimum Norm method are used in this study. To validate the various processing techniques, the ATLAS normal mode program is used to generate synthetic data which constitute a realistic signals environment. A deep-water, range-independent sound velocity profile environment, characteristic of the North-East Pacific, is being studied for two different 128 sensor arrays, a very long one cut for 30 Hz and operating at 20 Hz, and a shorter one cut for 107 Hz and operating at 100 Hz. The simulated sound source is 5 m deep. The full aperture and subaperture processing are being implemented with curved and plane wavefront replica vectors. The beamforming results are examined and compared to the ray-theory results produced by the Generic Sonar Model (GSM).

20. DISTRIBUTION / AVAILABILITY OF ABSTRACT
☐ UNCLASSIFIED/UNLIMITED ■ SAME AS RPT. ☐ DTIC USERS

21. ABSTRACT SECURITY CLASSIFICATION
UNCLASSIFIED

22a. NAME OF RESPONSIBLE INDIVIDUAL
W. S. Hodgkiss

22b. TELEPHONE *(Include Area Code)*
(619) 534-1798

22c. OFFICE SYMBOL
MPL

DD Form 1473, JUN 86 *Previous editions are obsolete* SECURITY CLASSIFICATION OF THIS PAGE
UNCLASSIFIED

High Resolution Beamforming on Large Aperture Vertical Line Arrays: Processing Synthetic Data

Jean-Marie Q.D. Tran
William S. Hodgkiss

Marine Physical Laboratory
Scripps Institution of Oceanography
San Diego, CA 92152

ABSTRACT

This technical memorandum studies the beamforming of large aperture line arrays deployed vertically in the water column. The work concentrates on the use of high resolution techniques. Two processing strategies are envisioned: full aperture coherent processing which offers in theory the best processing gain, and subaperture processing which consists in extracting subapertures from the array and recombining the angular spectra estimated from these subarrays. The conventional beamformer, the Minimum Variance Distortionless Response (MVDR) processor, the MUltiple SIgnal Classification (MUSIC) algorithm and the Minimum Norm method are used in this study. To validate the various processing techniques, the ATLAS normal mode program is used to generate synthetic data which constitute a realistic signals environment. A deep-water, range-independent sound velocity profile environment, characteristic of the North-East Pacific, is being studied for two different 128 sensor arrays, a very long one cut for 30 Hz and operating at 20 Hz, and a shorter one cut for 107 Hz and operating at 100 Hz. The simulated sound source is 5 m deep. The full aperture and subaperture processing are being implemented with curved and plane wavefront replica vectors. The beamforming results are examined and compared to the ray-theory results produced by the Generic Sonar Model (GSM).

Table of Contents

1. Introduction

This technical memorandum studies the beamforming of large aperture vertical line arrays with equally spaced sensors. The wavefield sampled by a vertical array is the superposition of correlated signal arrivals with curved wavefronts in a spatially colored ambient noise field. The interest in lower frequencies (10 to 100 Hz), triggered by their low attenuation in the water, lead to the development of low frequency acoustic vertical line arrays such as the MPL digital array [Sotirin1988]. The sampled wavefield is strongly influenced by the ocean boundaries since the physical dimensions of such arrays are of the same order as the ocean depth. Also, the lower frequency sound, which has a longer acoustic wavelength, significantly interacts with the bottom. One objective in developing these large aperture systems is to improve vertical resolution. An increased resolution allows the separation of the multipath arrivals impinging on the array, thus making possible a detailed study of the physics of sound propagation. Improved resolution can be obtained by having a longer aperture, or by using high resolution signal processing schemes yielding better resolution, or both.

Vertical arrival structure, usually, is obtained by processing the data sampled by a vertical array with a conventional beamformer using plane wave replica vectors. Generally, the assumptions of local plane wave propagation is justified by the moderate lengths (a few hundred meters) of the apertures deployed in the water column. The resolution that characterizes this conventional processing is the so-called Rayleigh resolution [Burdic1984] given by $\theta\,(rad) = \frac{\lambda}{L}$ where λ is the acoustic wavelength and L is the length of the aperture. Increasing the aperture length results in an improved resolution since $\theta \rightarrow 0$ as $L \rightarrow \infty$. In an isovelocity medium with sound speed of 1500 m/s, the 1500 m long array described in [Sotirin1988], has a Rayleigh resolution of approximately 0.6^o at 100 Hz and 6^o at 10 Hz. Even for such a long array, the resolution appears limited at low frequency.

High resolution techniques provide a substantial improvement of resolution depending on the encountered signal-to-noise ratio *SNR* . High resolution techniques can be divided in two classes, the adaptive and eigenvector techniques. In the following simulations, the adaptive Minimum Variance Distortionless Response (MVDR) beamformer [Capon1969], the eigenvector MUltiple SIgnal Classification (MUSIC) algorithm [Schmidt1986] and the Minimum Norm method [Orfanidis1988] are considered.

The strong potential of improved resolution with these high resolution techniques also results in poor performance as soon as the processed wavefield departs from the underlying signal model on which they are based. For example, the high resolution techniques fail to report correctly correlated arrivals produced by multipath propagation, which is common in a real oceanic environment. Spatial smoothing preprocessing techniques have been designed to limit these effects at the cost of substantial computational burden and of reduced effective aperture length (thus, a reduction in resolution).

The complexity of sound propagation has a definite impact on the resolution performance of the beamformers. Long range propagation is controlled by the variations of the sound speed profile with depth [Murphy1987] and this results in variations of the arrival angle with depth (wavefront curvature). This curvature can cause some important smearing and bias in angle in the arrival structure picture produced by the conventional processor as shown in [Tran1989]. It may affect the high resolution methods in a more critical way because of their higher sensitivity to mismatch. Wavefront Curvature must be taken into account by using replica vectors that properly model these wavefronts.

Coherent processing of the full aperture is commonly performed using the conventional beamformer, which is a very computationally efficient processor when implemented with Fast Fourier Transforms (FFTs). It is natural to envision high resolution full aperture processing of a long and well-filled array, although several aspects of this method are potentially unpractical. As a preliminary step, high resolution techniques require the estimation of the array covariance matrix. In practice, the array covariance matrix is estimated at a given frequency by averaging dyad products of FFT values at each sensor over successive time snapshots. The procedure is to average at least as many dyads as sensors, so that the matrix theoretically is of full rank. Assuming a time snapshot of 30 seconds (0.033 Hz FFT bin width) and an array of 120 elements, the averaging required represents an hour's worth of data. It is unlikely that the wavefield will be stationary for that long. Furthermore, the high resolution techniques involve computationally expensive matrix operations such as matrix inversion and eigen decomposition. Coherent processing of a long and well filled array requires considerable computational resources making real-time implementation costly and difficult [Speiser1985].

Beside full aperture coherent processing with high resolution techniques, another strategy with high resolution methods is to process subapertures extracted from the vertical array and to incoherently recombine the subaperture angular spectra. Such an approach is similar conceptually to some conventional time series techniques such as the Welch periodogram method [Marple1987]. Even though using smaller apertures, the subaperture approach should yield sufficient resolution due to the incorporation of the high resolution methods, and should enjoy a certain level of robustness due to the incoherent averaging. The estimation of the covariance matrices is easier with their smaller dimension and their further numerical manipulation facilitated. In addition to an angular spectrum estimate across the entire array through subarrays, this method produces angular spectra corresponding to different windows in the water column, thus providing information related to multipath variability in the vertical.

The rest of this technical memorandum does an intercomparison of the two different strategies discussed above:

(1) a full aperture coherent processing using the conventional and the MVDR beamformers

(2) a subaperture processing using the high resolution techniques (MVDR, MUSIC and the Minimum Norm methods).

The analysis is based on processing data simulated by an acoustic modeling program (based on a normal mode decomposition) that outputs the complex wavefield at range depth pairs of interest. The simulated wavefield models a realistic oceanic environment with correlated and curved wavefront arrivals.

2. Creation of Synthetic Data

A CW tone propagation experiment is simulated using the ATLAS normal mode model [Gordon1984] to generate the complex wavefield which outer product gives the array covariance matrix to be processed by the various methods. Normal mode models provide a complete solution of the wave equation including full diffraction effects [Boyles1984, p. 199] and should produce a realistic wavefield to process with the proposed processing methods to obtain estimates of vertical arrival structure.

2.1. Description of the Environment

The environment is characteristic of the North-East Pacific and a deep water situation. It is range independent with a water depth of 4667 m. The sound speed profile with depth is given in Table 2.1 and plotted in Figure 2.1. The sound speed varies in the water column between 1489.1 m/s and 1530 m/s. The sound axis is 500 m deep. The critical depth of the oceanic waveguide is on the order of 3313 m. Thus, the sound channel has a depth excess and convergence zone propagation may take place. The bottom is characterized by a frequency invariant bottom loss table (bottom loss in dB as a function of incidence angle), given in Table 2.2 and plotted in Figure 2.2. It is assumed that there is no surface loss.

A 5 m deep omnidirectional noise source is projecting a CW tone at 20 Hz or 100 Hz with a source level of 200 dB re 1 μPa at 1 m. The sound speed at the source is 1509.46 m/s so that its reciprocal depth is on the order of 3275 m. The environment is assumed to be noise free.

When the frequency analyzed is 20 Hz, the receiving vertical array is assumed to be cut for 30 Hz with an interelement spacing of 25 m. The array has 128 identical equispaced sensors and extends across most of the water column from 100 m to 3275 m. When the frequency is 100 Hz, the receiving vertical array is assumed cut for 107 Hz with an interelement spacing of 7 m. It extends from 300 m to 1189 m. The 20 Hz and

100 Hz cases differ by the receiving array used. The geometry in each case is summarized in Figure 2.3.

2.2. Analysis and Interpretation

Before processing a synthetic wavefield to get vertical arrival structure information, one must direct one's attention toward its analysis and interpretation. The ray tracing approach provides an easily understandable picture of the wave field in terms of ray diagrams, and guides the intuition in the study of the physics of the simulation [Urick1983]. The main appeal of a ray tracing program is the direct and quick availability of vertical arrival structure information across the array. The ray tracing program CONGRATS in the Generic Sonar Model (GSM) will be used in the following study [Weinberg1985].

Ray theory is widely used for high frequency, deep water problems [Jensen1988]. As rule of thumb, one may use in practice and consider the ray theory solution to be fairly accurate if the frequency f is such that $f \geq \frac{10c}{h}$, where c is the reference sound velocity and h the water depth [Cornyn1973]. This is not an absolute criterion since there is no certainty that the ray solution realistically models a given situation. It is well known that ray theory is a high frequency approximation to the solution of the wave equation, and that it breaks down near caustics [Boyles1984]. For this reason, ray theory has been generalized using a multipath expansion in the Fourier-Bessel integral representation of the pressure field to numerically solve the reduced wave equation under the WKB approximation [Weinberg1975]. This modified ray theory treats the caustic problem. The CONGRATS program in the GSM implements such modified ray theory and is used in the following. It is considered to do quite well at low frequency in its computation of eigenrays and pressure [Weinberg1985, p. 6-123]. Pressure or transmission loss is estimated by a phased summation of the different eigenray contributions [Weinberg1985, p. 6-139]. The GSM model is run with the same environmental inputs as the ATLAS model. The bottom loss table, Table 2.2, corresponds to the MGS bottom loss table Province type 3 of the GSM. The rays with launch angles of 0°, ± 5°, ± 10° and ± 15° from the source are plotted in Figure 2.4.

2.3. 20 Hz Simulation Results

The source at 5 m depth projects a 20 Hz CW tone. The transmission loss variations with range are computed by the ATLAS model and the results plotted on Figure 2.5. Panels A, B and C in Figure 2.5, respectively, correspond to receiver depths of 5 m, 50 m and 500 m. The transmission loss at a range of 80 km is 120 dB near the surface and on the order of 100 dB at greater depth. The same variations of transmission loss with range are computed with the GSM model and plotted in Figure 2.6. The GSM results have the same behavior as the ATLAS ones, although they show a well defined convergence zone between 50 and 60 km which is not reported by the ATLAS model. The acoustic wavelength at 20 Hz is of the order of 75 m so that the source can be considered at the surface. Both models report consistent transmission loss values at 80 km from the source.

The receiving array is assumed to be at 56 km from the source where the convergence zone should begin if it exists. The variations of the transmission loss as a function of depth across the 128 sensor array computed by the ATLAS and GSM models are respectively plotted in Figure 2.7 and Figure 2.8. Although the interference patterns across the water column do not match exactly, one notes the fair agreement between the two models below 1000 m where the transmission loss varies between 120 and 100 dB. As noted before, the GSM results yield above 1000 m a convergence zone which is not reported by the ATLAS model. The phase variations across the array, computed by the ATLAS model, are plotted in Figure 2.9.

The arrival angles of the eigenrays (rays propagating from a source to a receiver) between − 45° and 45° are given in Table 2.3 as calculated by the GSM at 56 km range and at the sound axis. Eigenray with positive source angle are downward going at the source and eigenrays with negative target angle are upward going [Weinberg1985, p. 7-37]. In order to present results consistent with the beamforming results for an array numbered from top to bottom, the signs of target angles are flipped when plotted, like in Figure 2.10 where eigenray angles are plotted as a function of depth at a range of 56 km from the source. In Figure 2.10, negative angle of arrival corresponds to downgoing ray at the array and positive angle of arrival to upgoing ray at the array. One observes eleven major arrivals between -45^{o} and 45^{o} at the array, their arrival angles at the array vary significantly with depth. The directionality picture is summarized by Figure 2.11 at the sound axis depth (500 m).

2.4. 100 Hz Simulation Results

The CW tone projected now by the 5 m deep source has a frequency of 100 Hz. The receiving array is cut for 107 Hz and extends from 300 m to 1189 m. The variations of transmission loss with range computed by the ATLAS model are plotted in Figure 2.12 for receiver depths of 5 m (Panel A), 50 m (Panel B) and 500 m (Panel C). These variations are similar to those of the GSM plotted in Figure 2.13. The better agreement between the two models is a result of the higher frequency. The GSM indicates a convergence zone between 50 and 60 km, clearly defined for a receiver at 50 m. Approximately at the same range, the transmission loss computed by ATLAS decreases slightly. The convergence zone is not as well defined as in the GSM results because low frequency sound diffracts in the shadow zone [Boyles1984, p. 199-201]. The existence of a convergence zone is confirmed by a contour plot of the 90 dB transmission loss level across the whole water column between 40 and 80 km from the source (Figure 2.14).

Like in the 20 Hz case, the receiving array is assumed to be at 56 km from the source, in the far field, and at the beginning of the convergence zone. The variations of transmission loss across the 128 sensors are plotted in Figure 2.15 and 2.16 for the

ATLAS and GSM results, respectively. The transmission loss varies rapidly in depth, indicating a complex interference pattern. It is for both cases on the order of 90 to 95 dB. In addition, the phase variations across the array, computed by the ATLAS model, are plotted in Figure 2.17.

The arrival angles of the GSM eigenrays between - 45° and 45° are given in Table 2.4 , as calculated by the GSM at the sound axis and for a range of 56 km. As above, eigenrays are plotted as a function of depth with their signs flipped in Figure 2.18 to be consistent with the sign convention that corresponds to beamforming an array numbered from top to bottom. One observe twelve major arrivals between - 45° and 45° on the array, their arrival angle at the array does not vary significantly with depth like in the 20 Hz case since the aperture is three times smaller. The directionality picture is summarized by Figure 2.19 at the sound axis depth (500 m).

Table 2.1	
Water Depth (m)	Sound Velocity (m/s)
0	1510.000
80	1501.400
120	1493.200
250	1483.700
400	1479.300
500	1479.100
700	1480.100
1000	1480.998
1750	1486.939
4667	1530.000

Table 2.2	
Vertical Angle (deg)	Loss (dB)
0	0
10	0.4
20	3.20
30	5.20
40	6.80
50	7.60
60	8.20
70	8.20
80	8.40
90	8.10

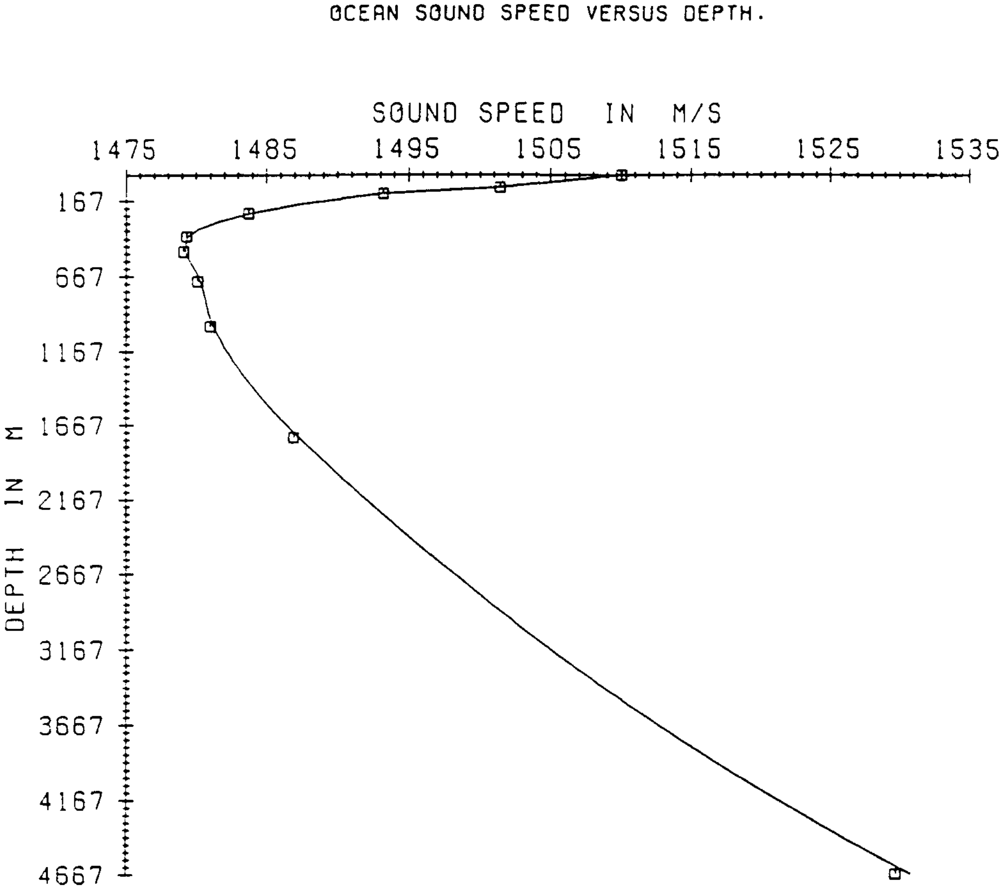

Figure 2.1: Sound speed profile.

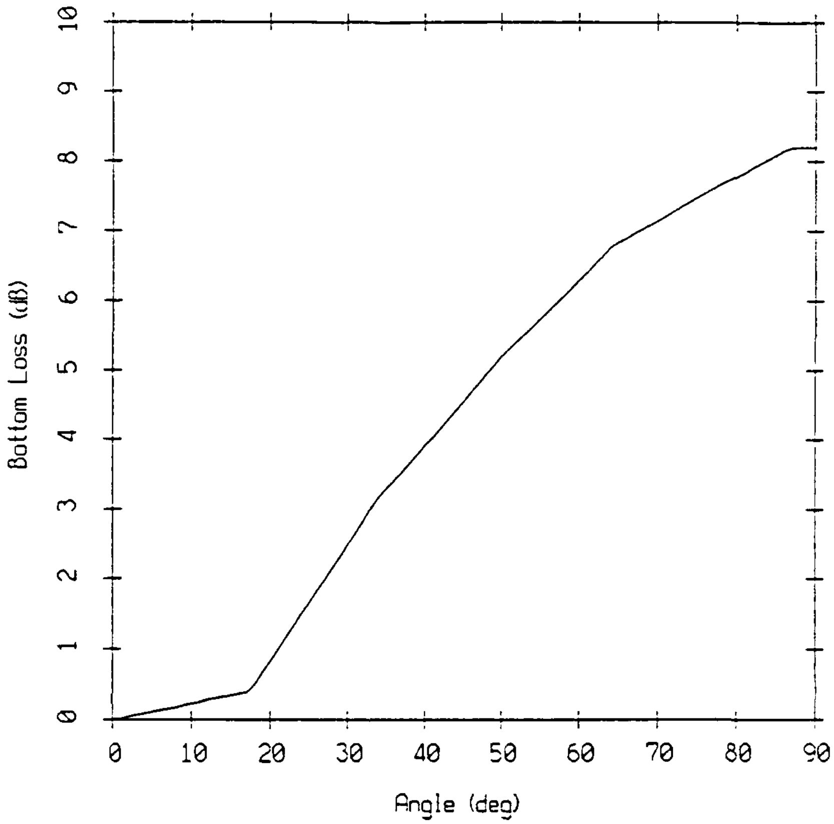

Figure 2.2: Bottom loss as a function of incidence angle.

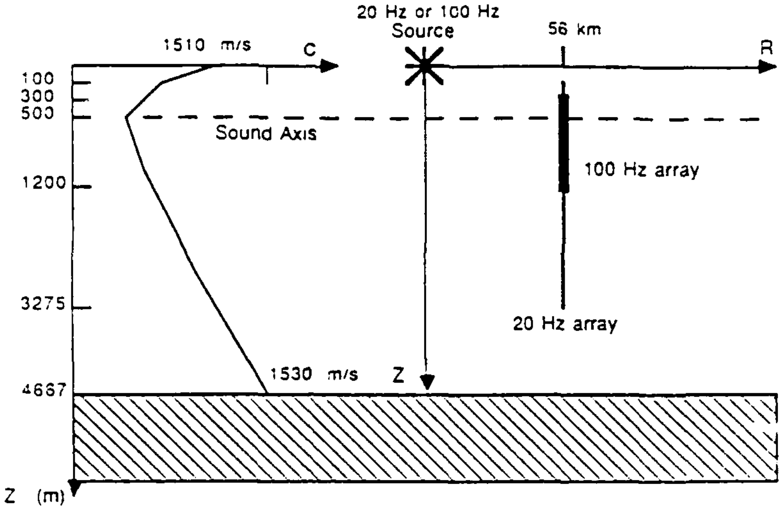

Figure 2.3: Summary of the problem geometry at 20 Hz and 100 Hz.

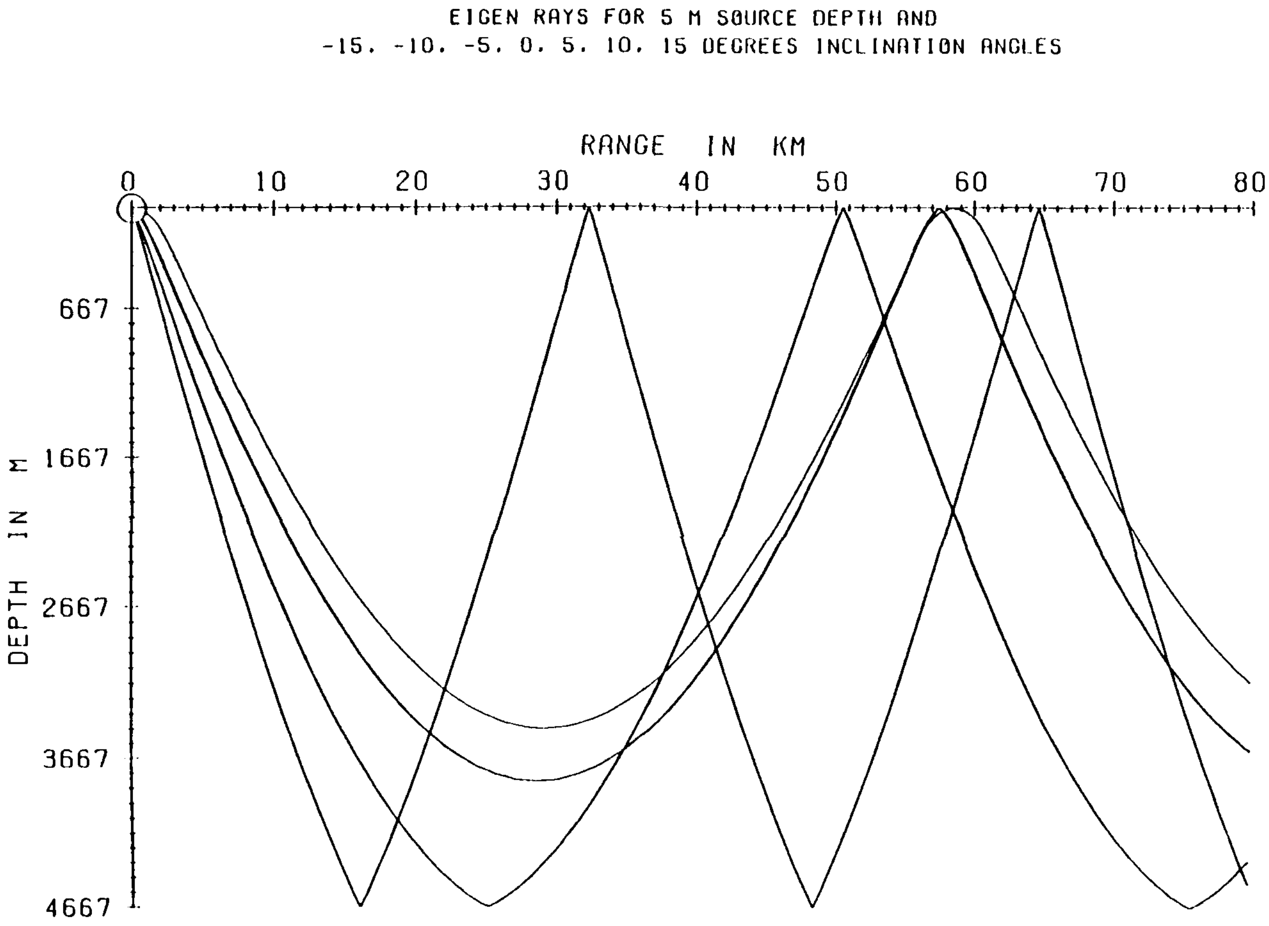

Figure 2.4: GSM ray diagram for launch angles of 0° ± 5° ± 10° ± 15°.

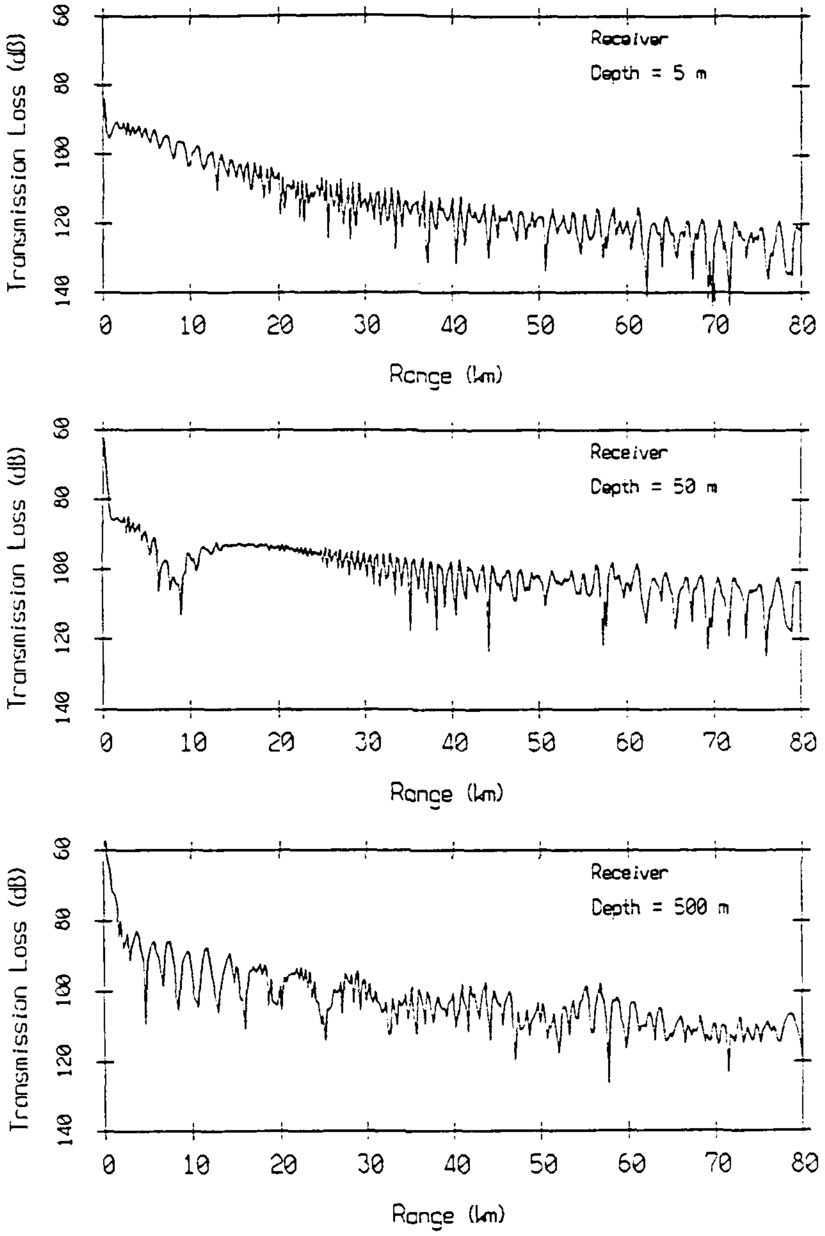

Figure 2.5: Transmission loss versus range computed by the ATLAS model at 20 Hz. A: receiver depth is 5 m, B: receiver depth is 50 m, C: receiver depth is 500 m.

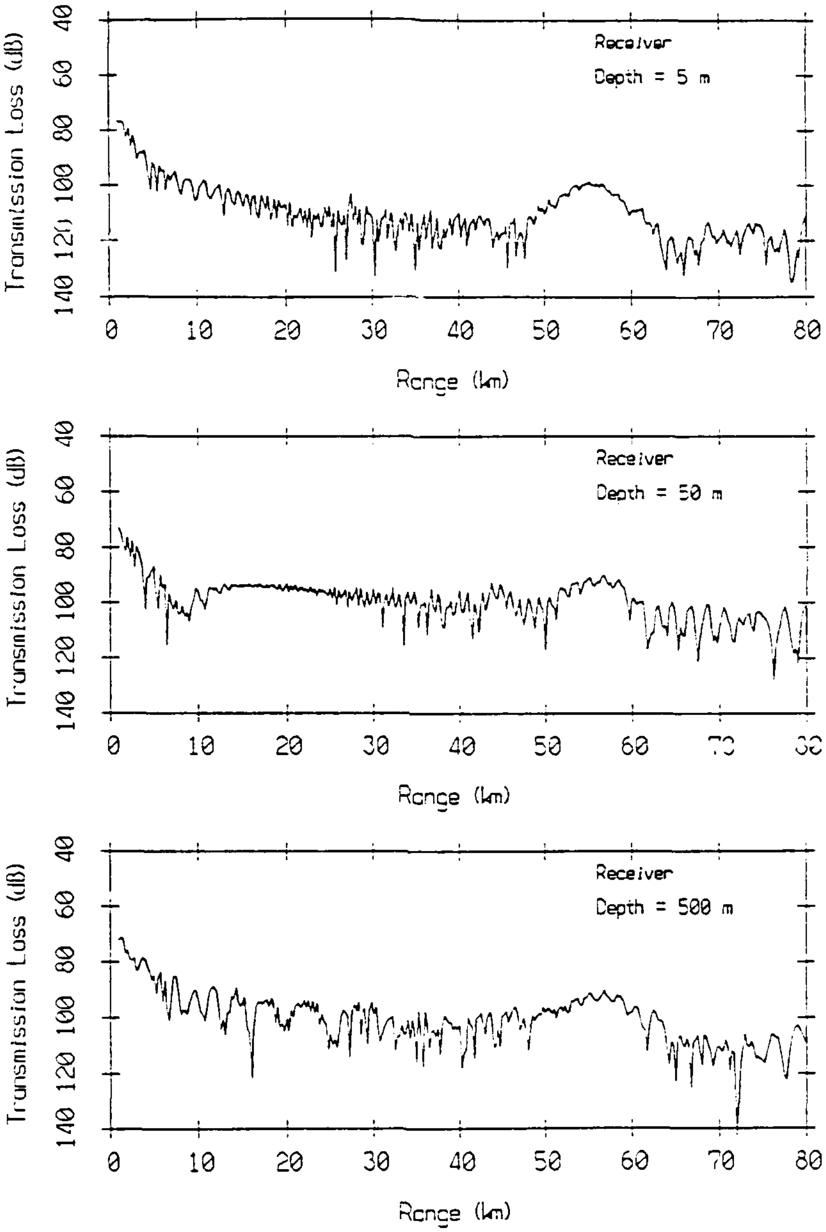

Figure 2.6: Transmission loss versus range computed by the GSM at 20 Hz. A: receiver depth is 5 m, B: receiver depth is 50 m, C: receiver depth is 500 m.

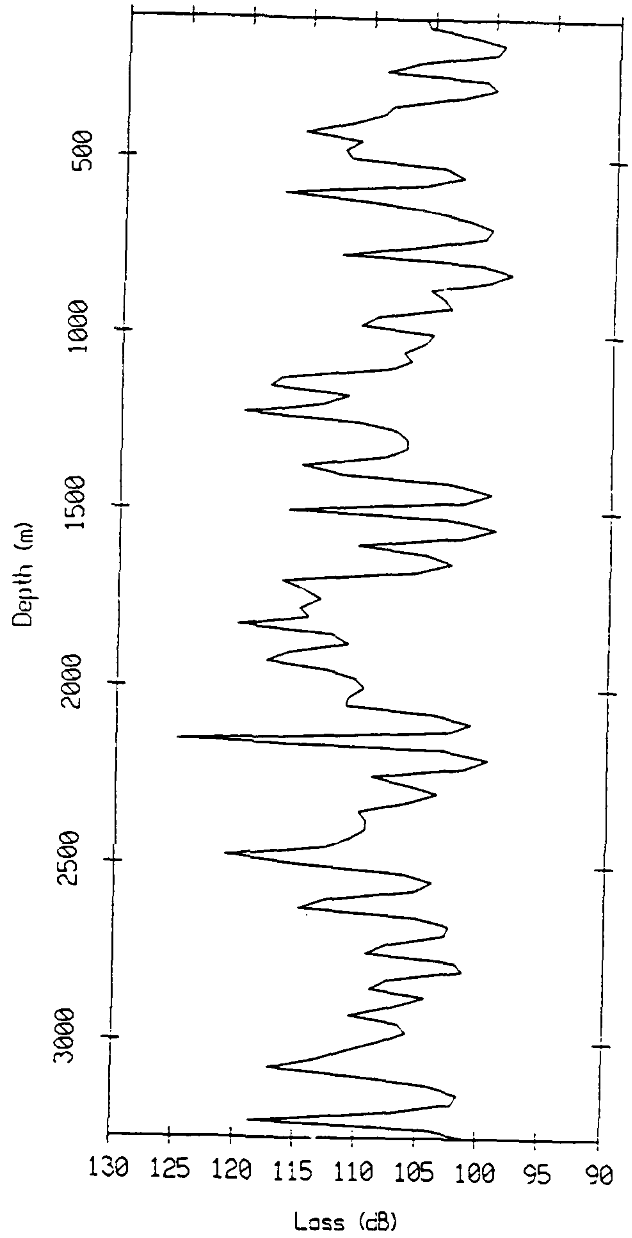

Figure 2.7: Transmission loss versus depth computed by the ATLAS model at 56 km and at 20 Hz.

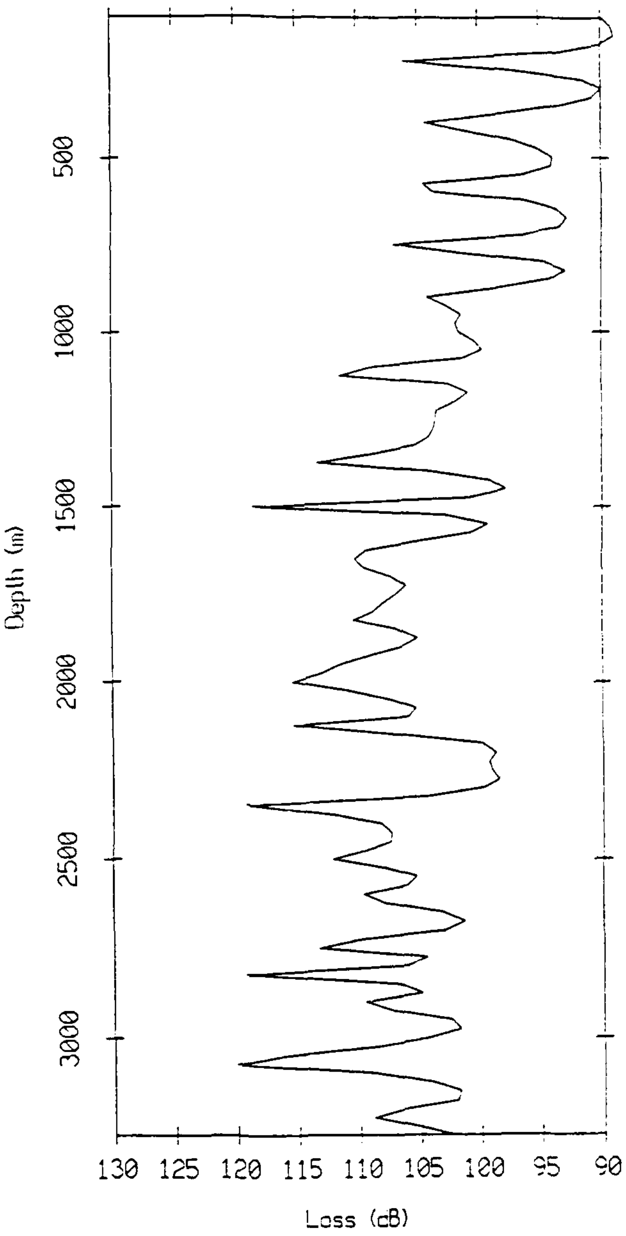

Figure 2.8: Transmission loss versus depth computed by the GSM at 56 km and at 20 Hz.

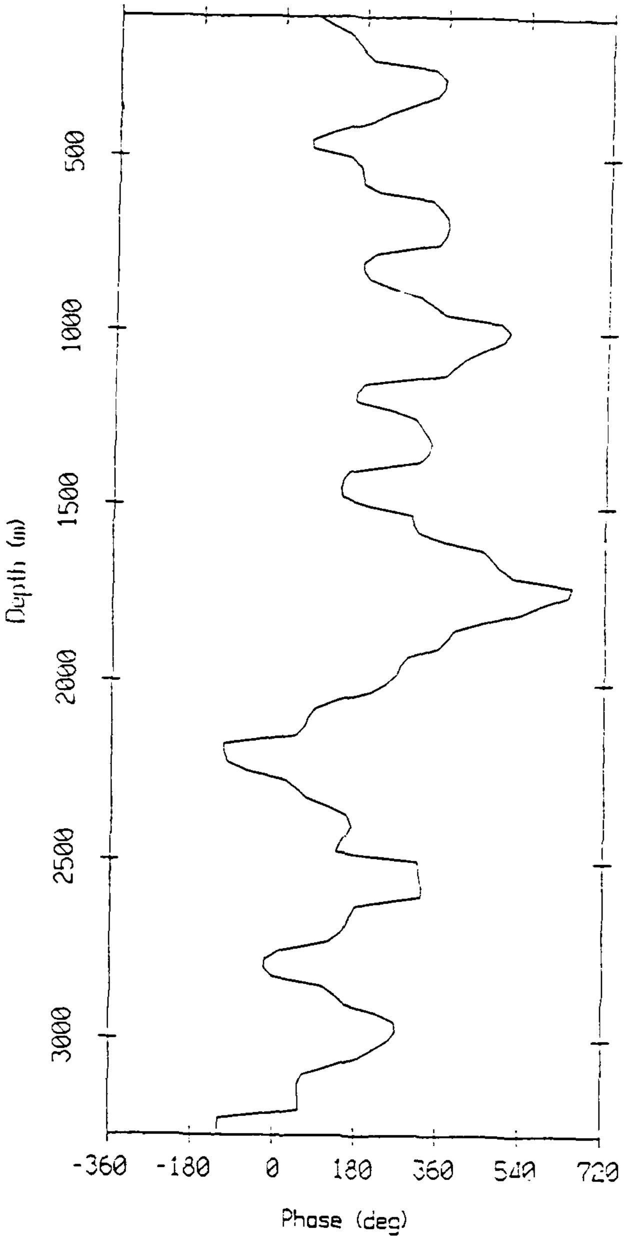

Figure 2.9: Phase versus depth computed by the ATLAS model at 56 km and at 20 Hz.

Table 2.3: GSM eigenray table at 20 Hz, 56 km range and at the sound axis.

```
GENERIC SONAR MODEL      VERSION  ANSI
-----------------------------------
RANGE =         56 KM
FREQUENCY =      0.020 KHZ
SOURCE DEPTH = 0.50000e+01 M
TARGET DEPTH = 0.50000e+03 M
FREQUENCY    = 0.20000e+02 HZ


                          ACOUSTIC EIGENRAYS
                          ------------------

   RANGE      TIME      SOURCE    TARGET     LEVEL      PHASE    NSRF  NBTM
    KM         S        ANGLE     ANGLE       DB         DEG     V = VERTEX
                         DEG       DEG

  56.0000   37.1411   -1.5278   11.5893  -120.341  -174.537     1     0
  56.0000   37.1411   -1.5278   11.5893  -119.013     4.016     1V    0
  56.0000   37.6891    9.7270  -15.0116  -104.809   -35.450     0     1
  56.0000   37.6800    7.1888  -13.5274   -90.161    -6.855     0     1V
  56.0000   37.6902   -9.7292  -15.0131  -104.785  -214.783     1     1
  56.0000   37.6808   -7.1344  -13.4990   -90.151  -172.267     1     1V
  56.0000   37.6926   -1.5283  -11.5894  -120.122  -196.057     1     1V
  56.0000   37.6926   -1.5283  -11.5894  -110.161   -20.023     1V    1V
  56.0000   37.8479    9.9744   15.1709  -101.809  -195.397     1     1
  56.0000   37.8038    2.8866   11.8418   -96.393  -117.572     1     1V
  56.0000   37.8038    2.8866   11.8418  -110.125  -173.055     1     1V
  56.0000   37.8020    0.8630   11.5214  -121.358  -164.297     1V    1V
  56.0000   37.8020    0.8630   11.5214  -103.110  -259.983     1V    1V
  56.0000   37.8491   -9.9790   15.1740  -101.757  -375.412     2     1
  56.0000   37.8044   -3.0893   11.8922   -95.952  -269.973     2     1V
  56.0000   37.8044   -3.0893   11.8922  -108.593  -334.472     2     1V
  56.0000   39.2268   17.1747  -20.5668  -100.216  -180.000     1     2
  56.0000   38.3622    1.9955  -11.6592  -121.459  -171.034     1     2V
  56.0000   38.3622    1.9955  -11.6592  -121.972  -283.141     1     2V
  56.0000   38.3434    0.5256  -11.5014  -120.052  -223.099     1V    2V
  56.0000   38.3434    0.5256  -11.5014  -119.186  -389.716     1V    2V
  56.0000   39.2288  -17.1846  -20.5749  -100.223  -360.000     2     2
  56.0000   38.3660   -2.1618  -11.6884  -121.994  -324.846     2     2V
  56.0000   38.3660   -2.1618  -11.6884  -119.284  -455.663     2     2V
  56.0000   39.4566   18.0335   21.2795  -100.720  -360.000     2     2
  56.0000   39.4586  -18.0433   21.2877  -100.726  -540.000     3     2
  56.0000   41.5867   25.5091  -27.8183  -108.986  -360.000     2     3
  56.0000   41.5896  -25.5178  -27.8262  -108.992  -540.000     3     3
  56.0000   41.8974   26.3122   28.5465  -109.566  -540.000     3     3
  56.0000   41.9003  -26.3208   28.5543  -109.572  -720.000     4     3
  56.0000   44.6877   32.8264  -34.5655  -119.397  -540.000     3     4
  56.0000   44.6913  -32.8338  -34.5724  -119.403  -720.000     4     4
  56.0000   45.0674   33.5283   35.2234  -119.939  -720.000     4     4
  56.0000   45.0711  -33.5356   35.2303  -119.944  -900.000     5     4
  56.0000   48.3927   39.0889  -40.4816  -130.361  -720.000     4     5
  56.0000   48.3969  -39.0952  -40.4876  -130.366  -900.000     5     5
  56.0000   48.8281   39.6892   41.0533  -130.838  -900.000     5     5
  56.0000   48.8323  -39.6954   41.0591  -130.842 -1080.000     6     5
  56.0000   52.5754   44.3965  -45.5571  -141.396  -900.000     5     6
  56.0000   52.5800  -44.4017  -45.5622  -141.400 -1080.000     6     6
  56.0000   53.0545   44.9058   46.0464  -141.793 -1080.000     6     6
  56.0000   53.0592  -44.9110   46.0514  -141.797 -1260.000     7     6
```

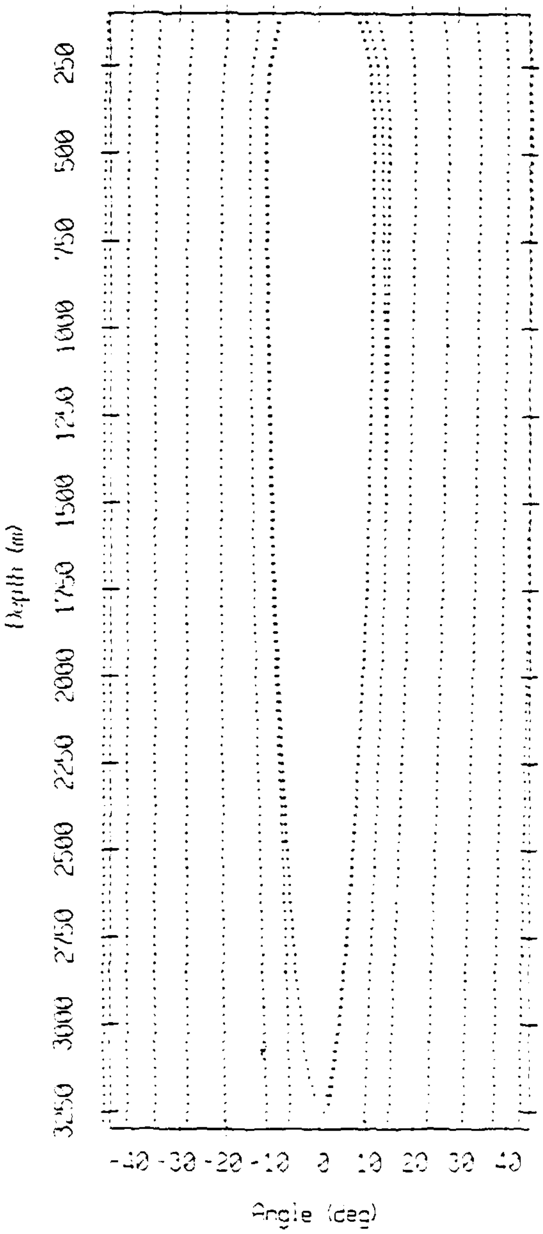

Figure 2.10: GSM eigenray arrival angles as a function of depth at 20 Hz.

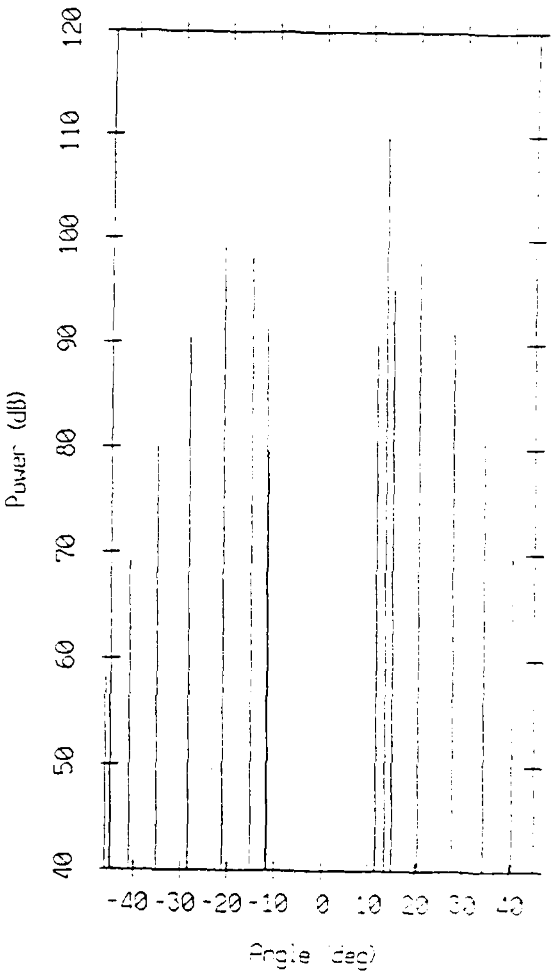

Figure 2.11: GSM eigenrays at the sound axis (500 m) and at 20 Hz.

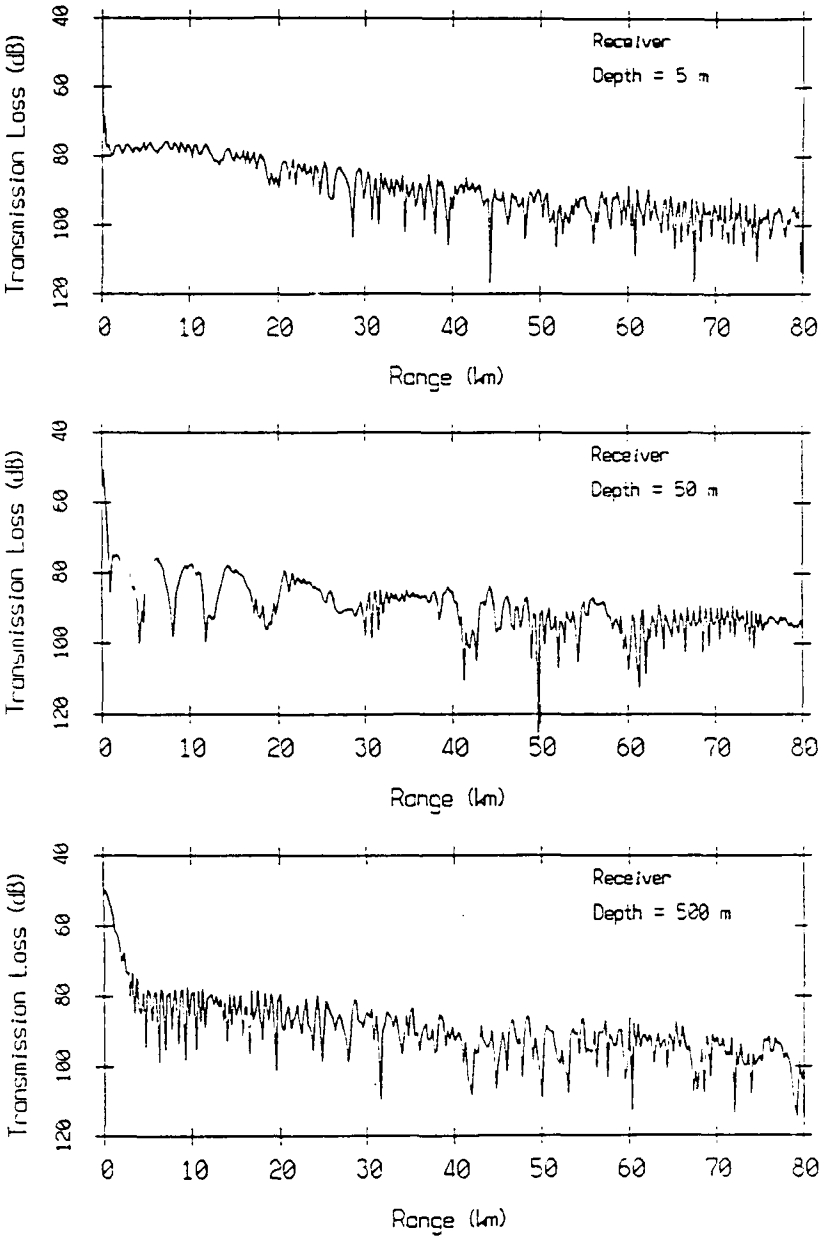

Figure 2.12: Transmission loss versus range computed by the ATLAS model at 100 Hz. A: receiver depth is 5 m, B: receiver depth is 50 m, C: receiver depth is 500 m.

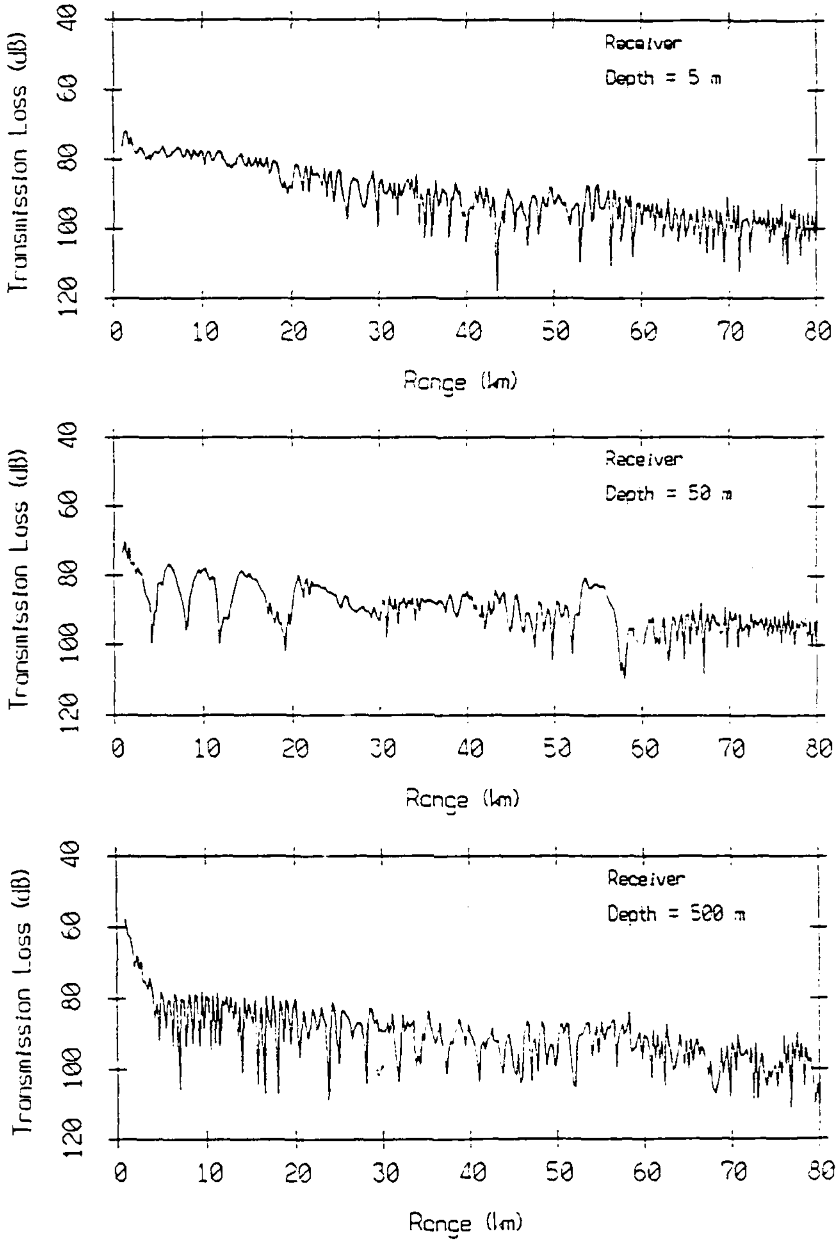

Figure 2.13: Transmission loss versus range computed by the GSM at 100 Hz. A: receiver depth is 5 m, B: receiver depth is 50 m, C: receiver depth is 500 m.

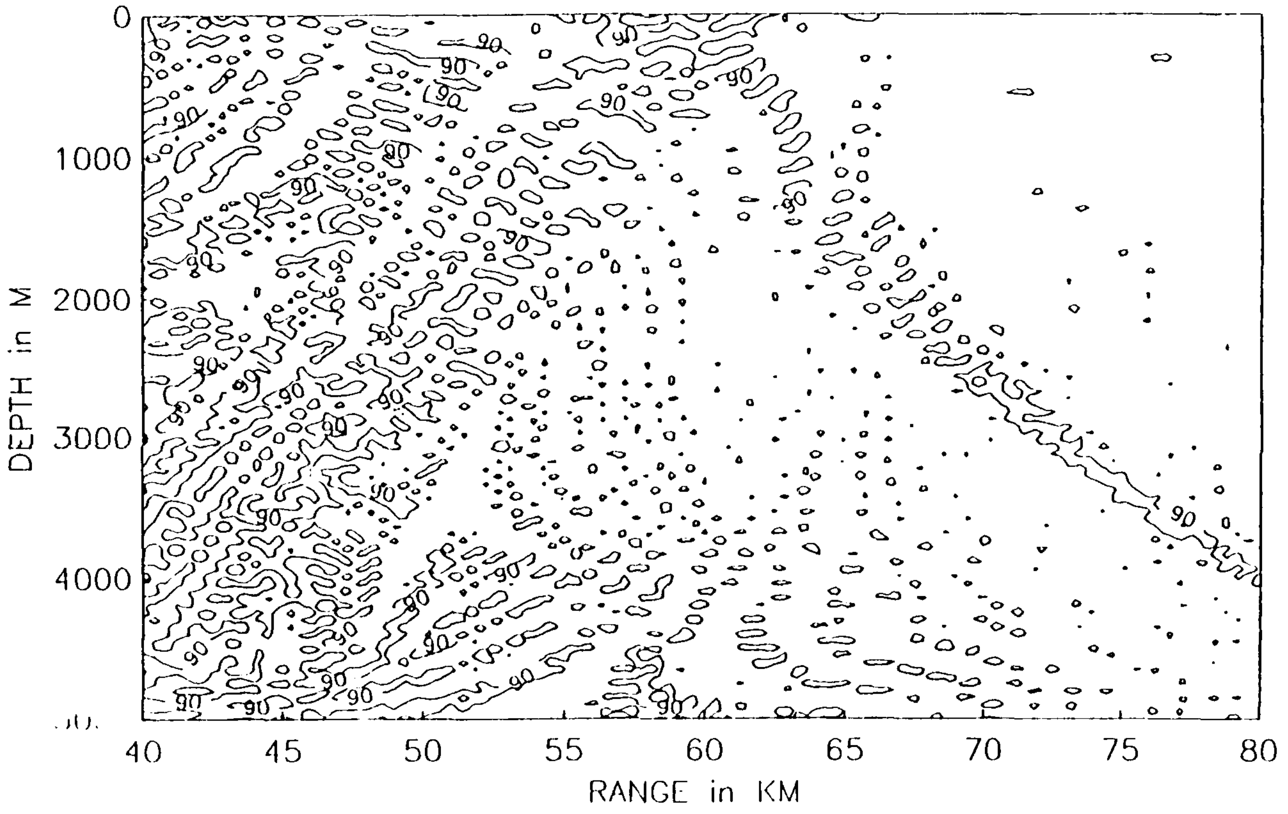

Figure 2.14: ATLAS 90 dB transmission loss contour plot at 100 Hz.

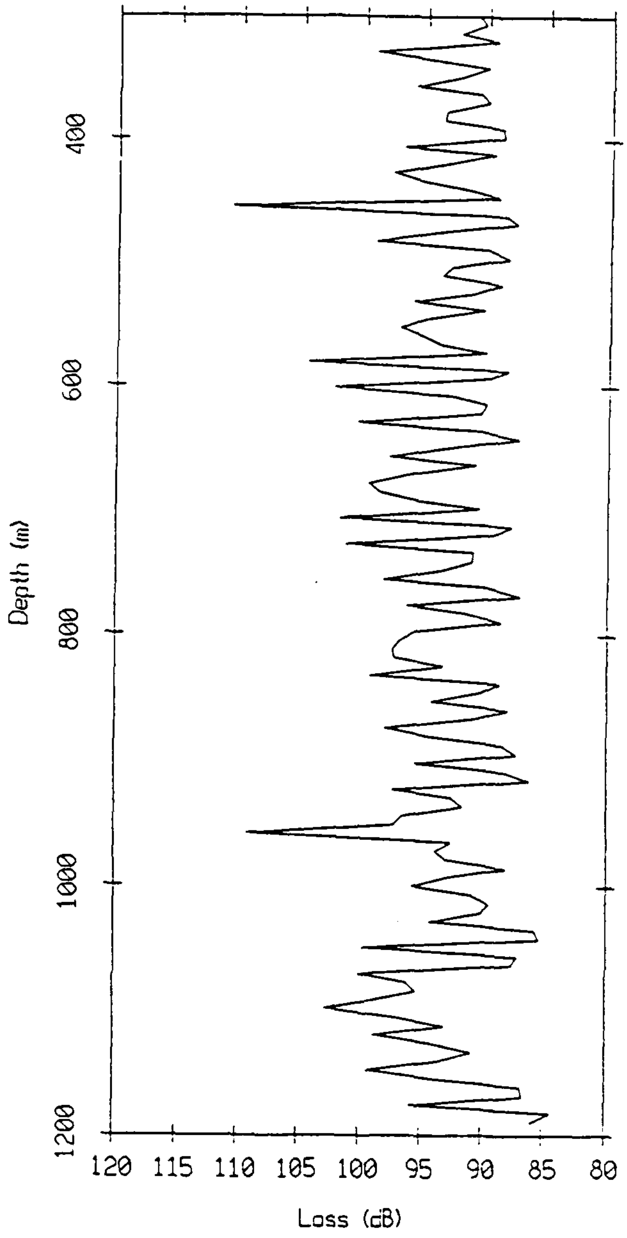

Figure 2.15: Transmission loss versus depth computed by ATLAS at 56 km and at 100 Hz.

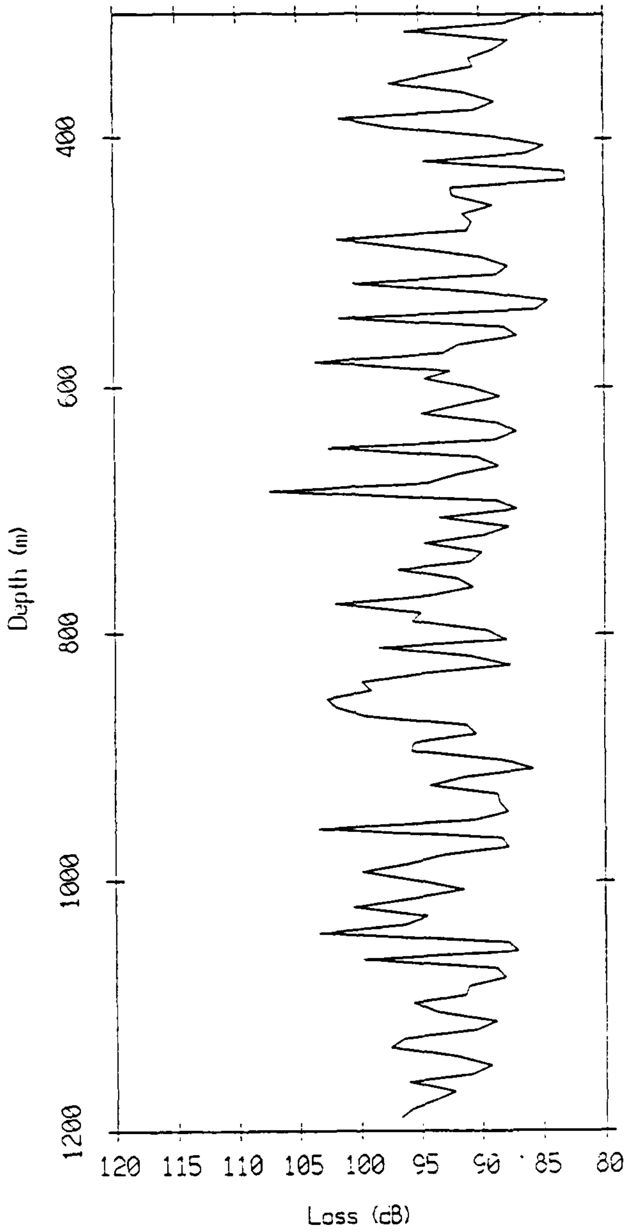

Figure 2.16: Transmission loss versus range computed by the GSM at 56 km and at 100 Hz.

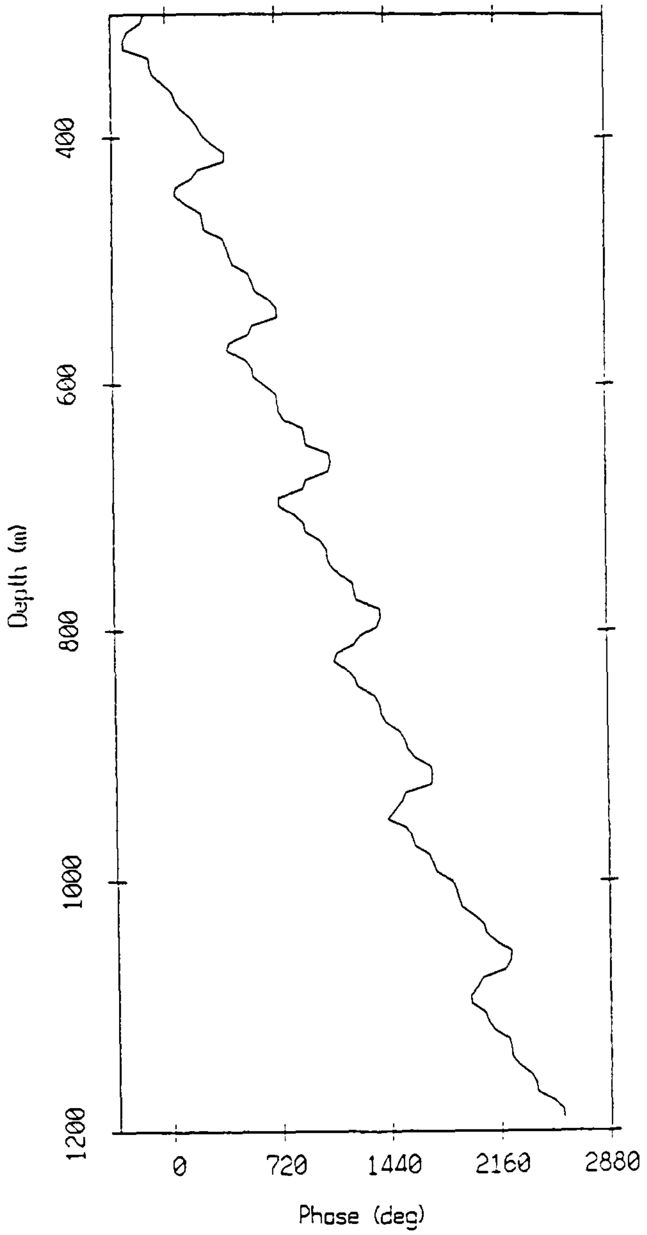

Figure 2.17: Phase versus depth computed by the ATLAS model at 56 km and at 100 Hz.

Table 2.4: GSM eigenray table at 100 Hz, 56 km range and at the sound axis.

```
GENERIC SONAR MODEL
-------------------
 RANGE        = 56 KM
 FREQUENCY    = 100 HZ
 SOURCE DEPTH = 5.0 M
 TARGET DEPTH = 503.0 M

                              ACOUSTIC EIGENRAYS
                              ------------------

  RANGE       TIME      SOURCE     TARGET     LEVEL       PHASE    NSRF  NBTM
   KM          S        ANGLE      ANGLE       DB          DEG     V = VERTEX
                         DEG        DEG

 56.0000    37.1415    -1.5278    11.5863   -122.187   -195.274     1     0
 56.0000    37.1415    -1.5278    11.5863   -122.889    -28.860     1V    0
 56.0000    37.6886     9.7266   -15.0091   -105.202    -23.184     0     1
 56.0000    37.6795     7.1971   -13.5293    -91.508      0.000     0     1V
 56.0000    37.6897    -9.7288   -15.0105   -105.128   -202.693     1     1
 56.0000    37.6803    -7.1430   -13.5010    -91.432   -180.000     1     1V
 56.0000    37.6922    -1.5282   -11.5864   -111.407   -205.347     1     1V
 56.0000    37.6922    -1.5282   -11.5864   -125.545   -203.759     1V    1V
 56.0000    37.8485     9.9753    15.1693   -101.239   -184.805     1     1
 56.0000    37.8042     2.8876    11.8392    -97.922   -109.703     1     1V
 56.0000    37.8042     2.8876    11.8392   -101.689   -197.855     1     1V
 56.0000    37.8024     0.8637    11.5185   -112.365   -159.014     1V    1V
 56.0000    37.8024     0.8637    11.5185    -97.888   -168.030     1V    1V
 56.0000    37.8496    -9.9800    15.1723   -101.164   -364.579     2     1
 56.0000    37.8048    -3.0899    11.8895    -97.262   -260.486     2     1V
 56.0000    37.8048    -3.0899    11.8895   -100.462   -361.665     2     1V
 56.0000    39.2261    17.1723   -20.5631   -100.316   -180.000     1     2
 56.0000    38.3618     1.9953   -11.6562   -124.018   -165.722     1     2V
 56.0000    38.3618     1.9953   -11.6562   -122.435   -391.638     1     2V
 56.0000    38.3430     0.5256   -11.4984   -123.519   -187.517     1V    2V
 56.0000    38.3430     0.5256   -11.4984   -123.498   -355.467     1V    2V
 56.0000    39.2281   -17.1821   -20.5713   -100.322   -360.000     2     2
 56.0000    38.3656    -2.1613   -11.6854   -126.535   -332.440     2     2V
 56.0000    38.3656    -2.1613   -11.6854   -123.004   -505.651     2     2V
 56.0000    39.4573    18.0360    21.2800   -100.822   -360.000     2     2
 56.0000    39.4593   -18.0458    21.2882   -100.828   -540.000     3     2
 56.0000    41.5858    25.5067   -27.8151   -109.091   -360.000     2     3
 56.0000    41.5886   -25.5154   -27.8229   -109.097   -540.000     3     3
 56.0000    41.8983    26.3146    28.5475   -109.675   -540.000     3     3
 56.0000    41.9013   -26.3231    28.5553   -109 681   -720.000     4     3
 56.0000    44.6866    32.8243   -34.5627   -119.510   -540.000     3     4
 56.0000    44.6902   -32.8317   -34.5696   -119.516   -720.000     4     4
 56.0000    45.0686    33.5303    35.2245   -120.056   -720.000     4     4
 56.0000    45.0723   -33.5376    35.2314   -120.062   -900.000     5     4
 56.0000    48.3914    39.0872   -40.4792   -130.484   -720.000     4     5
 56.0000    48.3956   -39.0934   -40.4851   -130.489   -900.000     5     5
 56.0000    48.8294    39.6910    41.0543   -130.964   -900.000     5     5
 56.0000    48.8336   -39.6972    41.0601   -130.969  -1080.000     6     5
 56.0000    52.5739    44.3949   -45.5551   -141.530   -900.000     5     6
 56.0000    52.5786   -44.4002   -45.5601   -141.534  -1080.000     6     6
 56.0000    53.0560    44.9073    46.0472   -141.930  -1080.000     6     6
 56.0000    53.0606   -44.9124    46.0522   -141.935  -1260.000     7     6
```

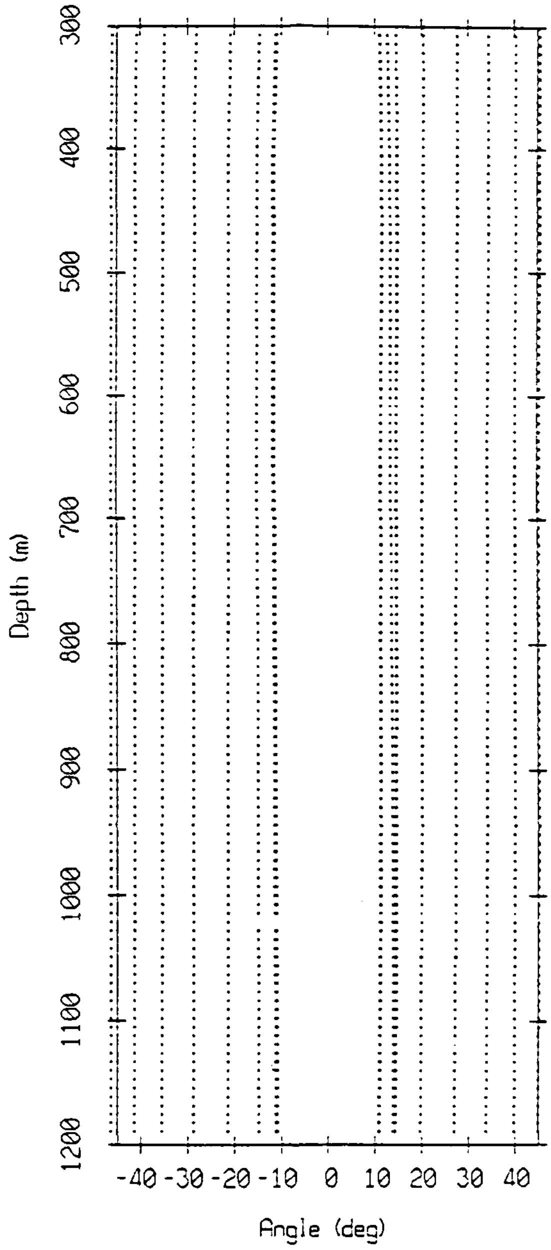

Figure 2.18: GSM eigenray arrival angles as a function of depth at 100 Hz.

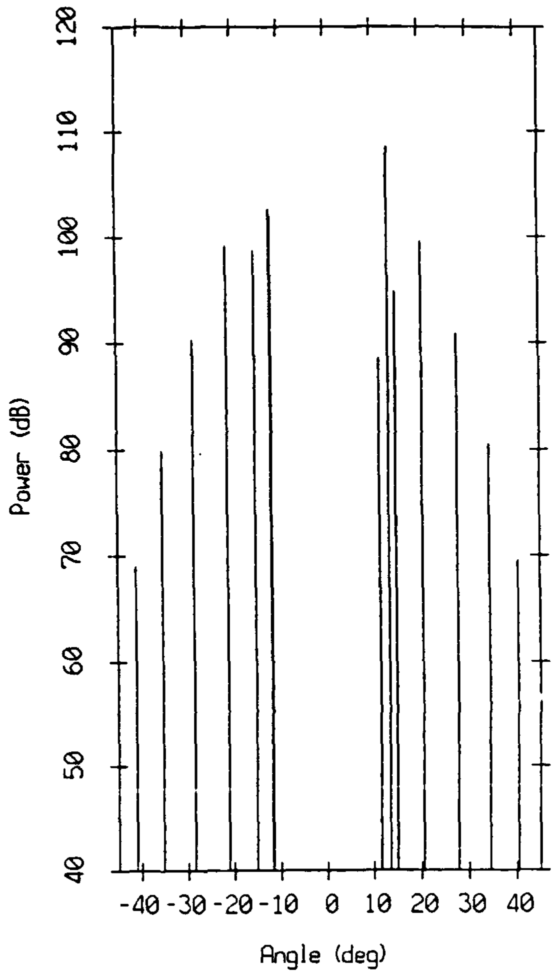

Figure 2.19: GSM eigenrays at the sound axis (500 m) and at 100 Hz.

3. Beamforming Results

3.1. Processor Implementation

The two complex wavefields created by the ATLAS normal mode program are now processed by the full aperture and subaperture approaches described in Section 1. The conventional beamformer is implemented with a rectangular window and a Kaiser-Bessel window with α parameter of 1.5 (yielding a 38 dB side lobe rejection). The angular spectra are normalized to yield power since one is interested in estimating discrete arrivals. The conventional beamformer using plane wavefront replica vectors and a rectangular window is given by

$$P_{rect} = \frac{1}{M^2} \mathbf{E}_p{}^H \, \mathbf{R} \, \mathbf{E}_p \tag{3.1}$$

where the plane wavefront replica vector $\mathbf{E}_p$ is such that $\mathbf{E}_p{}^H \mathbf{E}_p = M$. M is the number of sensors in the array (it is equal to 128). The $\frac{1}{M^2}$ normalization factor in Equation 3.1 produces a *power spectrum* (and not a power spectral density). $\mathbf{R}$ is the array covariance matrix given by

$$\mathbf{R} = \mathbf{X}\,\mathbf{X}^H \tag{3.2}$$

where $\mathbf{X}$ is the complex wavefield produced by the ATLAS normal mode model at the signal frequency of interest. When the Kaiser-Bessel window is used, the conventional processor associated to the planar array manifold is given by

$$P_{Kaiser} = \frac{1}{M^2} (\mathbf{W}\,\mathbf{E}_p)^H \, \mathbf{R} \, (\mathbf{W}\,\mathbf{E}_p) \tag{3.3}$$

where $\mathbf{E}_p$ and $\mathbf{R}$ are defined as in Equation 3.1 and $\mathbf{W}$ is defined by

$$\mathbf{W} = \frac{1}{\frac{1}{M} \sum_{i=0}^{M-1} a_i} \begin{bmatrix} a_0 & 0 & \cdots & 0 \\ 0 & a_1 & \cdots & \vdots \\ \vdots & \vdots & \ddots & \vdots \\ \vdots & \vdots & \cdots & 0 \\ 0 & 0 & \cdots & a_{M-1} \end{bmatrix} \tag{3.4}$$

where the a_i's are the Kaiser-Bessel window coefficients weighting the array, M is the number of sensors. Once again the power spectrum produced by Equation 3.3 is normalized for signals.

The phase at the i^{th} sensor corresponding to a plane wavefront replica vector, $\mathbf{E}_p$, is given by

$$\phi_i = \frac{2\pi f \sin\theta_0)}{c(z_0)}(z_i - z_0) \tag{3.5}$$

where the frequency of the signal is f, θ_o is the arrival angle with respect to the horizontal, c_o the sound speed (which is assumed constant throughout the whole medium), z_o a reference depth and z_i the depth of the i^{th} sensor. In a realistic oceanic medium, the sound speed varies with depth. The sound speed profile results in ray bending or wavefront curvature. Even for modest aperture length, such curvature can be important, especially for arrivals with small angle with respect to the horizontal [Tran1989]. Using Snell's law, a ray-geometric approximation of the wavefront phase was derived in [Tran1989]. The phase at the i^{th} sensor at a depth z_i is given by

$$\phi_i = 2\pi f \int_{z_0}^{z_i} \frac{Sgn(\theta(z_0))}{c(z_i)} \left\{ 1 - \cos^2\theta(z_0) \left[\frac{c(z_i)}{c(z_0)} \right]^2 \right\}^{1/2} dz \tag{3.6}$$

where Sgn is the signum function, and $\cos^2\theta(z_0)\left[\frac{c(z_i)}{c(z_0)}\right]^2 < 1$ is implicitly assumed for all z_i. As earlier, z_0 is the reference depth. The curved wavefronts phase, which enters in the curved wavefront replica vector $\mathbf{E}_c$, exists only if

$$\theta(z_0) \geq \cos^{-1}\frac{c(z_0)}{c(z_i)} \tag{3.7}$$

If Equation 3.7 is not satisfied, the corresponding ray has turned over and the complex exponential is replaced by zero at the sensor position i in the vector $\mathbf{E}_c$. Then, partial insonification takes place and the corresponding curved wavefront replica vector $\mathbf{E}_c$ is

$$\mathbf{E}_c{}^T = \left[0\,0 \cdots 0 * * \cdots * 0 \cdots 0 \right] \tag{3.8}$$

where the number of non zero entries in Equation 3.8, generically denoted by $*$, is M_i, the size of the insonified aperture $(M_i \leq M)$. The number of null entries and their position in the steering vector $\mathbf{E}_c$ depends on the sound speed profile and the particular array geometry (i.e. the relative position of the array with respect to the sound speed profile).

The conventional beamformer using curved wavefront replica vector is given by

$$P_{rect} = \frac{1}{M_i(\mathbf{E}_c)^2}\, \mathbf{E}_c{}^H\, \mathbf{R}\, \mathbf{E}_c \tag{3.9}$$

where the insonified window size M_i depends on a particular curved wavefront steering vector $\mathbf{E}_c$ or look direction, $\mathbf{E}_c^H\, \mathbf{E}_c = M_i(\mathbf{E}_c)$. $M_i(\mathbf{E}_c)$ is generally equal to M, except for low angle. The curved wavefront conventional processor using a Kaiser-Bessel window is similarly given by

$$P_{Kaiser} = (\mathbf{W}\,\mathbf{E}_c)^H\, \mathbf{R}\, (\mathbf{W}\,\mathbf{E}_c) \tag{3.10}$$

where E_c and $\mathbf{R}$ are defined as before and $\mathbf{W}$ is now defined by

$$\mathbf{W} = \begin{bmatrix} \mathbf{O}_{n_1,n_1} & \mathbf{O}_{n_1,M_i} & \mathbf{O}_{n_1,n_2} \\ \mathbf{O}_{M_i,n_1} & \mathbf{w}_{M_i,M_i} & \mathbf{O}_{M_i,n_2} \\ \mathbf{O}_{n_2,n_1} & \mathbf{O}_{n_2,M_i} & \mathbf{O}_{n_2,n_2} \end{bmatrix} \tag{3.11}$$

where $n_1 + M_i + n_2 = M$, $\mathbf{O}_{n_i,n_j}$ is a n_i by n_j covariance matrix with only zero entries. $\mathbf{w}$ is given by

$$\mathbf{w} = \frac{1}{\sum_{i=0}^{M_i-1} a_i} \begin{bmatrix} a_0 & 0 & \cdots & 0 \\ 0 & a_1 & \cdots & \cdot \\ \cdot & \cdot & \cdots & \cdot \\ \cdot & \cdot & \cdots & 0 \\ 0 & 0 & \cdots & a_{M_i}-1 \end{bmatrix} \tag{3.12}$$

where the a_i's are the Kaiser-Bessel window coefficients weighting the insonified part of the array, M_i in Equations 3.11 and 3.12 is equal to $M_i(\mathbf{E}_c)$, the number of insonified sensors.

The plane and curved wavefront replica vectors are referenced to the sound axis so that all the results obtained by the various processors, operating on the full aperture or on subapertures, are consistent with each other. 256 replica vectors between -90° and $+90^\circ$ are used, the quantization in angle is on the order of 0.7°. The array elements are numbered from top to bottom so that negative angles of arrival correspond to downgoing sound or uplooking beams and positive angles of arrival correspond to upgoing sound or downlooking beams. This sign convention is consistent with the results presented in

Section 2.

In addition to the full aperture plane and curved wavefront conventional beamforming, the MVDR processor is used to beamform the full aperture as well as subapertures extracted from the 128-sensor array. The MVDR beamformer, in the following, is given by

$$P_{MVDR} = \frac{1}{s_i(\mathbf{E}_e)} \frac{1}{\mathbf{E}_e{}^H F(\mathbf{R})_s{}^{-1} \mathbf{E}_e} \tag{3.13}$$

where $F(\mathbf{R})_s$ is the spatially smoothed covariance matrix on s-sensor subarrays across a M sensor array (the spatial smoothing subsegment length is s). When the full aperture is processed, M is equal to 128 and the spatial smoothing subsegment length s is 64 sensors. When subaperture processing is performed, M is chosen equal to 32 and the spatial smoothing subsegment length s equals 20. The curved wavefront steering vectors associated to each M-sensor array (each one has a particular geometry with respect to the sound speed profile) are passed through the spatial smoothing pre-processing operation from which the "best" replica vectors are obtained by an eigenvalue-eigenvector decomposition as explained in [Tran1989] ; hence the name of eigensteering vector $\mathbf{E}_e$. The eigensteering vector $\mathbf{E}_e$, of dimension $(s,1)$, is normalized to unit norm, $\mathbf{E}_e{}^H \mathbf{E}_e = 1$. In the case of partial insonification, the eigensteering vectors corresponding to low angle of arrival with respect to the horizontal are given by

$$\mathbf{E}_e = \begin{bmatrix} 0\,0 \cdots 0 * * \cdots * 0 \cdots 0 \end{bmatrix} \tag{3.14}$$

where the number of non zero entries in Equation 3.13 generically denoted by * is $s_i(\mathbf{E}_e)$, the size of the insonified equivalent aperture resulting from spatial smoothing with length s. As noted before, $s_i(\mathbf{E}_e)$, generally, is equal to s except for low angle of look. The normalization by $s_i(\mathbf{E}_e)$ in Equation 3.12 is performed to yield a power spectrum and not a power spectral density. $F(\mathbf{R})_s$ is stabilized before inversion by adding a small fraction of noise corresponding to 10^{-4} of the average power across the s sensor equivalent smoothed array (i.e. $10^{-4} tr(F(\mathbf{R})_s)$, where tr denotes the trace operation). This allows for a condition number (ratio of the smallest to the largest eigenvalue) on the order of 10^{-6}.

The MUSIC and Minimum Norm eigenvector methods are used to do subaperture processing, like the MVDR beamformer. The MVDR, MUSIC and Minimum Norm methods will operate on 32-element subapertures using the corresponding eigensteering vectors for spatial smoothing with subsegment length of 20 sensors. Subaperture processing is performed on 48 subarrays sliding from the top to the bottom of the full aperture array by two elements (i.e. the first array extends from sensor 1 to 32, the second subarray extends from sensor 3 to 34 and so on). The angular spectra are computed on each subaperture and then incoherently averaged to produce a full aperture composite angular spectrum.

The subaperture processing is also performed on four non-overlapping 32 sensor subarrays, using the corresponding eigensteering vectors as described above. The composite angular spectrum, then, is the results of averaging on those four subarrays. Such processing appears more realistic, being more practical in its computational requirements.

The MUSIC algorithm is given by

$$P_{MUSIC} = \frac{1}{s_i(\mathbf{E}_e)} \frac{1}{\mathbf{E}_e{}^H \mathbf{R}_{noise} \mathbf{E}_e} \tag{3.15}$$

where $s_i(\mathbf{E}_e)$ and $\mathbf{E}_e$ are defined as before. $\mathbf{R}_{noise}$ is the noise only covariance matrix. It is obtained by choosing a number of arrivals or signals n_{signal} and doing an eigenvalue-eigenvector decomposition of the spatially smoothed covariance matrix $F(\mathbf{R})_s$. $\mathbf{R}_{noise}$ is given by

$$\mathbf{R}_{noise} = \frac{1}{s - n_{signal}} \sum_{i=1}^{s-n_{signal}} \mathbf{V}_i \mathbf{V}_i^H \tag{3.16}$$

where the $\mathbf{V}_i$'s are the unit norm noise eigenvectors ($\mathbf{V}_i \mathbf{V}_i^H = 1$). The orthonormal eigenvectors $\mathbf{V}_i$ of $F(\mathbf{R})_s$ corresponds to the $s - n_{signal}$ lowest eigenvalues. To ensure numerical stability in the computation of the quadratic form in Equation (3.15), the noise only covariance matrix is stabilized by adding a small fraction of noise to main diagonal, i.e.

$10^{-7} tr(\mathbf{R}_{noise})$, where tr denotes the trace operation. This results in clipping the peaks SNR theoretically infinite to 70 dB.

The Minimum Norm method is given in [Orfanidis1988, p. 363]

$$P_{MINORM} = \frac{1}{s_i(\mathbf{E}_e)} \; \frac{1}{\mathbf{E}_e{}^H \mathbf{d}\mathbf{d}^H \mathbf{E}_e} \tag{3.17}$$

where $\mathbf{E}_e$ is a (s,1) unit norm eigensteering vector as defined earlier, and $\mathbf{d}$ a $(s,1)$ vector given by

$$\mathbf{d} = \left[\sum_{i=1}^{s-n_{signal}} \mathbf{V}_i \mathbf{V}_i^H \right] \mathbf{U}_o \tag{3.18}$$

where $\mathbf{U}_o^T = [1\ 0\ 0\ \cdots\ 0]$, and $\mathbf{V}_i$ like in MUSIC is the i^{th} noise eigenvector of the spatially smoothed covariance matrix $F(\mathbf{R})_s$. To ensure numerical stability of the computation of the quadratic form in Equation 3.7, the (s, s) matrix $\mathbf{d}\mathbf{d}^H$ is stabilized by adding a small fraction of white noise to the main diagonal, $10^{-7}\frac{tr(\mathbf{d}\mathbf{d}^H)}{s}$, where tr denotes the trace operation. As in the case of the MUSIC algorithm, this results in clipping theoretically infinite peaks SNR to 70 dB.

3.2. 20 Hz Simulation Results

The results of conventional processing on the 20 Hz synthetic data using rectangular and Kaiser-Bessel windows, and the plane wave array manifold are plotted in Figures 3.1. These angular spectra correspond to the output of a classic FFT beamformer commonly performed on vertical line arrays. The situation is of high signal-to-noise ratio since there is no ambient noise. The highest power arrivals lay between -30° and $+30^\circ$. The use of a tapering window appears necessary to protect the estimate from sidelobe leakage, the high angle power level drops off 20 dB when one switches from the rectangular window to the Kaiser-Bessel window.

The use of curved wavefront replica vectors with the conventional beamformer gives results similar to the case of plane wavefront replica vectors. The angular spectra for the curved wavefront array manifold are plotted in Figures 3.2 for rectangular and Kaiser-Bessel windows. The arrivals are reported at slightly different angles. The conventional beamformer using curved wavefront replica vectors reports high power levels on the order of 90 dB at near horizontal angles. This is due to the partial insonification of the aperture which results in higher sidelobes and lower resolution. The insonified aperture in the 128 element array is plotted as a function of arrival angle in Figure 3.3. Near horizontal arrivals insonify a very limited part of the aperture, thus explaining the high power levels reported at low angle by the curved wavefront processor. Horizontal arrivals in this case do not physically exist since they insonify only the sensor number 13 as shown in Figure 3.3.

The results of the conventional beamformer using plane and curved wavefront replica vectors are overlaid with the GSM eigenrays in Figure 3.4. The GSM multipath pattern at the sound axis is similar to the angular spectra obtained from the ATLAS data with all arrival angles steeper than $\pm 10^\circ$. The peak powers indicated by the GSM are slightly higher than the ones in the ATLAS angular spectra. This is consistent with the acoustic modeling performed on Section 2 which shows that the convergence zone reported by the GSM is much better defined than the ATLAS one. One can note a slight increase in resolution when curved wavefront replica vectors are used, especially for low arrival angles. There is also a better agreement with the GSM eigenray arrival angles for the two arrivals near -15° and 20° for the curved processor. Furthermore, the curved wavefront processor yields arrival peak to in-between peak levels larger than the plane wavefront processor for physically upgoing arrivals with angles up to +40° and also downgoing arrivals with arrival angles larger than -30°. The upgoing arrival angular estimates produced by the curved processor are also closer to the GSM eigenray arrival angle than the ones produced by the plane wave processor. This is also true for the downgoing arrival close to -15°. The planar replica vectors produce slightly lower arrival angles, especially for upgoing sound (positive angles). The conventional processor produces similar results for steep arrival angles with either type of replica vectors. In this case, it is known than the phase relationships entering in the plane and curved wavefront replica vectors are almost equivalent [Tran1989].

The output of the MVDR processor operating on the full aperture with a spatial smoothing subsegment length of 64 sensors is plotted in the top panel of Figure 3.5. A large amount of smoothing is necessary in order to decorrelate over a dozen multipath arrivals which can be close together, as indicated by the GSM eigenray angles. Therefore, the MVDR estimate may still suffers large signal cancellation due to arrival correlation. The peak power of the arrivals is up to 20 dB lower than the ones produced by the conventional processor. Loss can also be due to incorrect wavefront modeling, even if eigensteering vectors are used, and unsufficient sampling in angle. The MVDR beamformer is known to be very sensitive to mismatch, especially at high signal-to-noise ratio. The near horizontal angles (at 0°) exhibits an increase in power which is due, like in the case of the conventional curved wavefront processor, to the partial insonification of the spatially smoothed equivalent aperture. The eigensteering vectors which corresponds to this equivalent aperture have, at low arrival angles, zero entries much like the actual physical aperture, as shown in Figure 3.6. The results of the MVDR full aperture processing are overlaid with the curved wavefront conventional processing results and the GSM eigenrays in the bottom panel of Figure 3.5. Although the equivalent aperture is reduced by half after spatial smoothing, the MVDR beamformer, using the eigensteering vectors, yields a much larger resolution than the conventional beamformer.

The results of the 32 sensor subaperture processing by the MVDR method, after spatial smoothing with a subsegment length of 20 and using the eigensteering vectors, are presented in Figures 3.7, 3.8 and 3.9. Figure 3.7 is the waterfall plot of the angular spectra corresponding to each subarray and referenced to the sound axis. Increasing subarray number corresponds to increasing depth. This plot shows that the number of peaks, as well as their power, are not correctly reported. Because of the short aperture, only limited spatial smoothing can be performed. This leads to an unsufficient decorrelation of the multipaths and signal cancellation takes place. The flat area at low angles in the waterfall plot corresponds to an angular region where no arrivals or sound can physically exist according to the ray geometric approach selected here. It is the result of the partial insonification phenomena discussed earlier. In Figure 3.8 are plotted the traces with depth of the local maxima of these spectra, each angular spectrum is associated to the depth of the corresponding subarray center. A peak is detected and indicated in Figure 3.8 if it is a local maximum in the angular spectrum (null derivative and negative second derivative). This plot shows the great variability of the detected arrival angles with depth (even though referenced to the sound axis). It is largest in the middle and the upper half of the 128 sensor aperture. As a result of this great variability, the incoherent averaging of the 48 angular spectra (all referenced to the sound axis) does not produce good results, as shown in Figure 3.9. The arrivals have peak powers which are greatly lower than the conventional beamformer peak powers. In addition the arrival structure is significantly different from the one obtained by full aperture coherent processing with either the conventional beamformer or the MVDR processor.

The same processing is performed by the MUSIC algorithm. The number of signals is 12. The MVDR and MUSIC methods are known to yield similar results at very high signal to noise ratios [Nickel1988]. Since the situation studied is ambient noise free, it is the case here and the MUSIC angular "spectra" waterfall plot of Figure 3.10 is qualitatively similar to the MVDR angular spectra waterfall plot of Figure 3.7. The traces with depth of the local maxima of these spectra, plotted in Figure 3.11, show the same variability as in the case of the MVDR beamformer. The incoherent average of the MUSIC "spectra", plotted in Figure 3.12, is almost identical to the MVDR results in Figure 3.9, with an imperceptible improved resolution. This can be observed easily by looking at Figure 3.13 on which are overlaid the average of the 48 subaperture spectra for the MVDR beamformer and the MUSIC algorithm, and the GSM eigenray angles. The spectra are normalized to their respective minimum value. One observes a good agreement in angle estimation between the MUSIC averaged "spectrum" and the GSM results for low arrival angles. However, the angular estimate differ for steeper angle of arrival which also corresponds to lower powers.

The Minimum Norm method is used with the same spatial smoothing subsegment length of 20 and a number of signals set to 12. The waterfall plot of the Minimum Norm "spectra" in Figure 3.14 shows a substantial increase in resolution compared to the MUSIC results, with more defined peaks. The traces with depth of the local maxima of these "spectra" are plotted in Figure 3.15. The variability is even larger than with MUSIC. As a result, the incoherent averaging of the 48 Minimum Norm "spectra" produces a complicated picture with a high density of peaks in Figure 3.16. The MUSIC and Minimum Norm averaged "spectra" are normalized by their respective minimum value and overlaid with the GSM eigenray arrival angles in Figure 3.17. There is a good agreement in angle estimation at low angles of arrival. The Minimum Norm estimate has line pairs in place of single arrival. This appears similar to the line splitting phenomenon common for high resolution spectral estimation methods such the auto-regressive model based methods [Marple1987].

The averaged angular spectra based on four nonoverlapping subarrays of 32 sensors (with a spatial smoothing with subsegment length of 20) are plotted in Figures 3.18, 3.19 and 3.20 for the MVDR, MUSIC and Minimum Norm methods, respectively. The composite angular spectrum is the average of the spectra calculated over four nonoverlapping 32-sensor subarray. Averaging over four subarrays in some cases produces better results than averaging over 48 subarrays, as done earlier, because of the great variability of the angular spectra in the vertical. The improvements are characterized by a better resolution of the peaks, and are especially obvious for the Minimum Norm results where the multipath arrival structure is fairly close to the eigenray structure produced by the GSM. The MUSIC and Minimum Norm results are overlaid with the GSM eigenray angles in Figure 3.21. One notes for both MUSIC and the Minimum Norm the qualitative improvement.

3.3. 100 Hz Simulation Results

The 100 Hz case is characterized by an aperture length smaller than in the 20 Hz case, over which sound speed does not vary as much. Therefore, the effects of the wavefront curvature should have less impact. The angular spectra produced by the conventional beamformer, using planar replica vectors, with a rectangular window and a Kaiser-Bessel window, are plotted in Figure 3.22. The angular spectra produced by the conventional processor using curved wavefront replica vectors are plotted in Figure 3.23. As in the 20 Hz case, a tapering window is necessary to minimize sidelobe leakage. The curved wavefront conventional processor produces high power in the horizontal because of the partial insonification of the aperture, which results in large sidelobe leakage [Tran1989]. The insonified aperture is plotted in Figure 3.24 which shows that the 0° arrival insonifies only three sensors.

The results of the conventional processing with plane and curved wavefronts are overlaid with the GSM eigenrays in Figure 3.25. As expected, the conventional processor, using curved and plane wavefront replica vectors, are identical, except for the spurious horizontal arrival of the curved wavefront processor. They match closely the multipath arrival structure reported by the GSM. The correspondence between the ATLAS angular spectrum estimate and the GSM eigenrays is still excellent when looking at the absolute power levels of the arrivals.

The output of the MVDR processor operating on the full aperture array, after spatial smoothing with a subsegment length of 64 sensors, is plotted in the top panel of Figure 3.26. The MVDR angular spectrum is overlaid with the results of the conventional processor using curved wavefront replica vectors and the GSM eigenrays in the bottom panel of Figure 3.26. As in the 20 Hz case, the MVDR processor on the full aperture method, using eigensteering vectors, produces a better resolution than the conventional processor, even with a reduction by half of the aperture length due to spatial smoothing.

The peak power levels in this angular spectrum are up to 20 dB lower than the ones of the conventional processing. There may still be some strong signal cancellation in addition to mismatch loss due to imperfect wavefront modeling and unsufficient sampling in angle. The slight increase of power, at low arrival angles, corresponds to the partial insonification of the spatially smoothed equivalent aperture. The insonified part of this equivalent aperture, based on the eigensteering vectors is plotted in Figure 3.27.

The results of the 32 sensor subaperture processing by the MVDR method, after spatial smoothing with subsegment length of 20 and using the eigensteering vectors, are presented in Figures 3.28, 3.29 and 3.30. Figure 3.28 is a waterfall plot of the angular spectrum corresponding to each subarray. As in the 20 Hz case, these spectra are referenced to the sound axis. The number of peaks in Figure 3.28 is roughly half of what is detected in the full aperture coherent processing. This is due to the limited spatial smoothing performed on the short subaperture. Here, spatial smoothing does not fully decorrelate the multipaths. Thus, signal cancellation takes place and results in lower power levels. Another cause of peak power reduction is mismatch due to imperfect wavefront modeling. The peaks levels are up to 20 dB below the conventional processor peak levels. The traces with depth of the local maxima of these spectra are plotted in Figure 3.29. The high power level and low angle arrivals are stable, while the lower level, high angle arrivals exhibit a large variability both in power and angle. The composite angular spectrum, calculated by incoherently averaging the 48 angular spectra, is plotted in Figure 3.30. The strong and low angle arrivals detected by this composite estimator have power levels on the same order as the full aperture MVDR processor.

The subaperture processing, performed by the MVDR processor, is now repeated using the MUSIC algorithm, with a number of signals set to 12. The waterfall plot of the MUSIC "spectrum" in Figure 3.31 shows some resolution improvement. The traces with depth of the local maxima of these "spectra", plotted in Figure 3.32, still indicate a large variability for steeper arrivals. The limited spatial smoothing does not allow decorrelation of all the multipath arrivals. 13 spatial averages are performed to transform the array covariance matrix. Based on the output of full aperture processors, at least 15 multipath arrivals impinge on the array. Incoherent averaging of the MUSIC "spectra" in Figure 3.33 produces a very good estimate of the arrival structure for arrival angles between -35° and $+35^\circ$, even if it does not have as high signal to floor levels as in the case of the full aperture processors. For steeper arrival angles, which have also lower power levels, the MUSIC algorithm fails to report the correct arrival angles.

The subaperture composite spectra for the MVDR and MUSIC are normalized by their respective minimum value and overlaid with the GSM eigenray angles in Figure 3.34. Both processors detect the highest level arrivals with no or little angle bias at low arrival angle. The bias in angle is larger for steeper and lower level arrivals. As suggested earlier, this is due to insufficient decorrelation achieved by limited spatial smoothing.

The Minimum Norm method now is used to perform the subaperture processing performed by the MVDR and MUSIC techniques, with a 20 sensor subsegment length spatial smoothing and a number of signals set to 12. The waterfall plot of the Minimum Norm angular "spectrum" with depth, in Figure 3.35, shows a substantial increase in resolution, with peaks more defined. The traces with depth of the local maxima of these "spectra" are plotted in Figure 3.36 and exhibit a larger variability for higher arrival angles. On the other hand the lower angle arrivals are very stable with depth. As a result, the average of the "spectra" estimated on the 48 subarrays, plotted in Figure 3.37, has strong and well defined peaks at low angles, and more choppy noise-like structure at higher angles. This is due to unsufficient decorrelation achieved by the spatial smoothing with a subsegment length of 20, which only allows the resolution of the strongest arrivals.

The averaged Minimum Norm and MUSIC "spectra" are normalized by their respective minimum value and overlaid with the GSM eigenray angles in Figure 3.38. We observe a very good agreement between the GSM eigenray angles and the arrival angle estimates obtained from the MUSIC and the Minimum Norm techniques. The Minimum Norm method allows an easier detection of arrivals compared to the MUSIC algorithm, yielding larger signal-to-noise ratios.

The subaperture processing on four 32 sensor nonoverlapping subarrays is now presented in Figures 3.39, 3.40 and 3.41 for the MVDR, MUSIC and Minimum Norm techniques respectively. Both the MVDR composite spectrum and the MUSIC composite "spectrum" based on the 4 subarrays are similar to the composite spectra based on the 48 subarrays. It appears in Figures 3.39 and 3.40 that doing 48 averages or only four averages has no or little effects on the detection of the main low angle arrivals. On the other hand, the Minimum Norm composite "spectrum", based on only 4 non-overlapping subarrays, allows the detection of additional arrivals which impinge on the array with steeper angles, compared to the MUSIC algorithm (Figure 3.42).

4. Conclusions

This report introduces several approaches to beamform large vertical line arrays. Full aperture beamforming using the conventional and the MVDR processors is proposed. Conventional beamforming using plane and curved wavefront replica vectors is performed. Full aperture MVDR processing is accomplished using curved wavefront replica vectors which are modified to minimize mismatch after spatial smoothing. A subaperture processing is described and implemented using three high resolution methods, the MVDR, MUSIC and Minimum Norm techniques with curved wavefront replica vectors modified to minimize mismatch after spatial smoothing.

A simulation is designed to assess the relative performance of these various processing schemes. It does not include ambient noise and thus corresponds to infinitely high signal-to-noise ratios. The ATLAS normal mode model is used to create realistic environment signals to be processed. Careful modeling allows a good correspondence to be achieved between the ATLAS beamforming results and the GSM eigenrays, with only marginal differences in angle of arrival and power levels. Two cases are treated. The 20 Hz case is of a very large array operating at low frequency, where almost the whole water column is covered. The 100 Hz case corresponds to mid-low frequencies and arrays currently available such as the MPL digital array [Sotirin1988].

The use of curved wavefront replica vectors with the conventional beamformer appears to be desirable in the 20 Hz case. The use of plane wavefront replica vector can result in arrival angle bias in arrival angle, especially for low angle of arrival with respect to the horizontal where curvature is the largest [Tran1989]. The use of curved wavefront also yield in some cases better peak resolution. In the 100 Hz case where the array is 900 m long, the simulation shows that there is no advantage of using curved wavefront replica vectors with the conventional processor. In this case, the output of the conventional beamformer is almost the same whether planar or curved wavefront replica vectors are used.

Because the simulation does not include any ambient noise model, the signal-to-noise ratios are infinitely high and loss due to mismatch can become a limiting factor for the performance of the high resolution methods. The use of curved wavefront replica vectors, modified to accommodate the spatial smoothing pre-processing (which is required in order to decorrelate the multipaths), is necessary in both the 20 Hz and the 100 Hz cases. The MVDR processor is used to process coherently the full aperture and produces better resolution than conventional beamforming. On the other hand, loss due to mismatch and signal cancellation due to multipath arrivals still occur and result in lower power levels than in conventional beamforming. The stabilization noise added to the smoothed covariance matrix in order to invert it, sets a noise floor in the angular spectra.

The subaperture processing, which requires less integration time to estimate the *array covariance matrix*, does not produce as good signal-to-noise-floor levels as the full aperture processing. Based on the simulation, the high resolution eigenvector based methods, MUSIC and the Minimum Norm, have fairly good resolution capabilities, even if the parameters used in this work are such that the amount of spatial smoothing is potentially insufficient to decorrelate all the multipath arrivals.

The simulation brings up the problem of selecting the location and the number of subarrays to process in order to obtain the averaged angular spectrum of arrival. The vertical arrival structure appears highly variable depending on the amount of incoherent averaging performed (e.g. when 48 subarrays or 4 nonoverlapping subarrays are processed by the MUSIC and the Minimum Norm methods). Increasing the number of subarrays does not necessarily enhance the angular spectrum. Too much incoherent averaging may result in smearing the peaks in the angular spectrum.

This simulation shows that the two processing strategies envisioned are viable and that the high resolution methods using a ray geometric model of curvature, based on the sound speed profile at the array, produce good results. By using the high resolution methods, one enhances resolution in the angular spectra. The cost to pay in this simulation is a reduction of signal-to-noise-floor level essentially because of the absence of ambient noise.

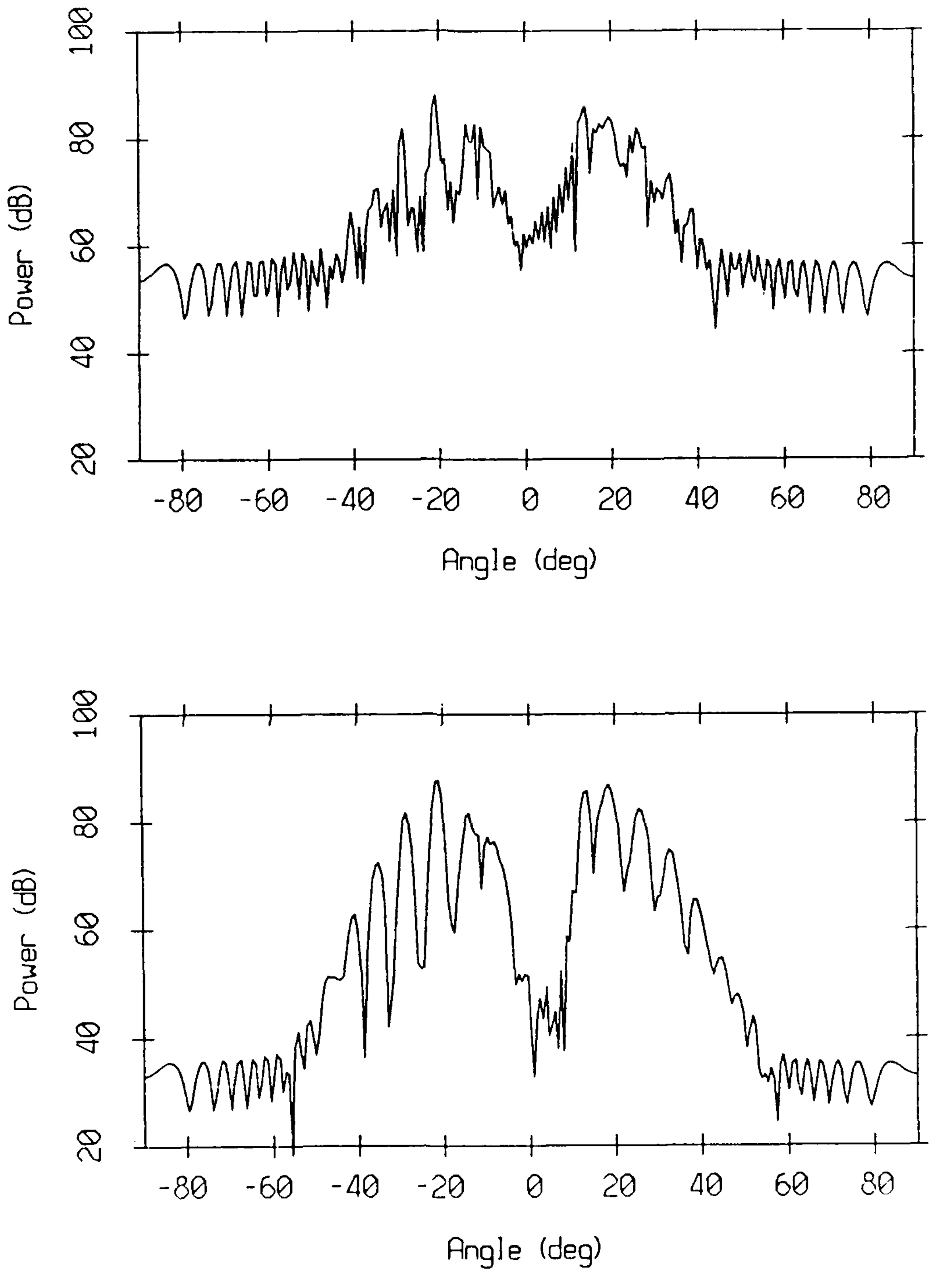

Figure 3.1: 20 Hz output of the conventional beamformer using plane wavefront replica vectors. Data are weighted in the top panel by the rectangular window, and in the bottom panel by a Kaiser-Bessel ($\alpha = 1.5$) window.

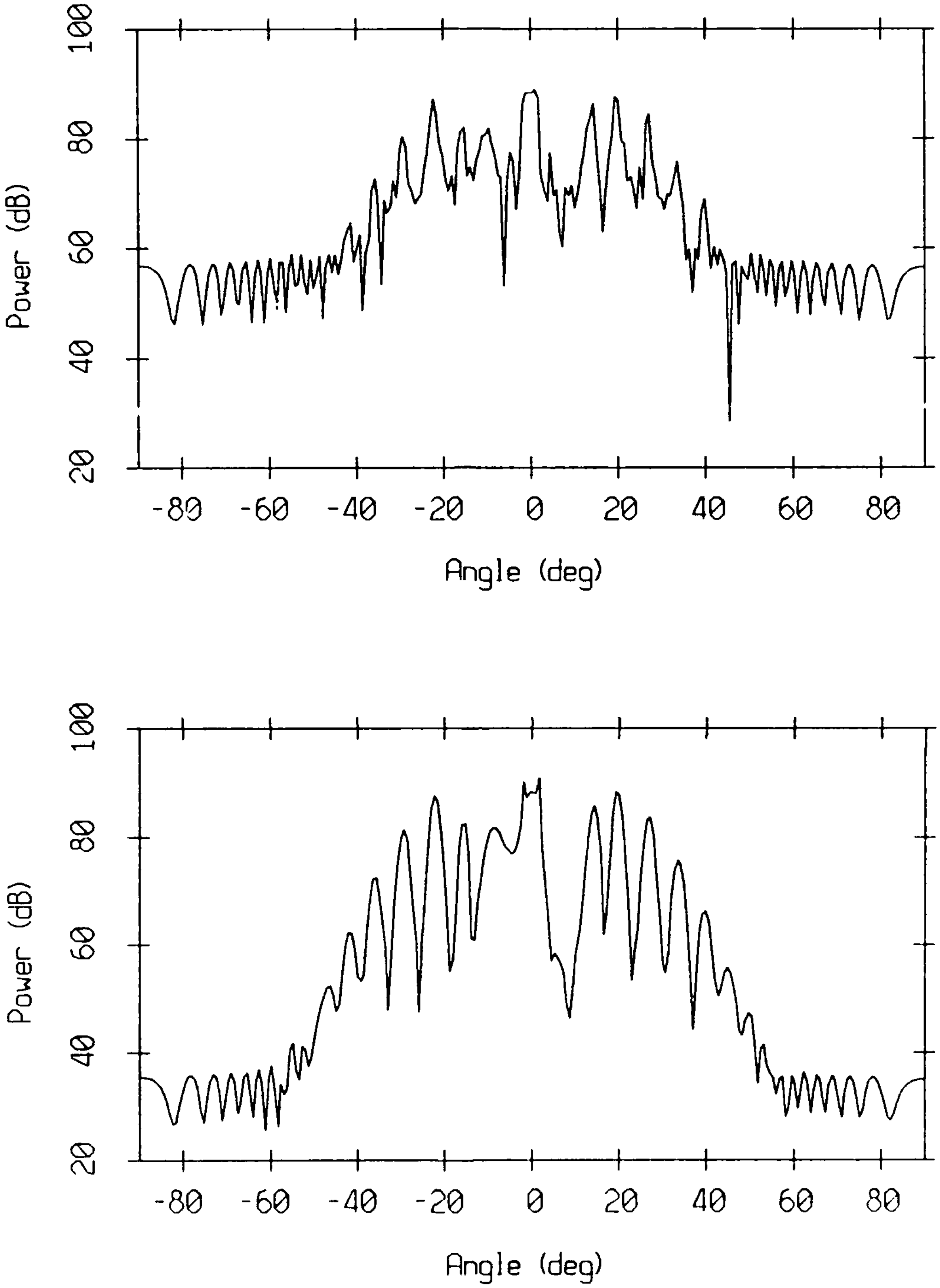

Figure 3.2: 20 Hz output of the conventional beamformer using curved wavefront replica vectors. Data are weighted in the top panel by the rectangular window, and in the bottom panel by a Kaiser-Bessel (α = 1.5) window.

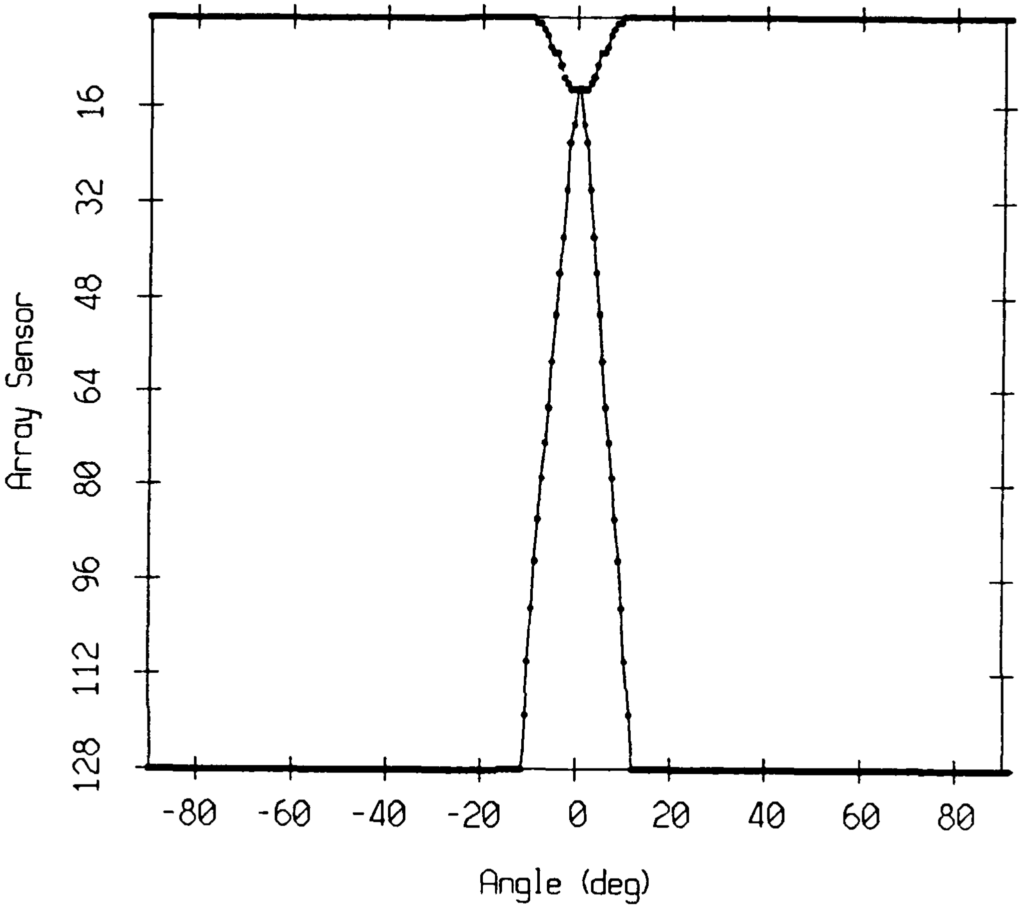

Figure 3.3: Insonification of the 128-sensor aperture by the curved wavefront arrivals betwen -90° and 90°.

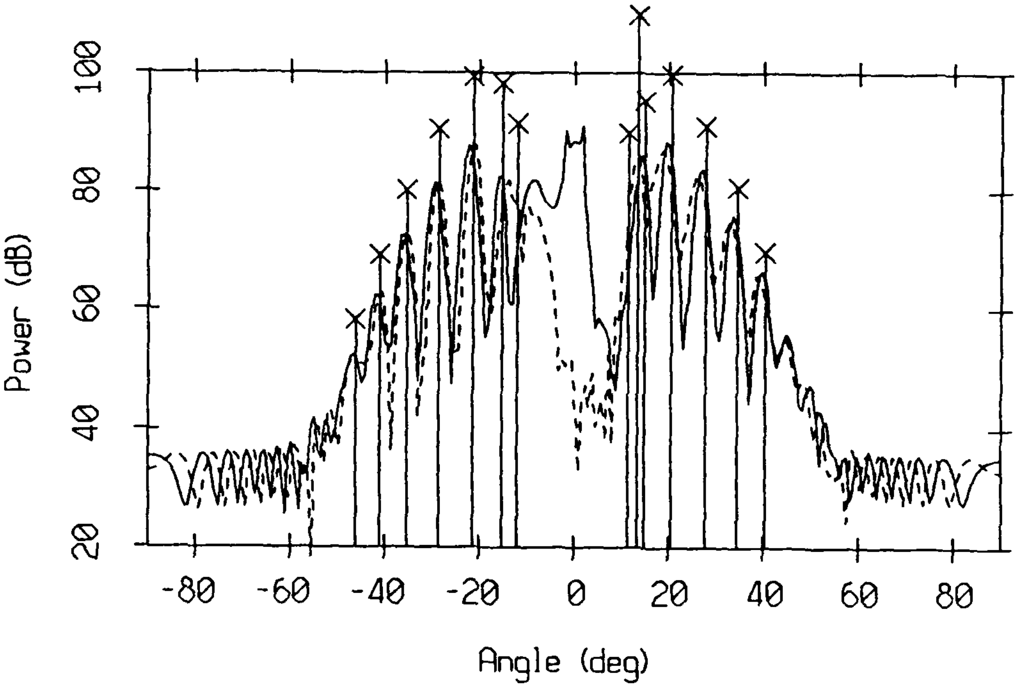

Figure 3.4: 20 Hz output of the conventional beamformer with a Kaiser-Bessel window with α parameter of 1.5 using curved wavefront replica vectors (solid line), plane wavefront replica vectors (dotted line) overlaid with the GSM eigenrays at the sound axis.

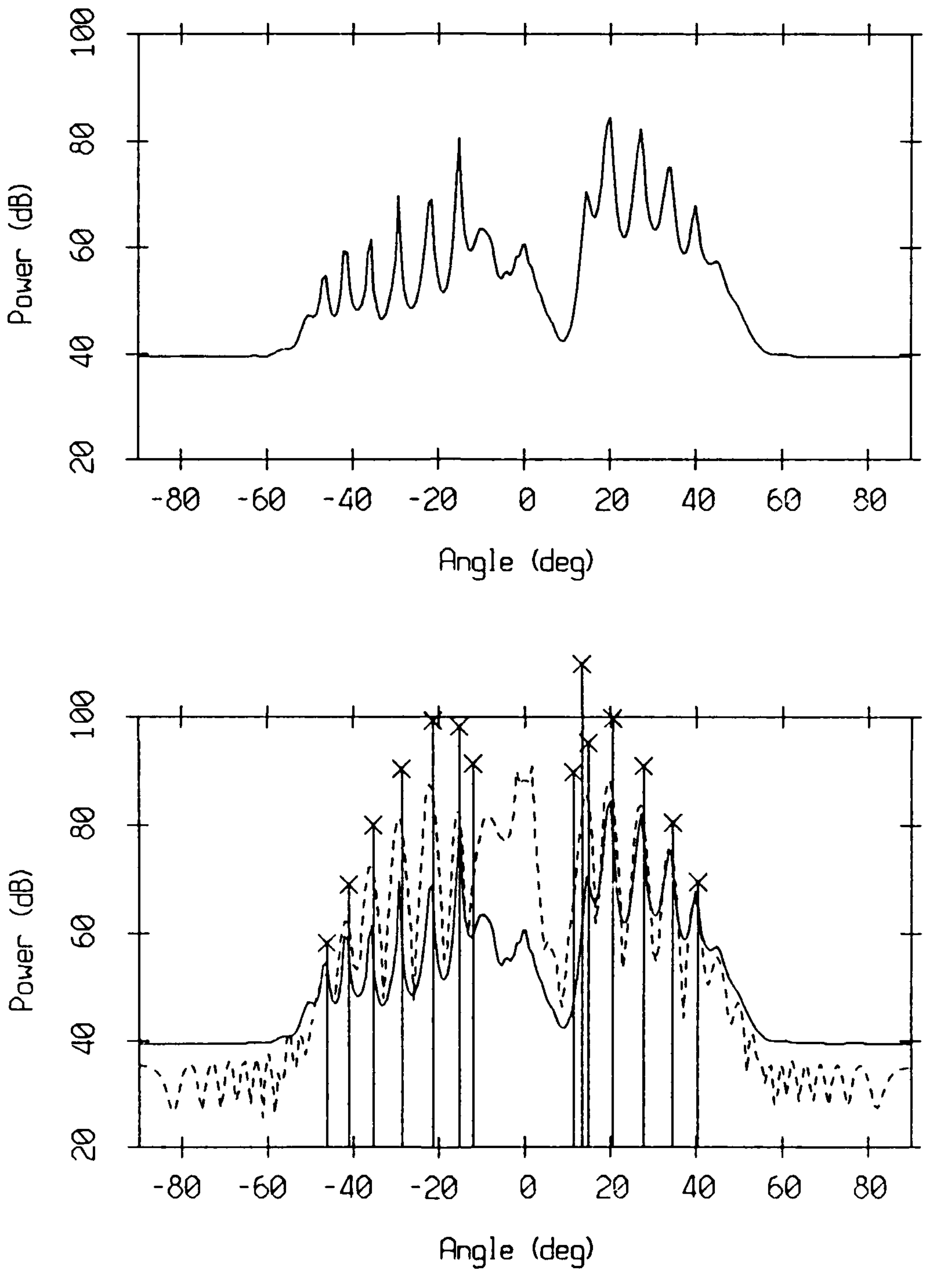

Figure 3.5: Top panel: 20 Hz output of the MVDR beamformer processing the full aperture. Bottom panel: overlaid MVDR (solid line) and conventional (dotted line) angular spectra with the GSM eigenrays.

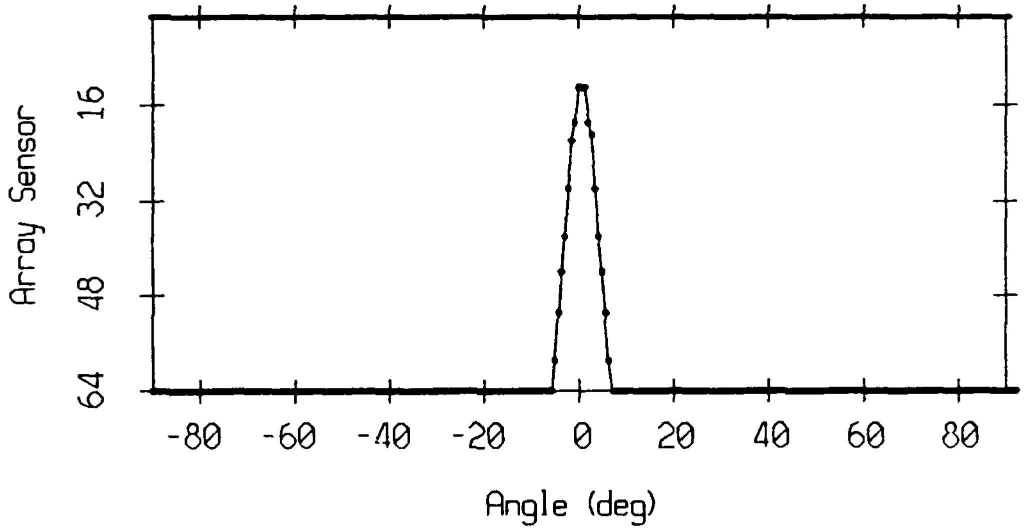

Figure 3.6: Insonification of the 64-sensor spatially smoothed equivalent aperture by the eigensteering vectors between -90° and 90°.

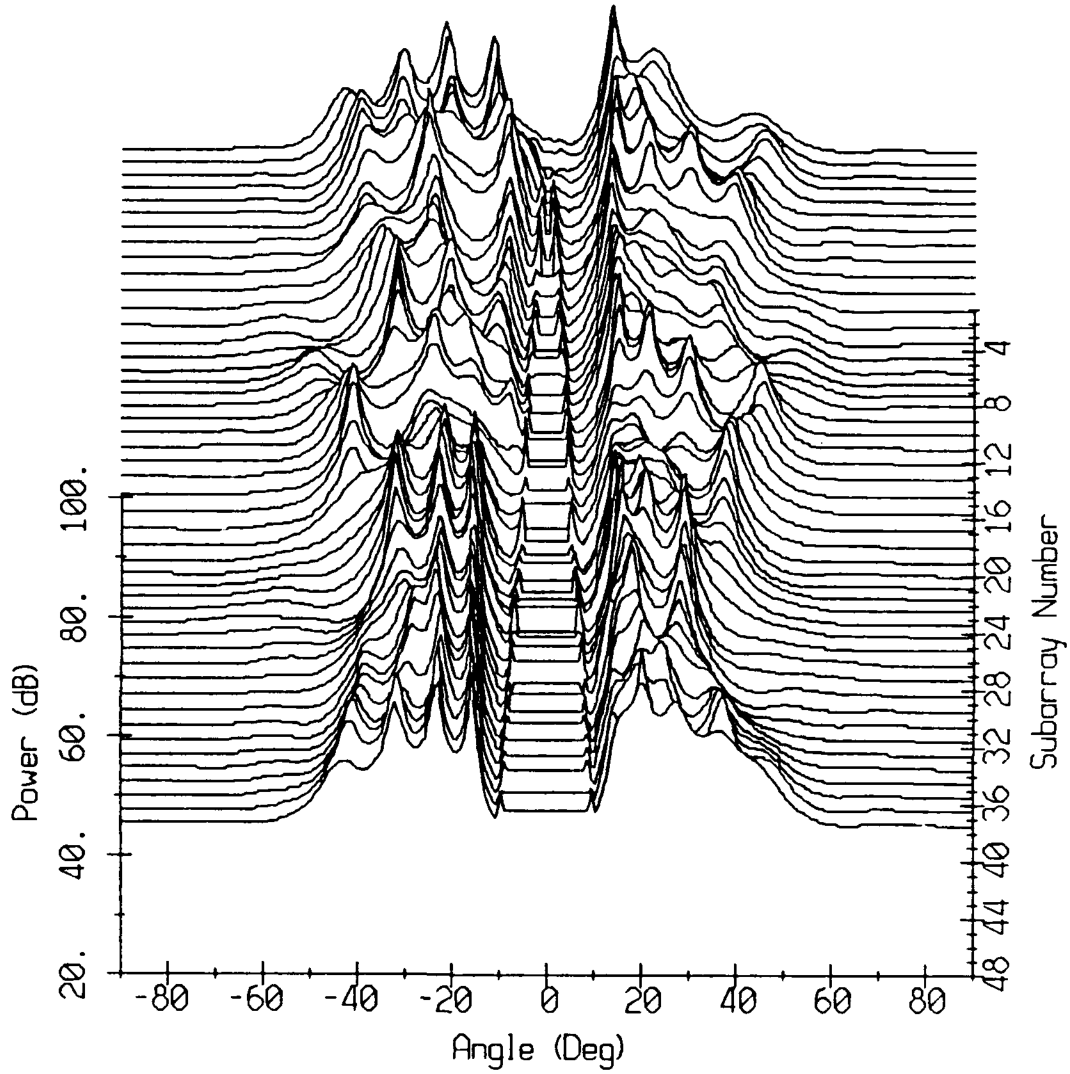

Figure 3.7: Waterfall plot of the 32 sensor subarray MVDR angular spectra at 20 Hz after spatial smoothing with subsegment length of 20 sensors and using the eigensteering vectors.

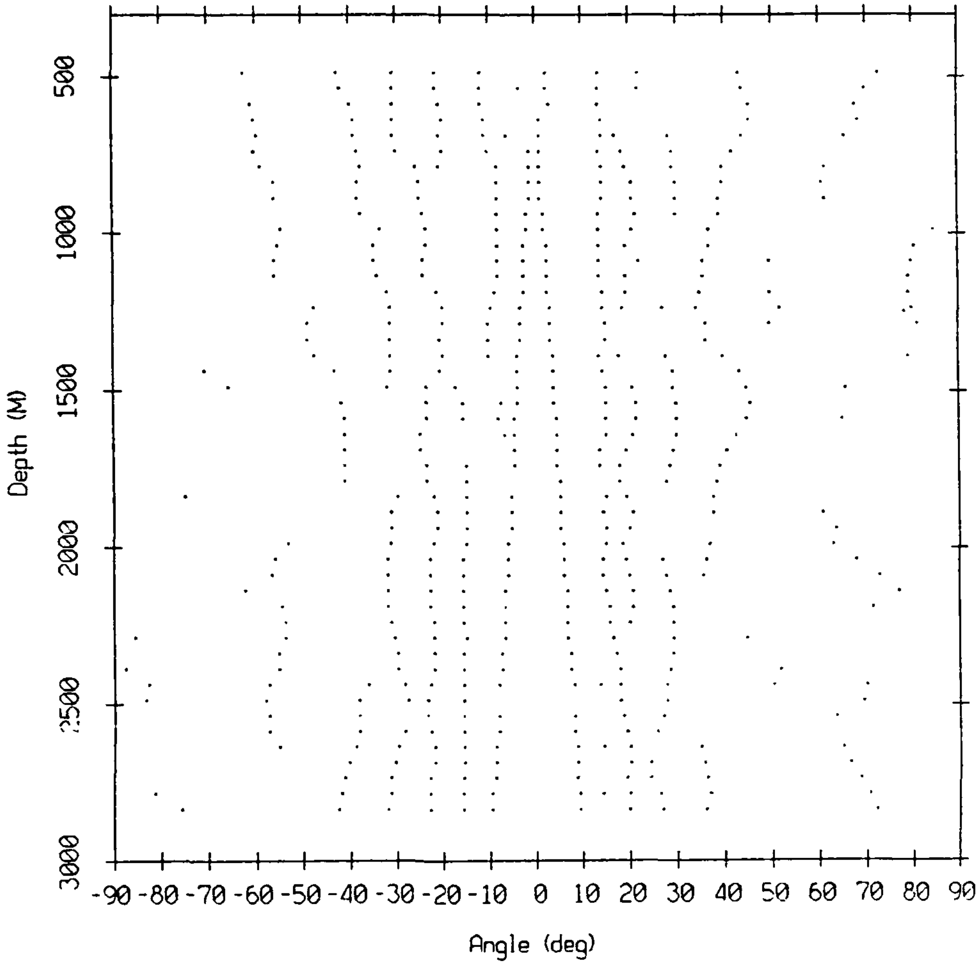

Figure 3.8: Traces with depth of the local maxima of the 32 sensor subarray MVDR angular spectra at 20 Hz.

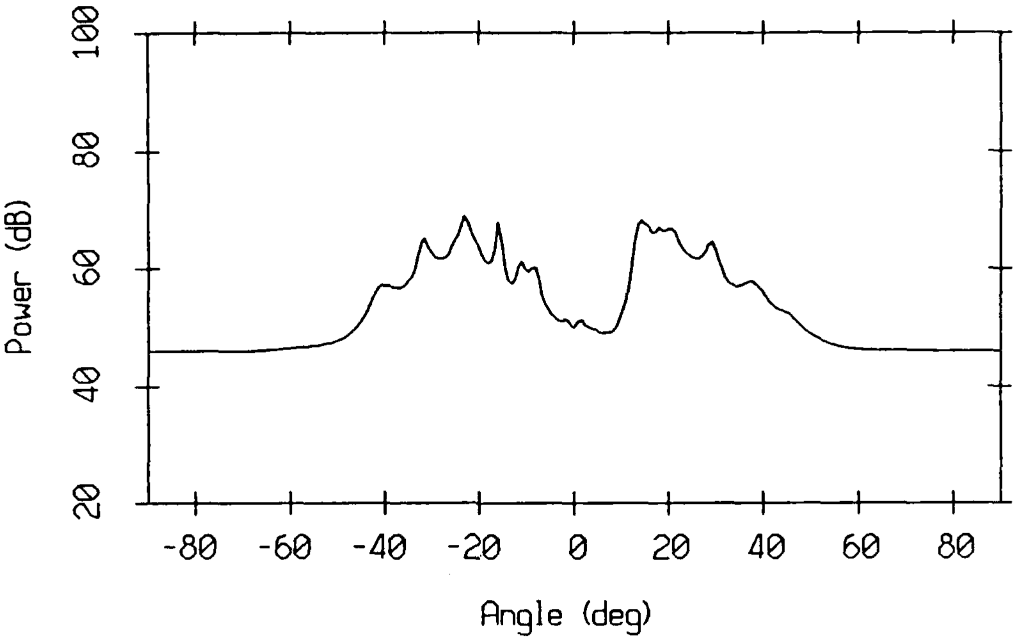

Figure 3.9: Composite MVDR angular spectrum at 20 Hz.

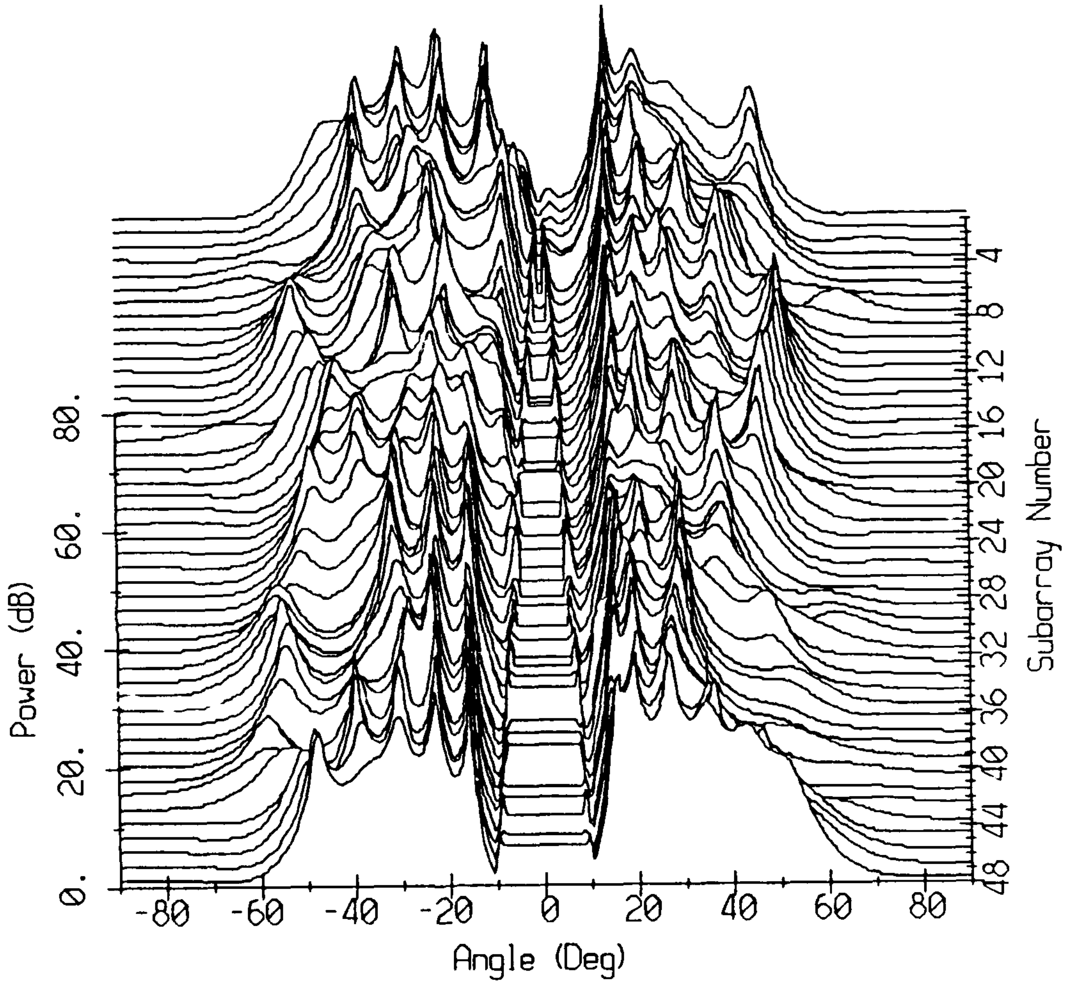

Figure 3.10: Waterfall plot of the 32 sensor subarray MUSIC "spectra" at 20 Hz after spatial smoothing with a subsegment length of 20 sensors, using the eigensteering vectors, and with a number of signals set to 12.

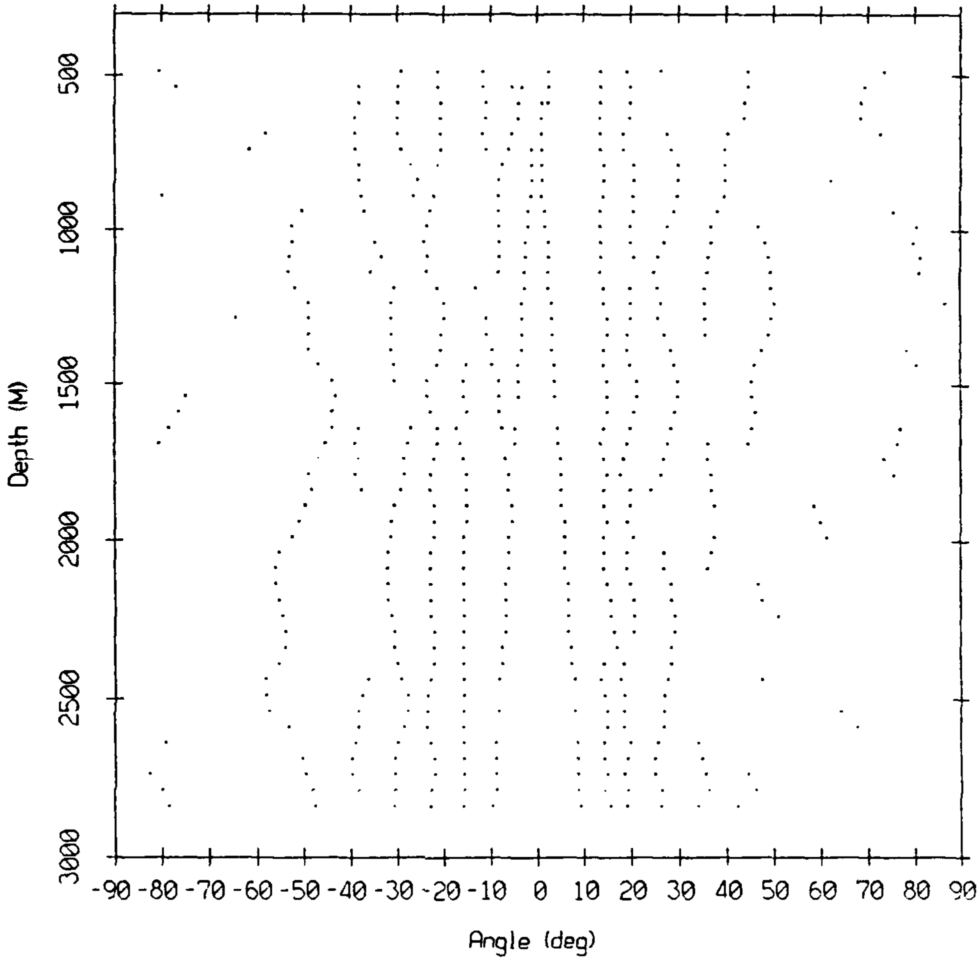

Figure 3.11: Traces with depth of the local maxima of the 32 sensor subarray MUSIC "spectra" at 20 Hz.

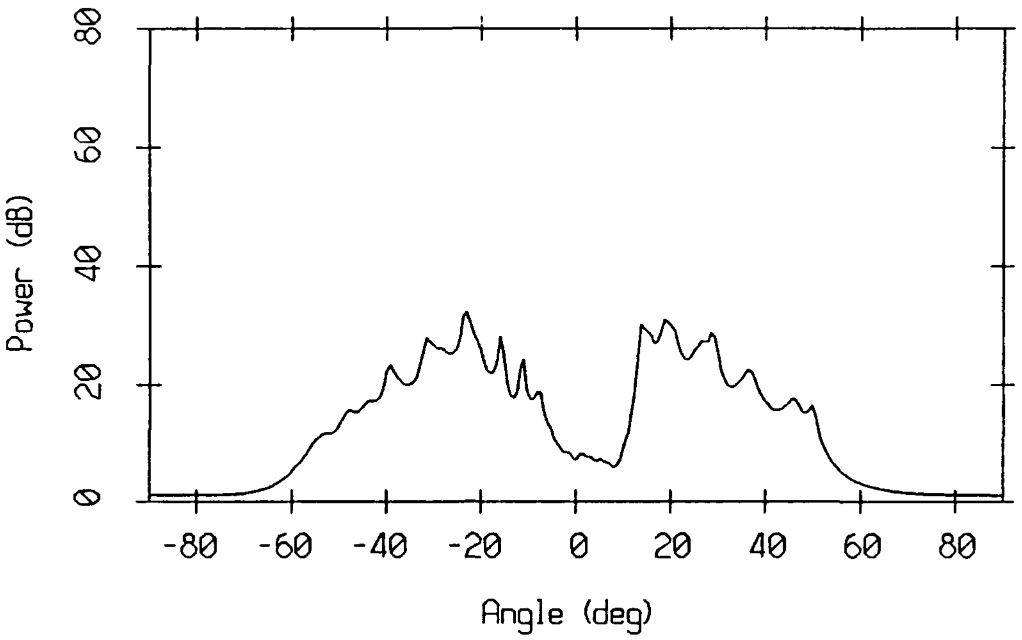

Figure 3.12: Composite MUSIC "spectrum" at 20 Hz.

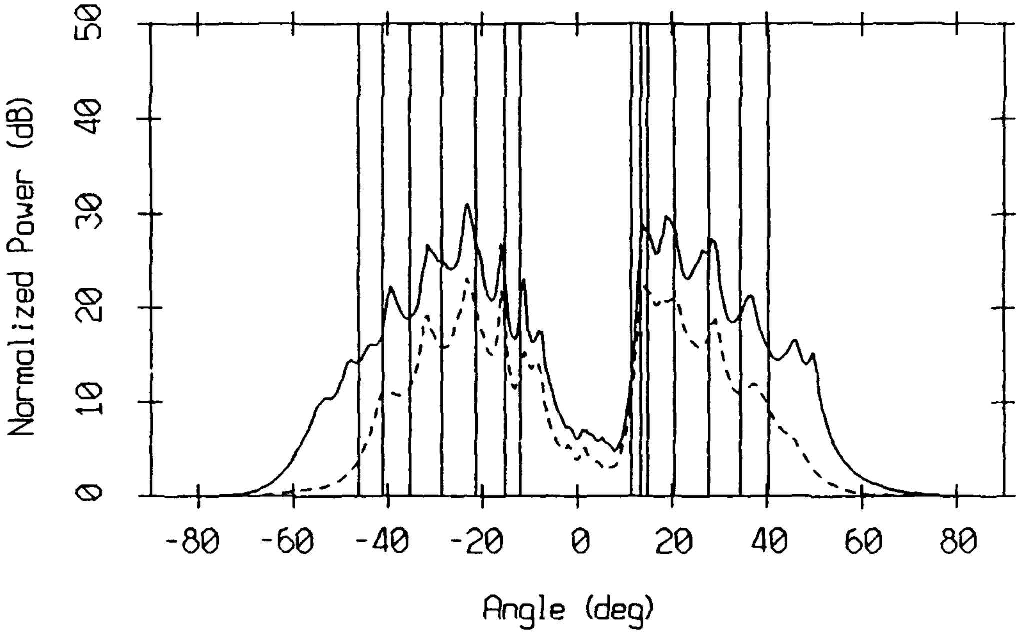

Figure 3.13: Composite MUSIC (solid line) and MVDR (dotted line) spectra overlaid with the GSM eigenray angles at the sound axis and at 20 Hz.

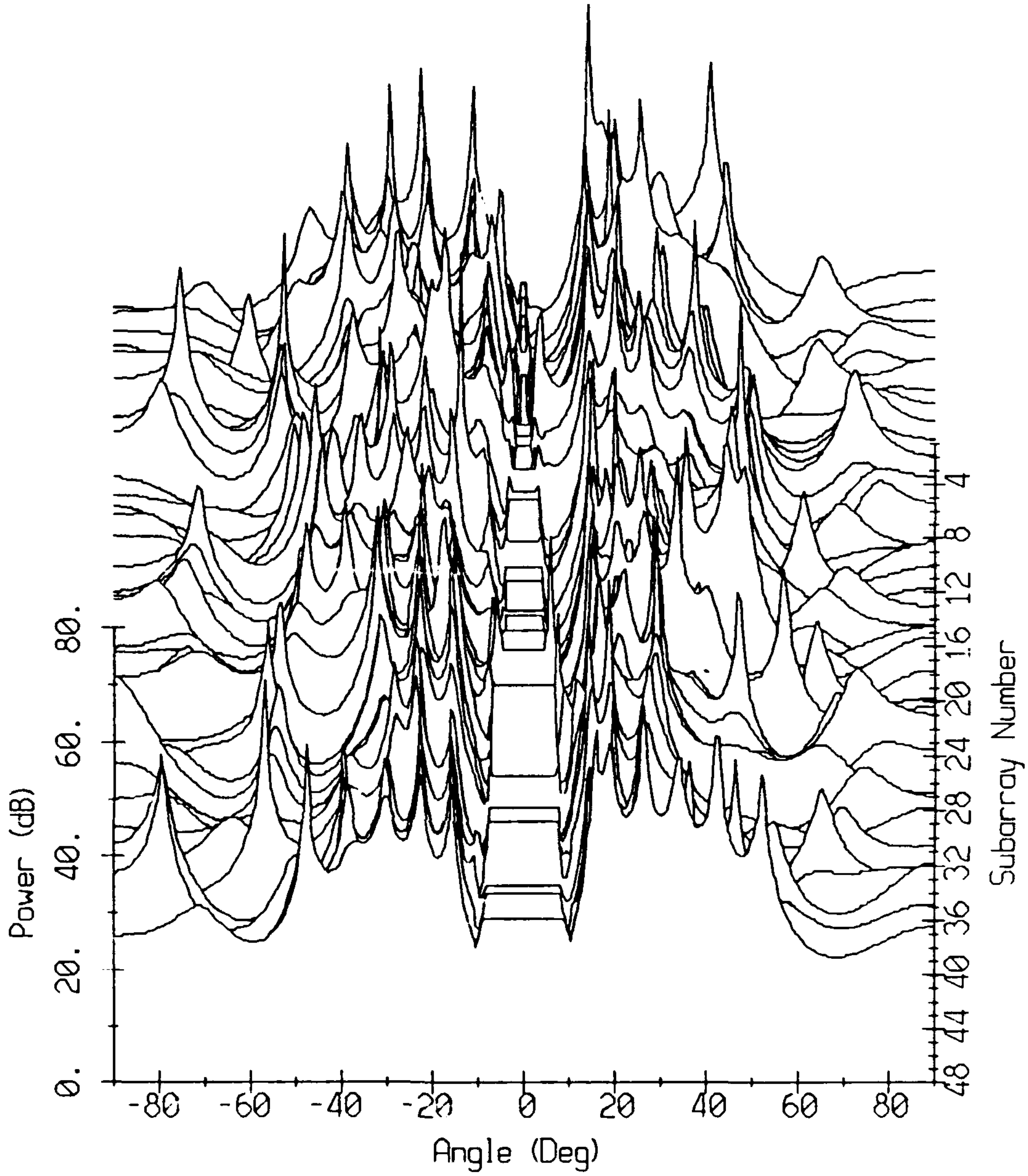

Figure 3.14: Waterfall plot of the 32 sensor subarray Minimum Norm "spectra" at 20 Hz after spatial smoothing with subsegment length of 20 sensors using the eigensteering vectors and with a number of signals set to 12.

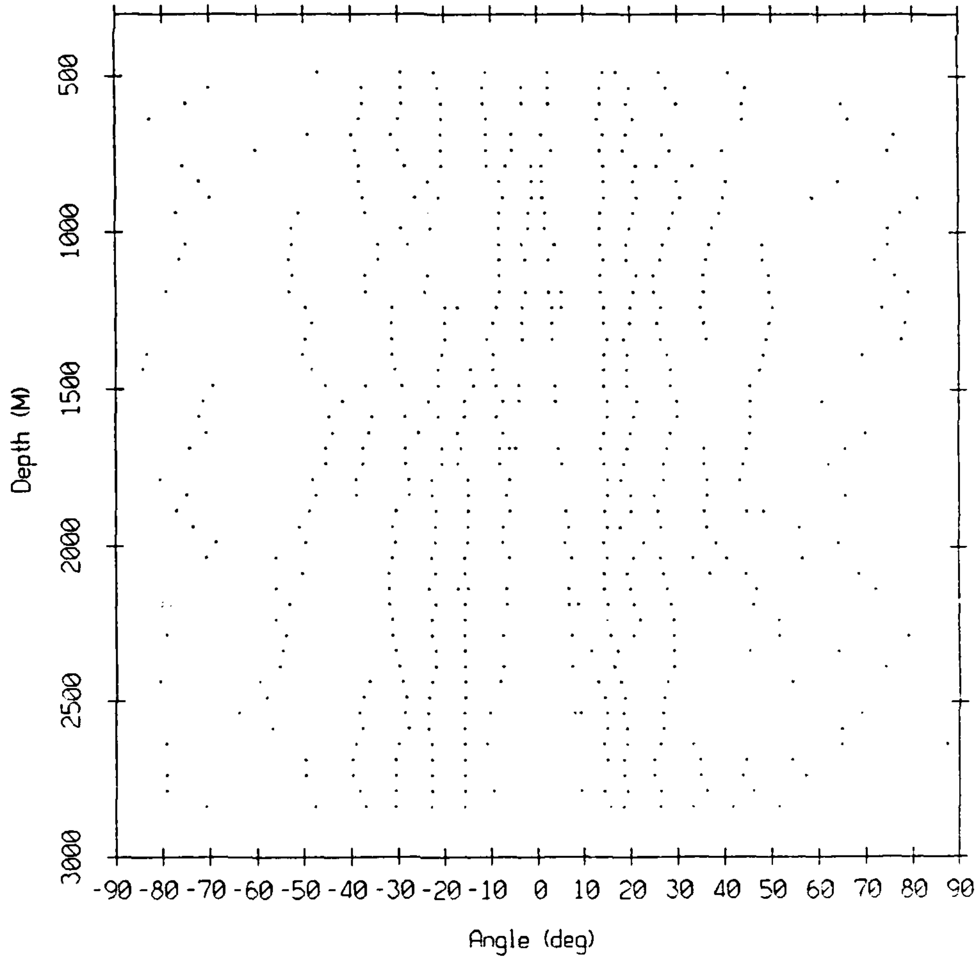

Figure 3.15: Traces with depth of the local maxima of the 32 sensor subarray Minimum Norm "spectra" at 20 Hz.

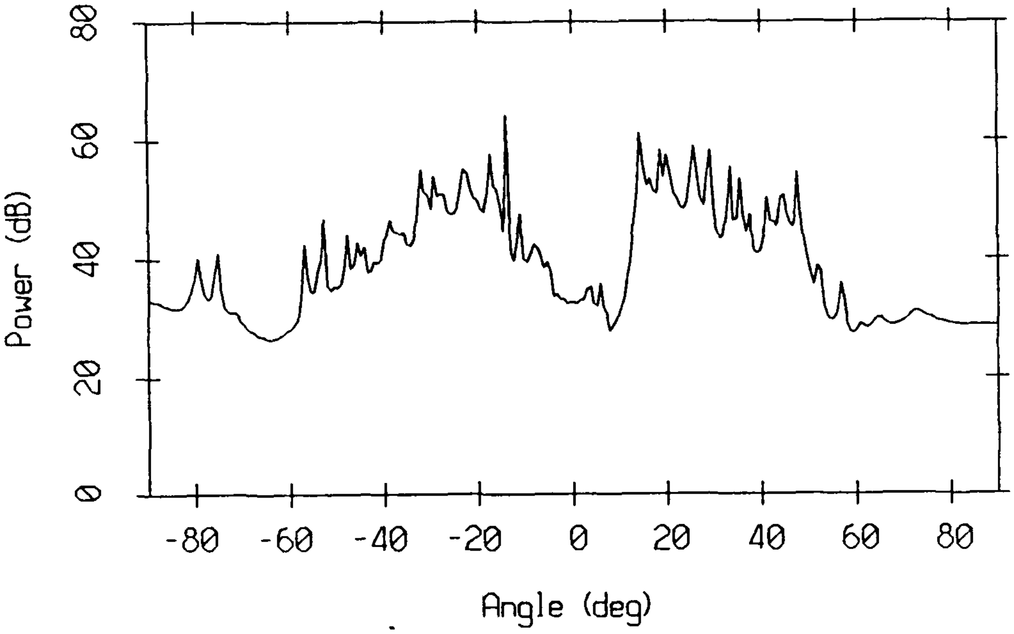

Figure 3.16: Composite Minimum Norm "spectrum" at 20 Hz.

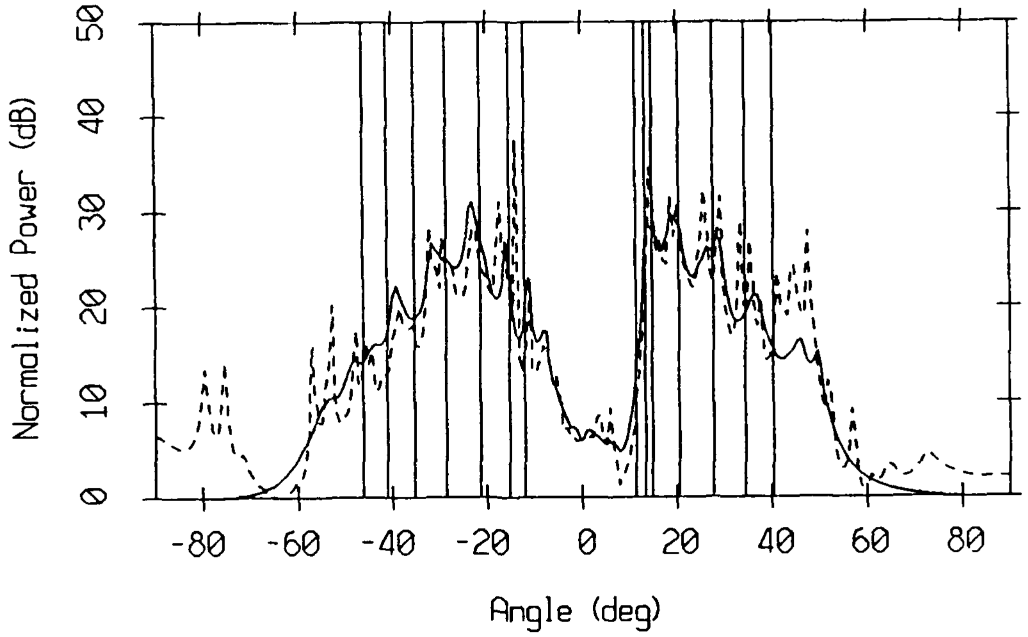

Figure 3.17: Composite subarray MUSIC (solid line) and Minimum Norm (dotted line) "spectra" overlaid with the GSM eigenray angles at the sound axis and at 20 Hz.

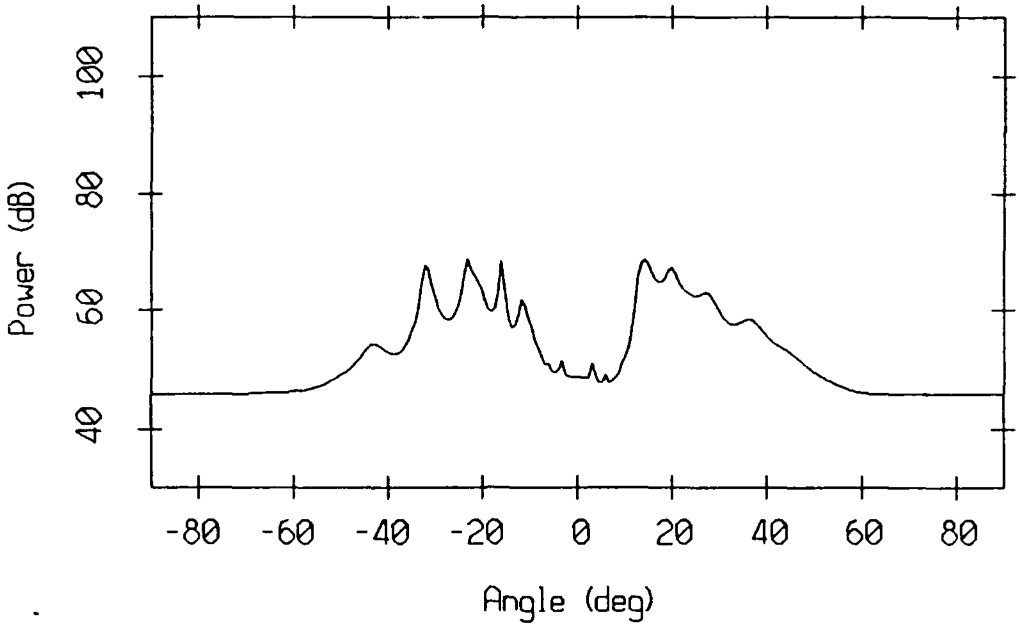

Figure 3.18: MVDR angular spectrum (average on 4 non-overlapping 32 sensor subarray spectra at 20 Hz). Spatial smoothing is performed with a subsegment length of 20 sensors.

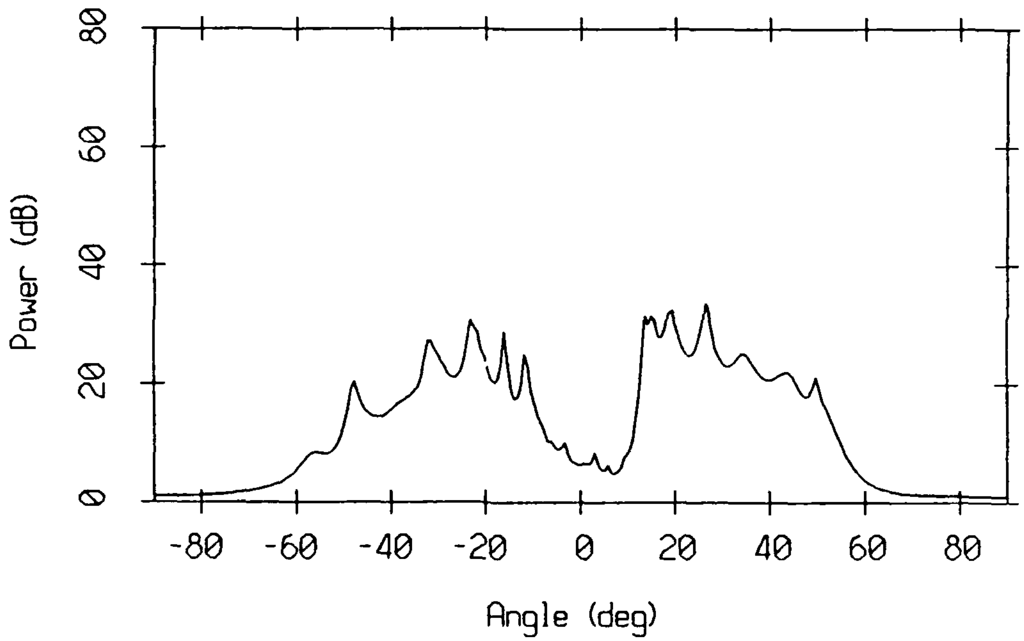

Figure 3.19: MUSIC "spectrum" (average on 4 non-overlapping 32 sensor subarray spectra at 20 Hz). Spatial smoothing is performed with subsegment length of 20 sensors. The number of signals is set to 12.

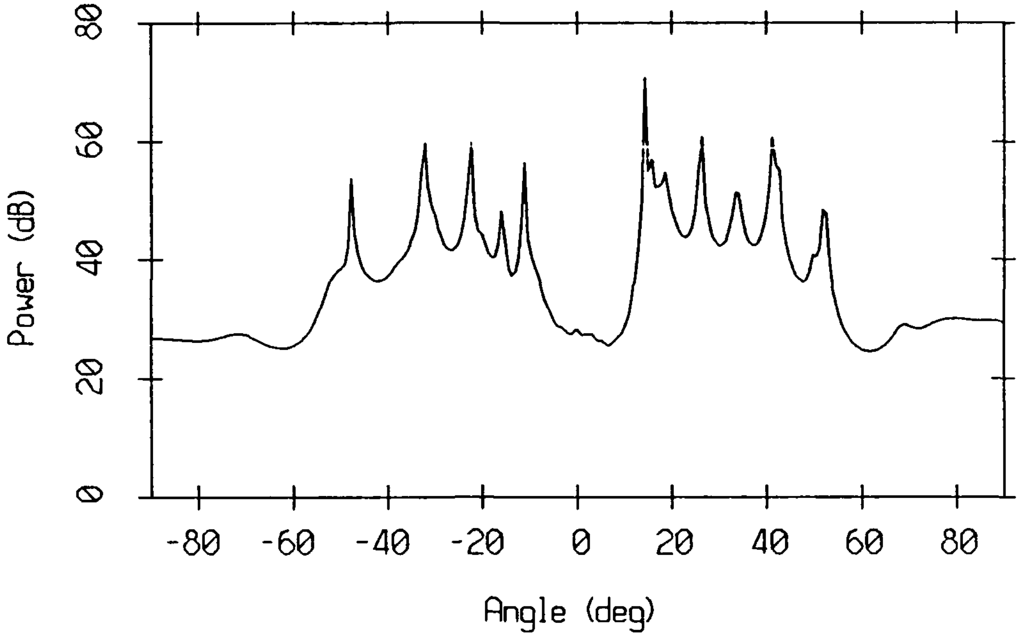

Figure 3.20: Minimum Norm "spectrum" (average on 4 non-overlapping 32 sensor subarray spectra at 20 Hz). Spatial smoothing is performed with subsegment length of 20 sensors. The number of signals is set to 12.

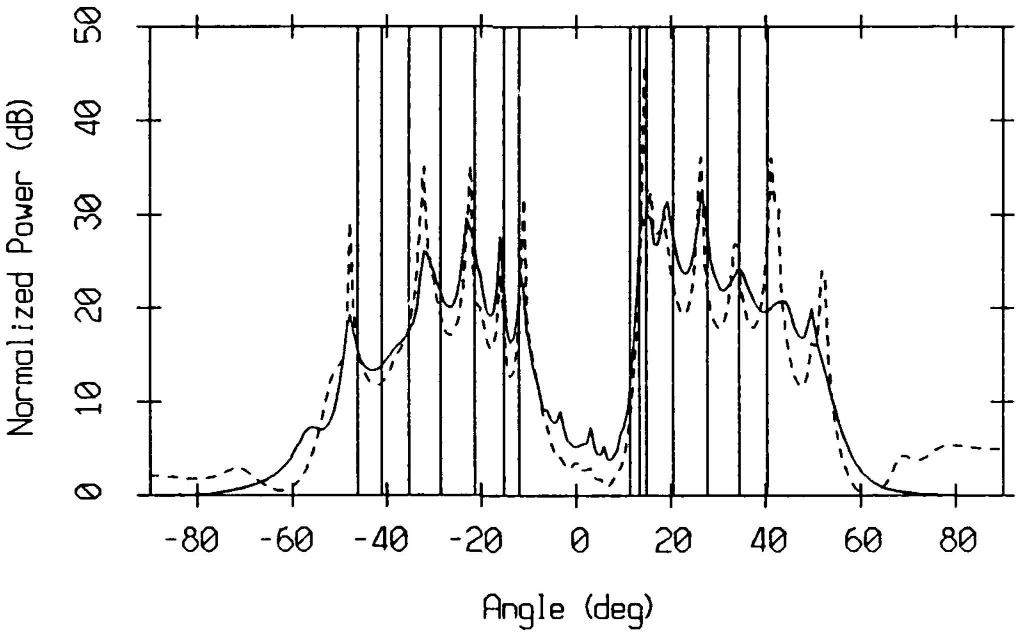

Figure 3.21: MUSIC (solid line) and Minimum Norm (dotted line) subaperture "spectra" (averaged on 4 non-overlapping 32 sensor subarrays) overlaid with the GSM eigenray angles at the sound axis and at 20 Hz.

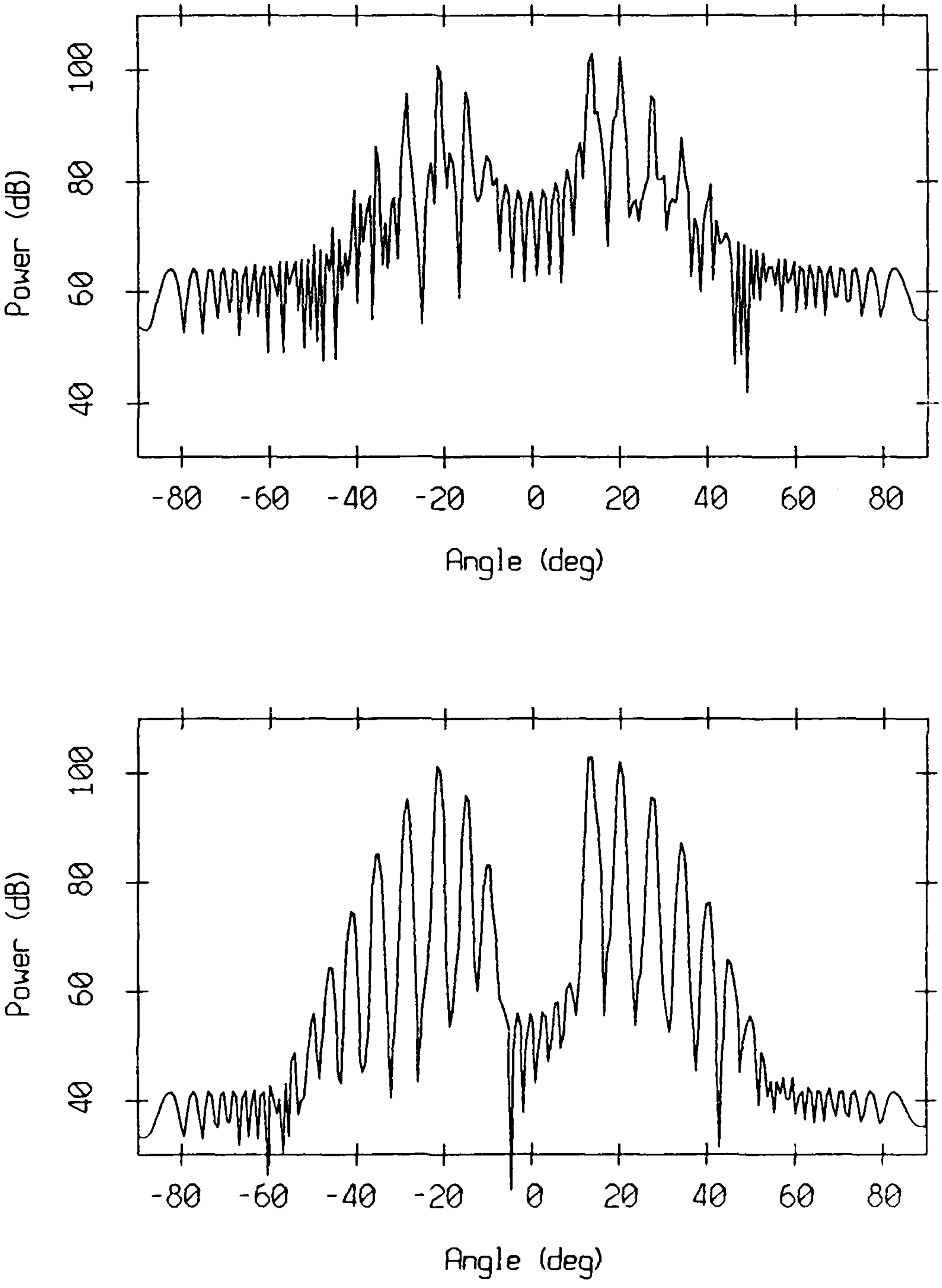

Figure 3.22: 100 Hz output of the conventional beamformer using plane wavefront replica vectors. Data are weighted by the rectangular window in the top panel and by the Kaiser-Bessel ($\alpha = 1.5$) window in the bottom panel.

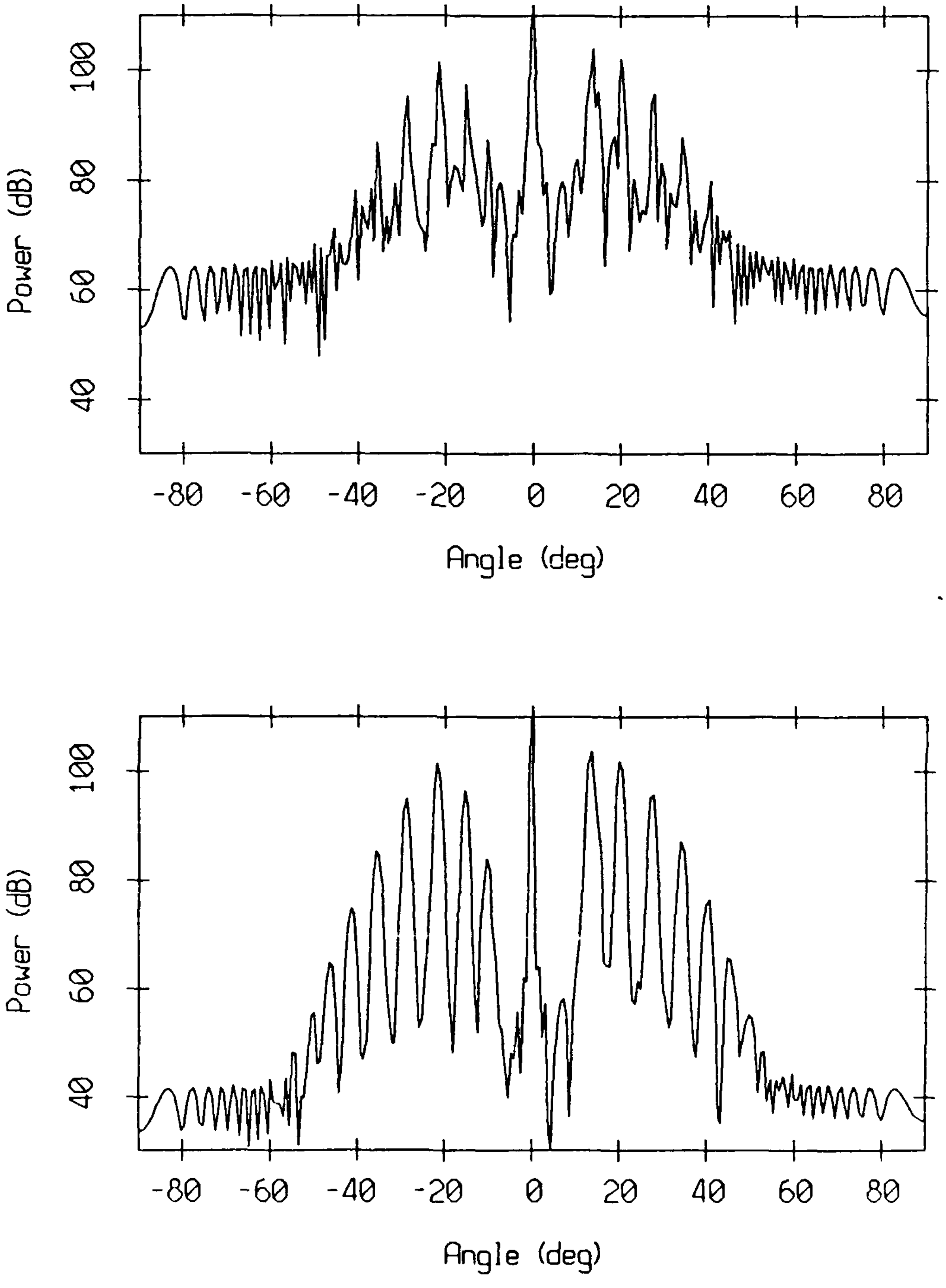

Figure 3.23: 100 Hz output of the conventional beamformer using curved wavefront replica vectors. Data are weighted by the rectangular window in the top panel and by the Kaiser-Bessel window $\alpha = 1.5$ in the bottom panel.

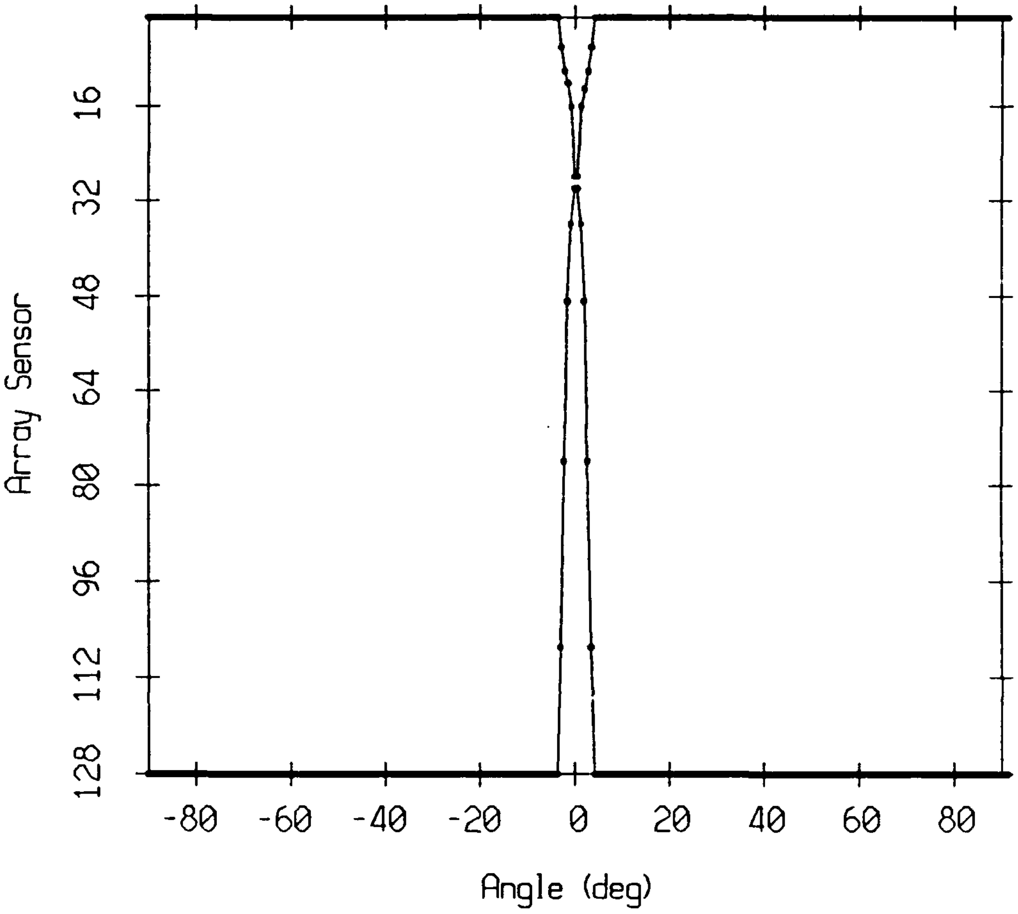

Figure 3.24: Insonification of the 128-sensor aperture by the curved wavefront arrivals between -90° and 90°.

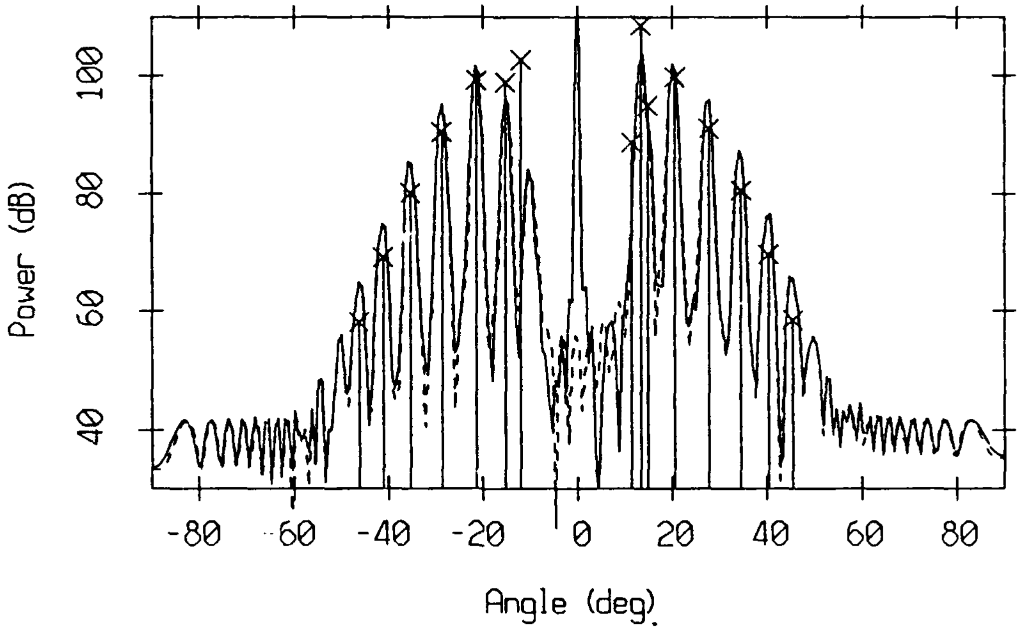

Figure 3.25: Angular spectra at 100 Hz produced by the conventional beamformer with a Kaiser-Bessel window with α parameter of 1.5 using curved wavefront replica vectors (solid line), plane wavefront replica vectors (dotted line) overlaid with the GSM eigenrays at the sound axis.

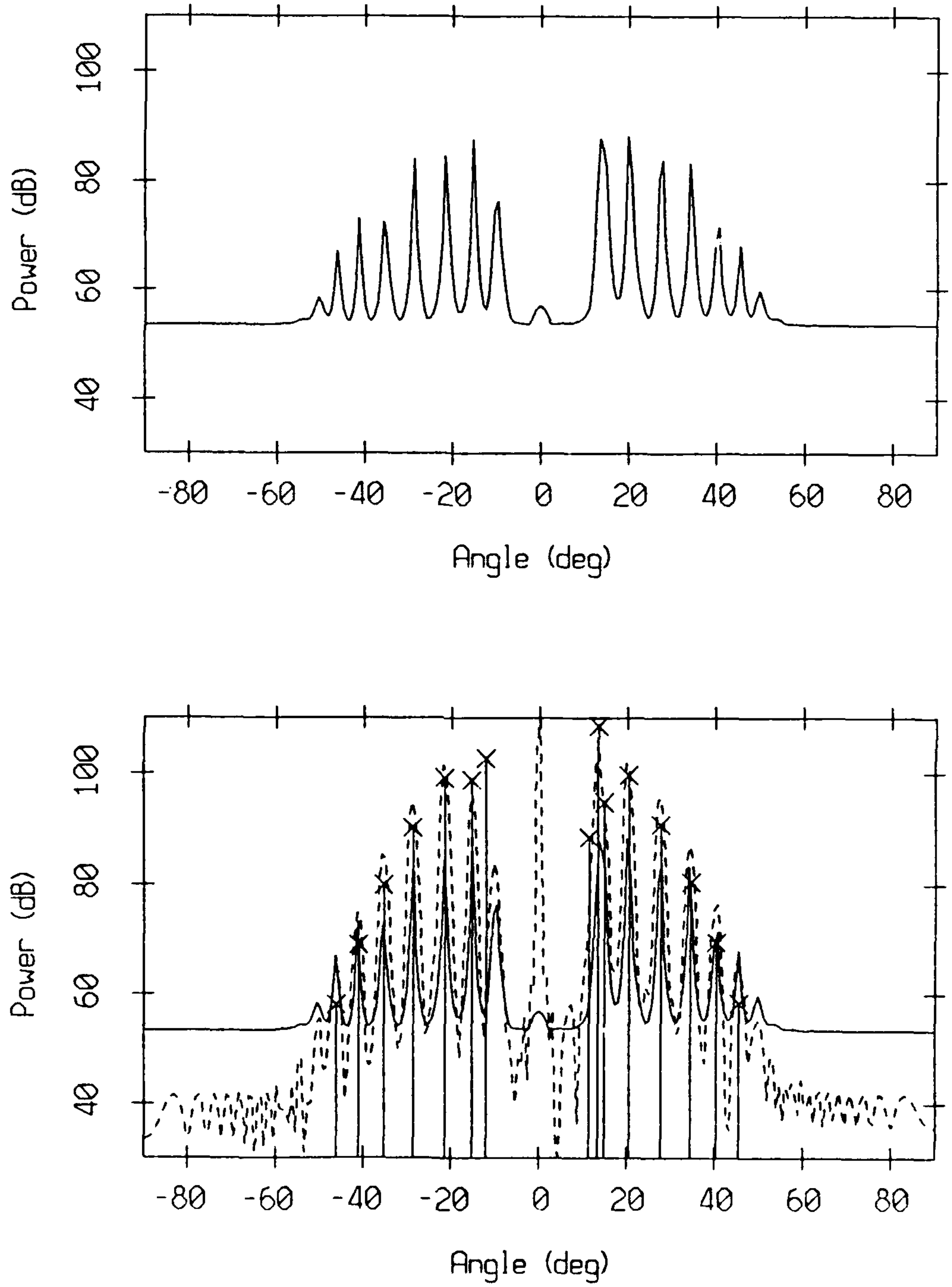

Figure 3.26: Top panel: 100 Hz output of the full aperture MVDR beamformer. Bottom panel: overlaid MVDR (solid line) and conventional (dotted line) spectra and GSM eigenrays at the sound axis.

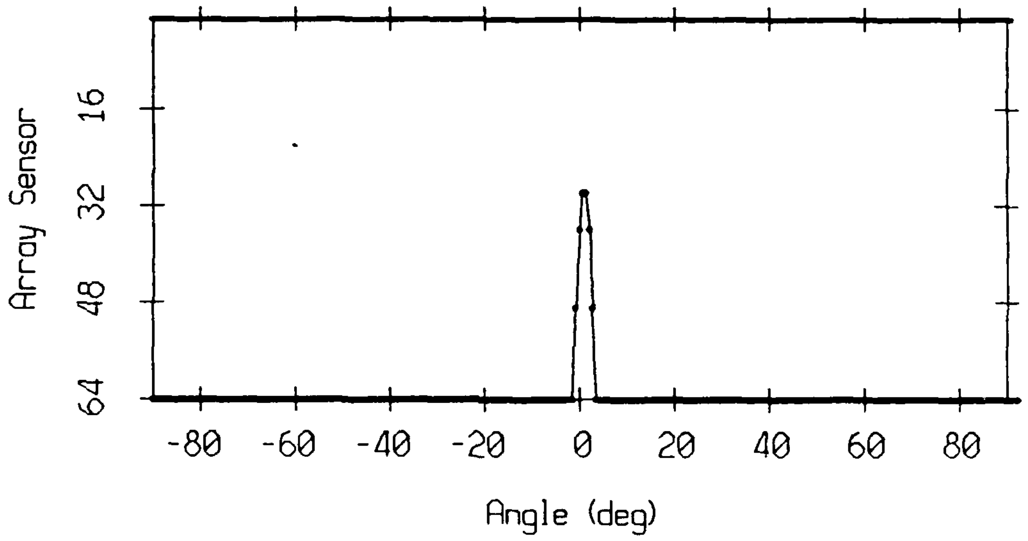

Figure 3.27: Insonification of the 64-sensor spatially smoothed equivalent aperture by the eigensteering replica vectors between -90° and 90°.

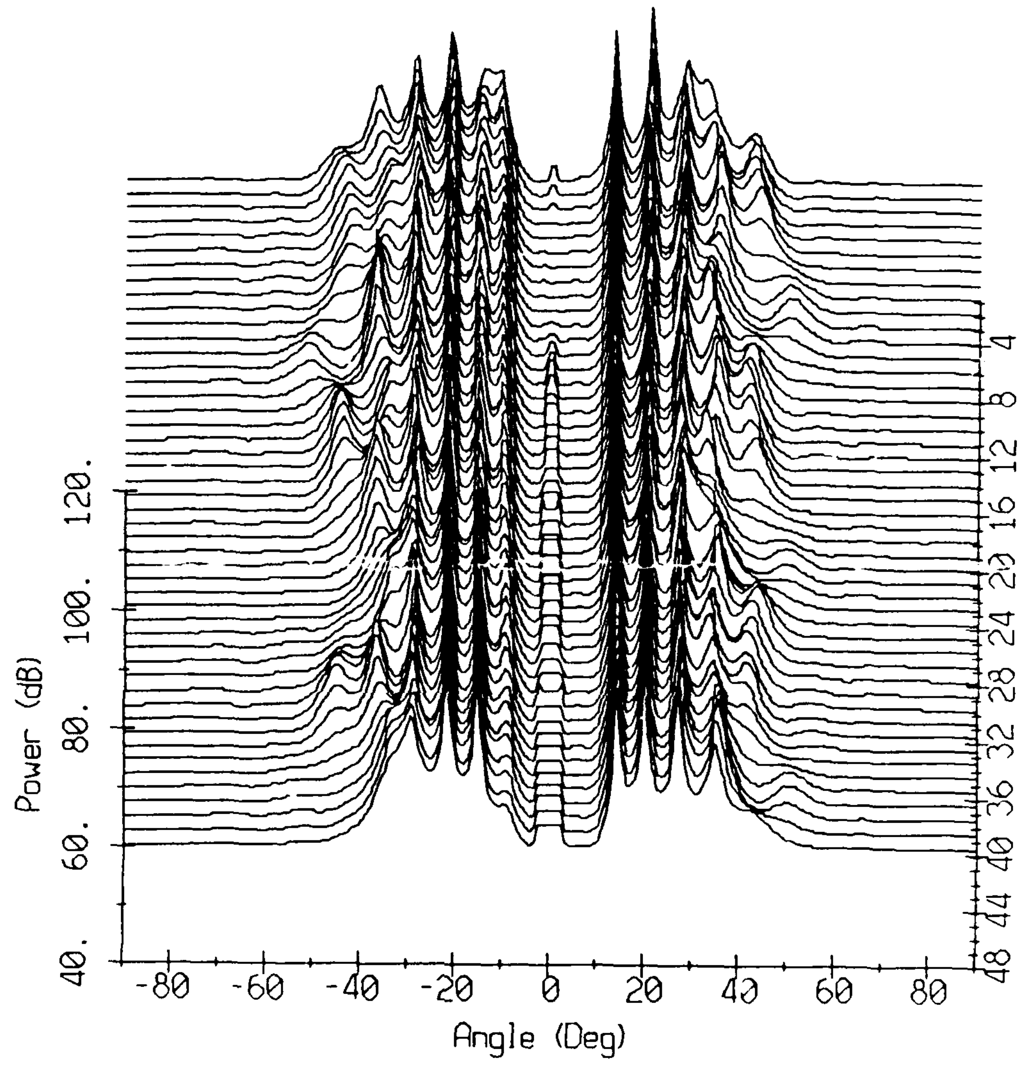

Figure 3.28: Waterfall plot of the 32 sensor subarray MVDR angular spectra at 100 Hz after spatial smoothing with subsegment length of 20 sensors and using the eigensteering vectors.

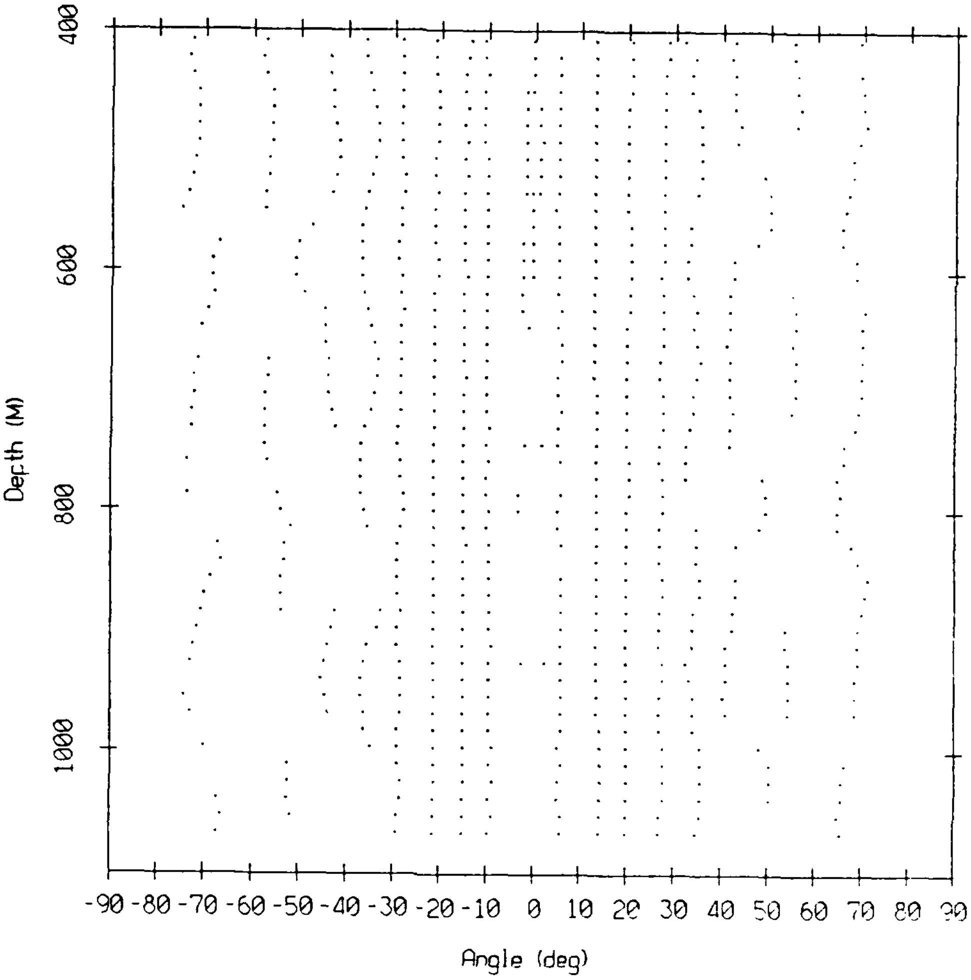

Figure 3.29: Traces with depth of the local maxima of the 32 sensor subarray MVDR angular spectra at 100 Hz.

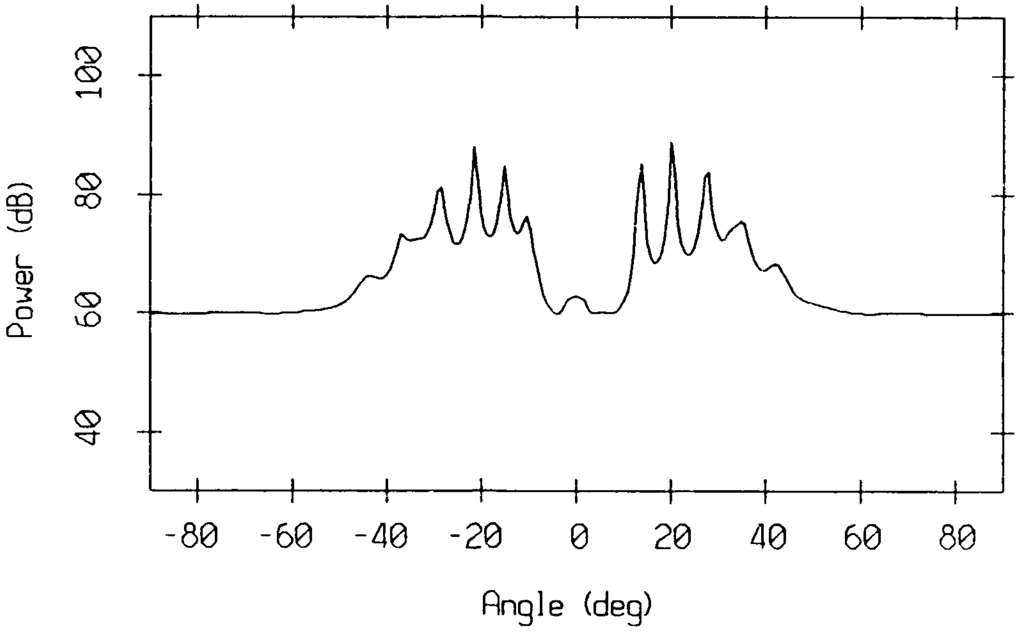

Figure 3.30: Composite MVDR angular spectrum at 100 Hz.

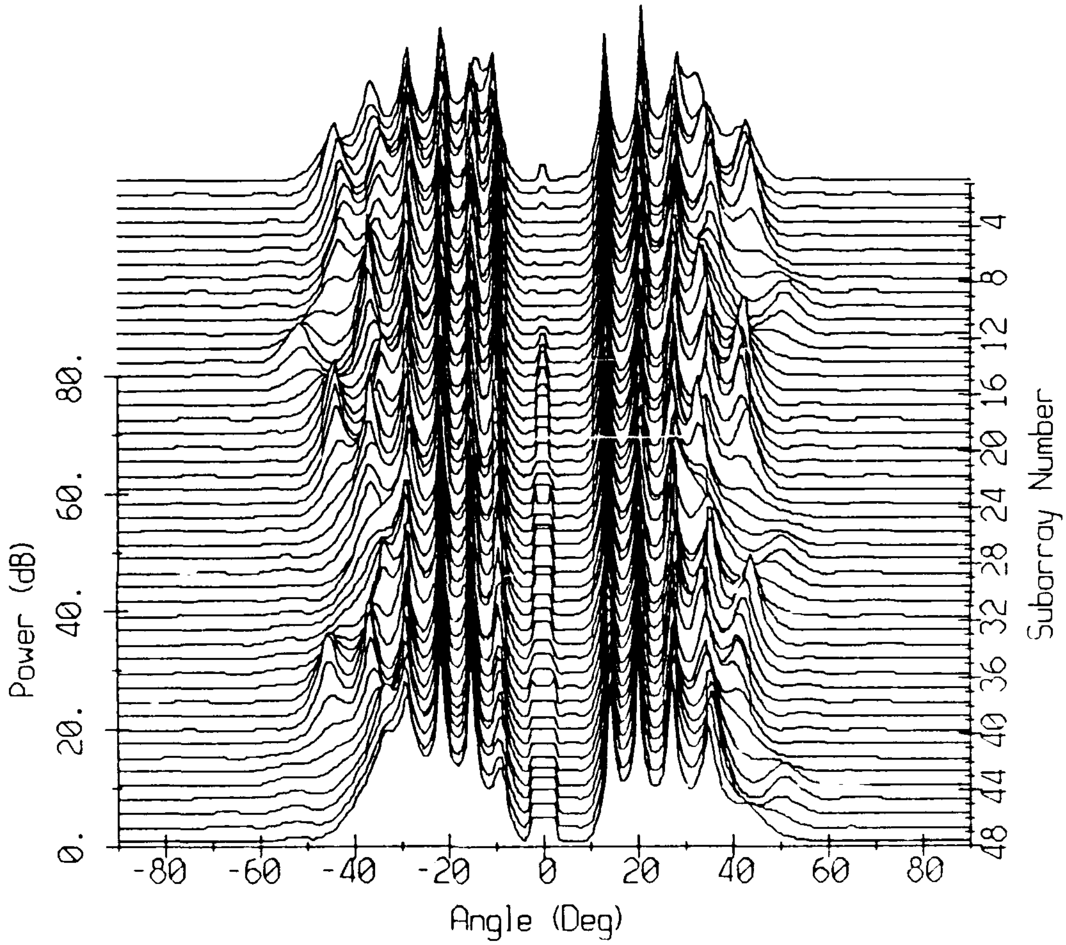

Figure 3.31: Waterfall plot of the 32 sensor subarray MUSIC "spectra" at 100 Hz after spatial smoothing with a subsegment length of 20 sensors, using the eigensteering vectors, and with a number of signals set to 12.

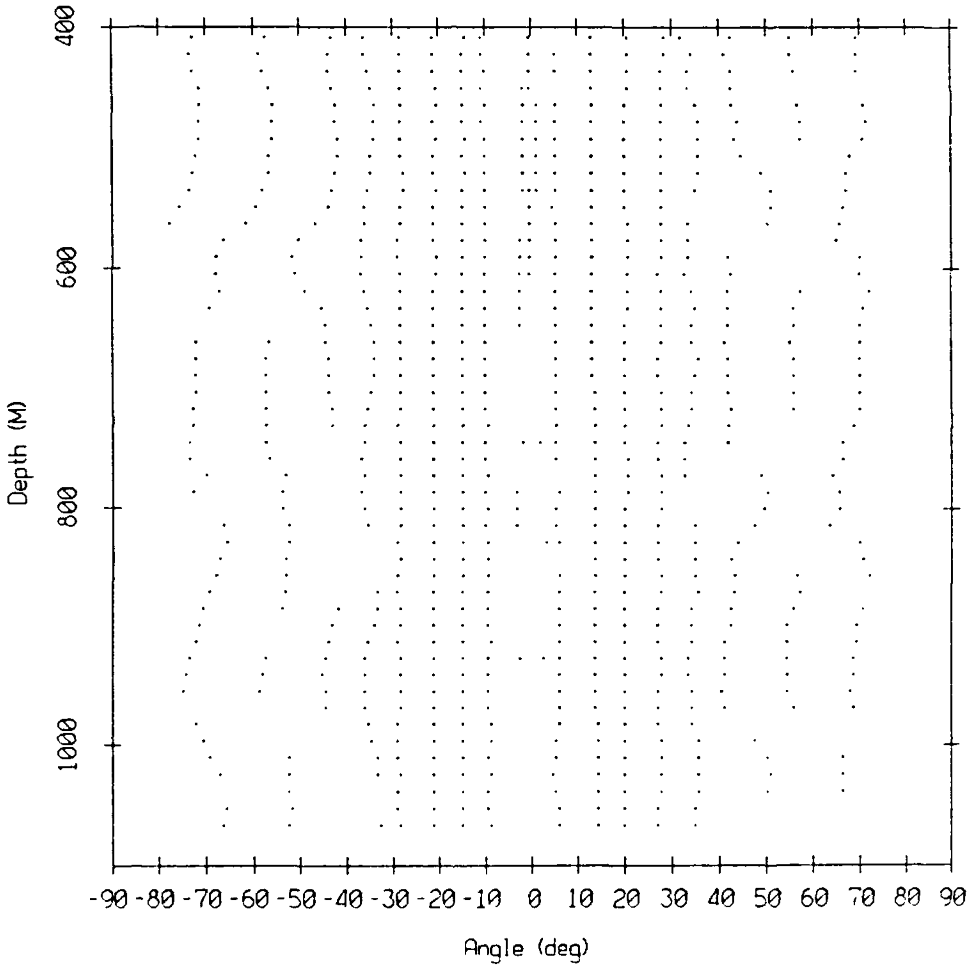

Figure 3.32: Traces with depth of the local maxima of the 32 sensor subarray MUSIC "spectra" at 100 Hz.

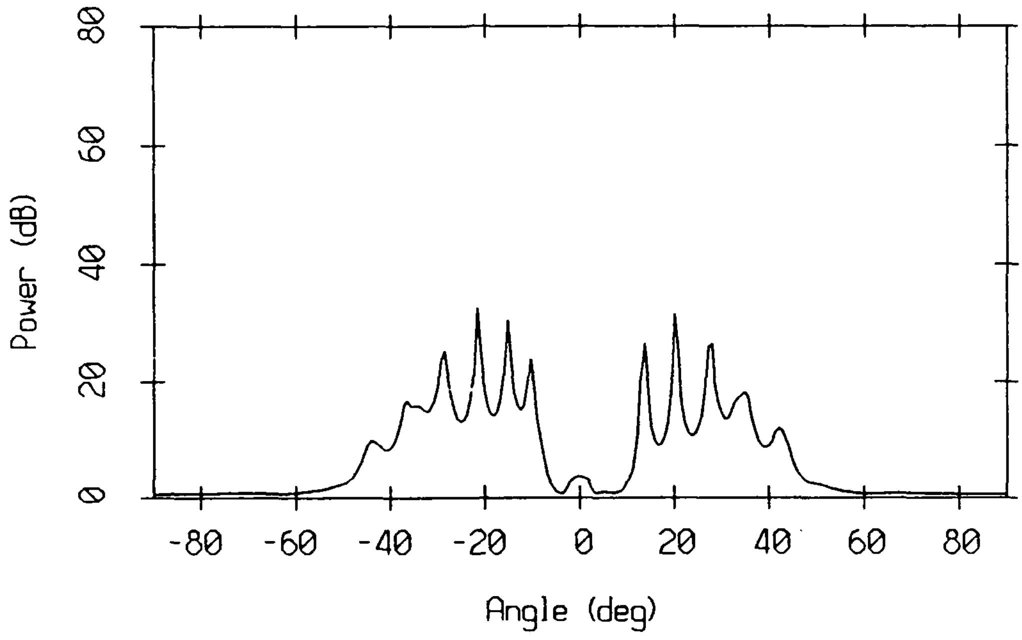

Figure 3.33: Composite subarray MUSIC "spectrum" at 100 Hz.

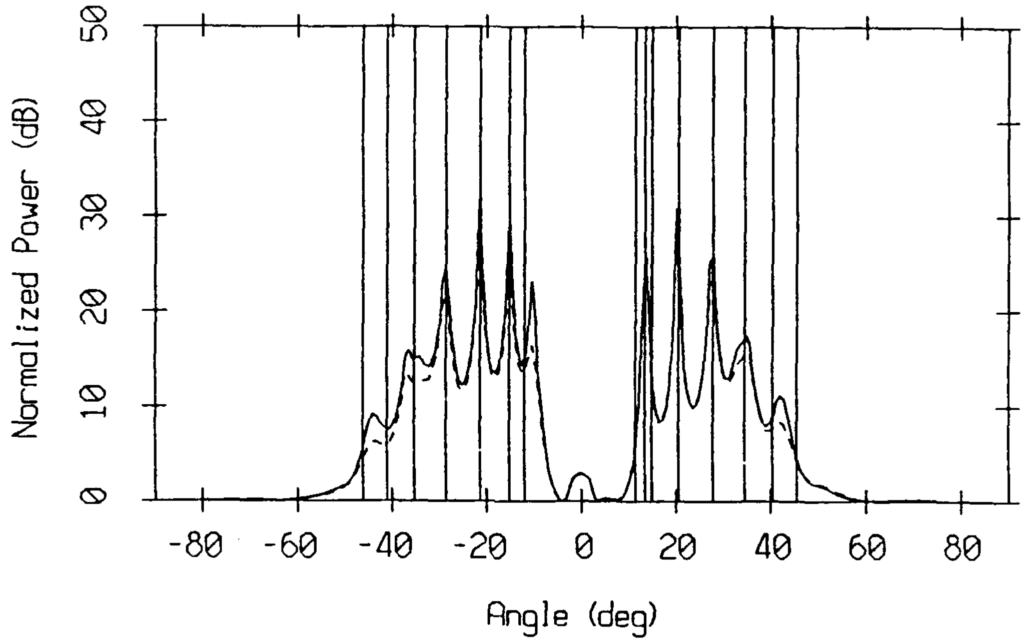

Figure 3.34: Composite MUSIC (solid line) and MVDR (dotted line) spectra overlaid with the GSM eigenray angles at the sound axis and at 100 Hz.

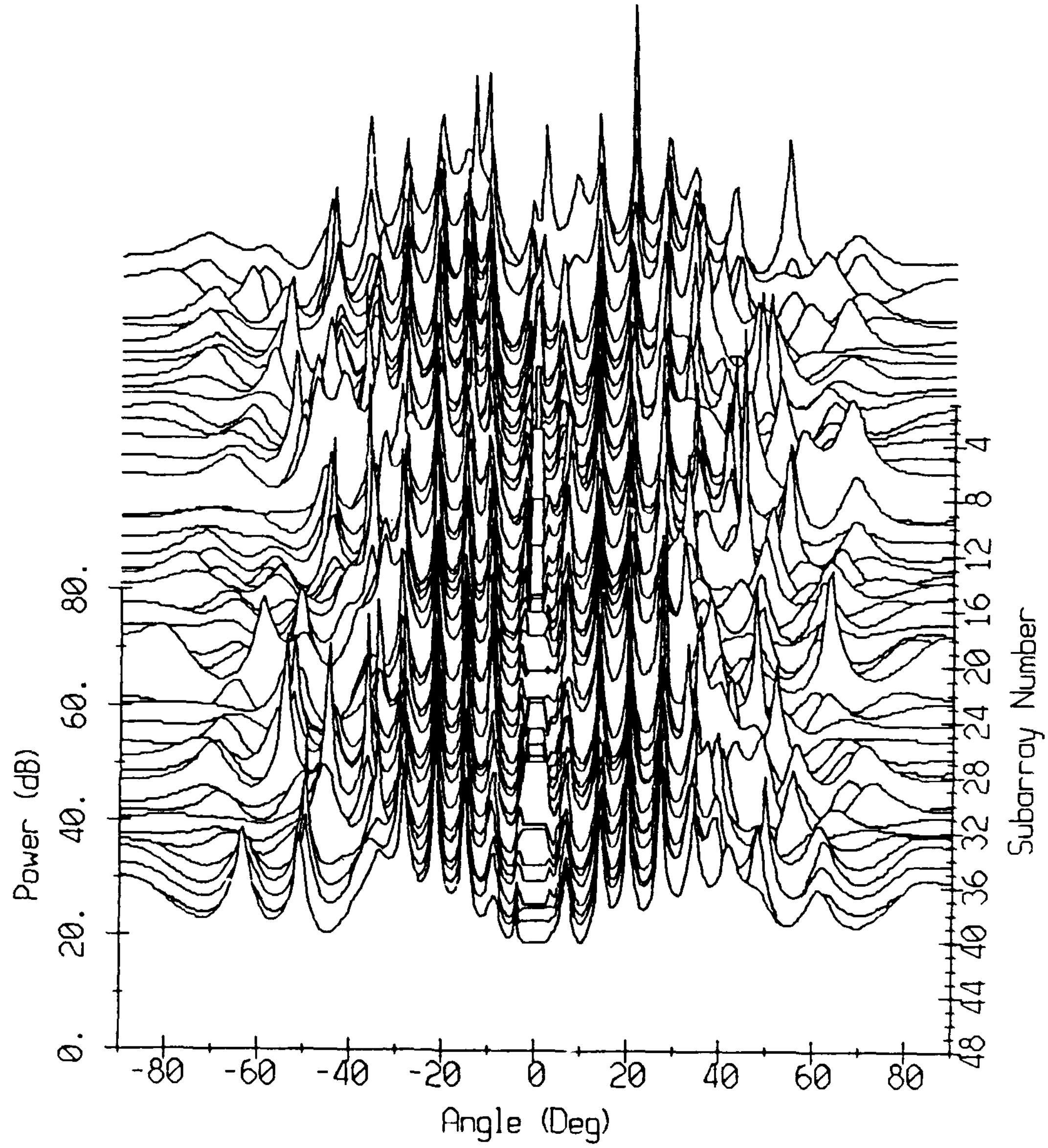

Figure 3.35: Waterfall plot of the 32 sensor subarray Minimum Norm "spectra" at 100 Hz after spatial smoothing with subsegment length of 20 sensors using the eigensteering vectors and with a number of signals set to 12.

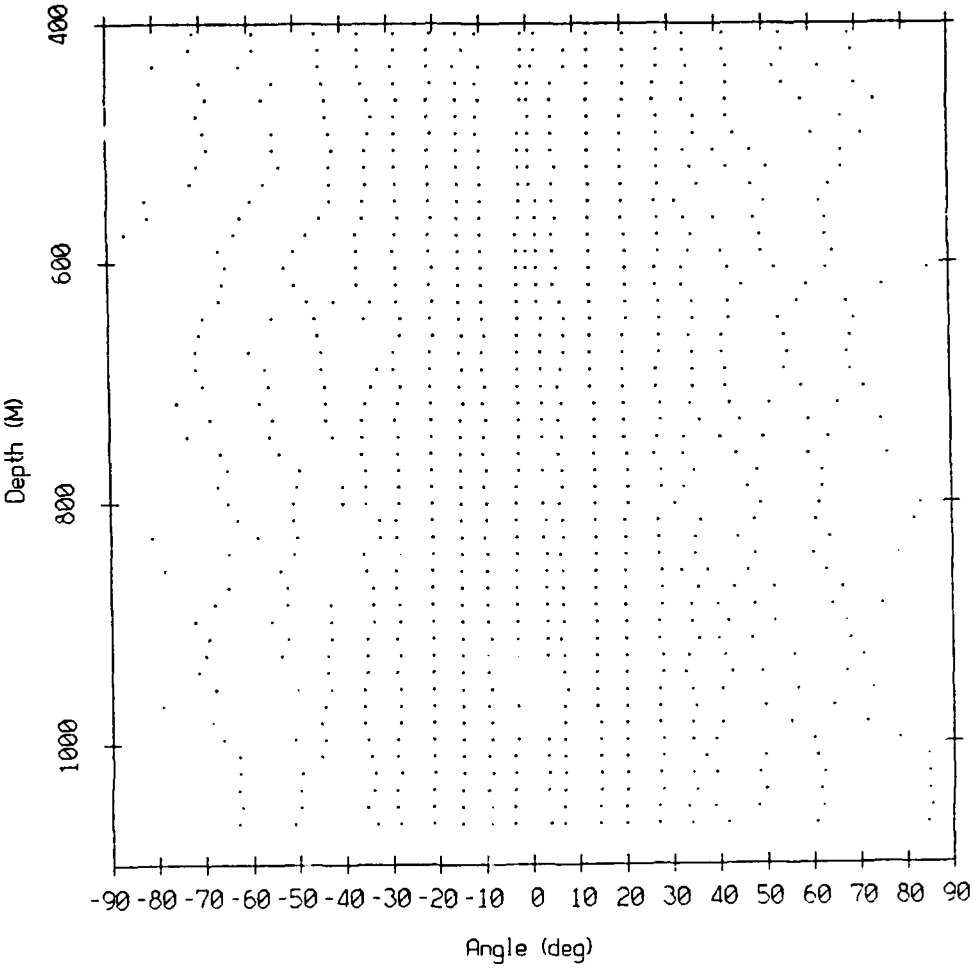

Figure 3.36: Traces with depth of the local maxima of the 32 sensor subarray Minimum Norm "spectra" at 100 Hz.

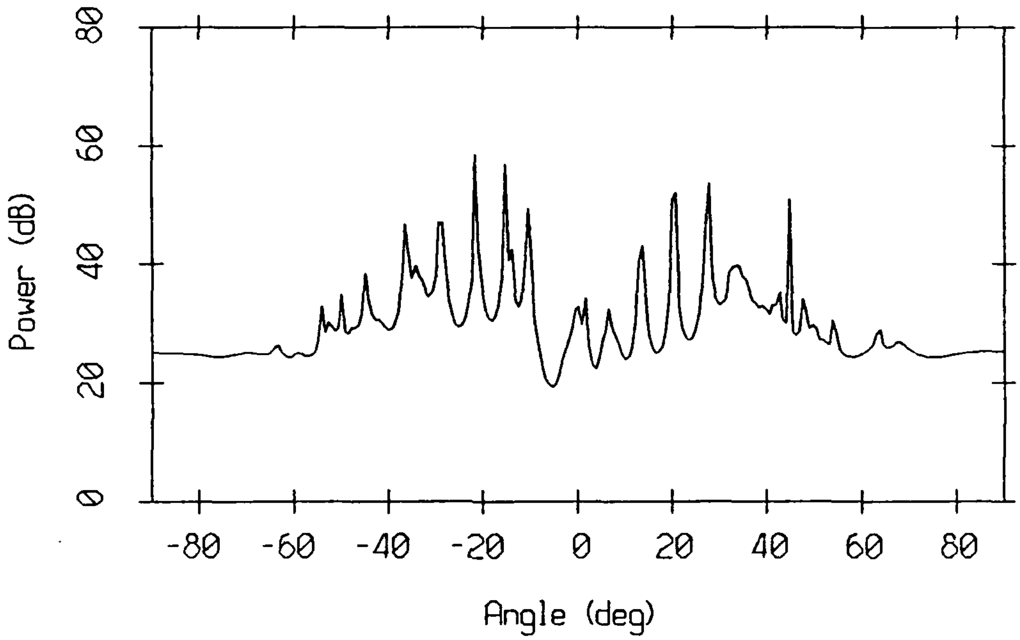

Figure 3.37: Composite subarray Minimum Norm "spectrum" at 100 Hz.

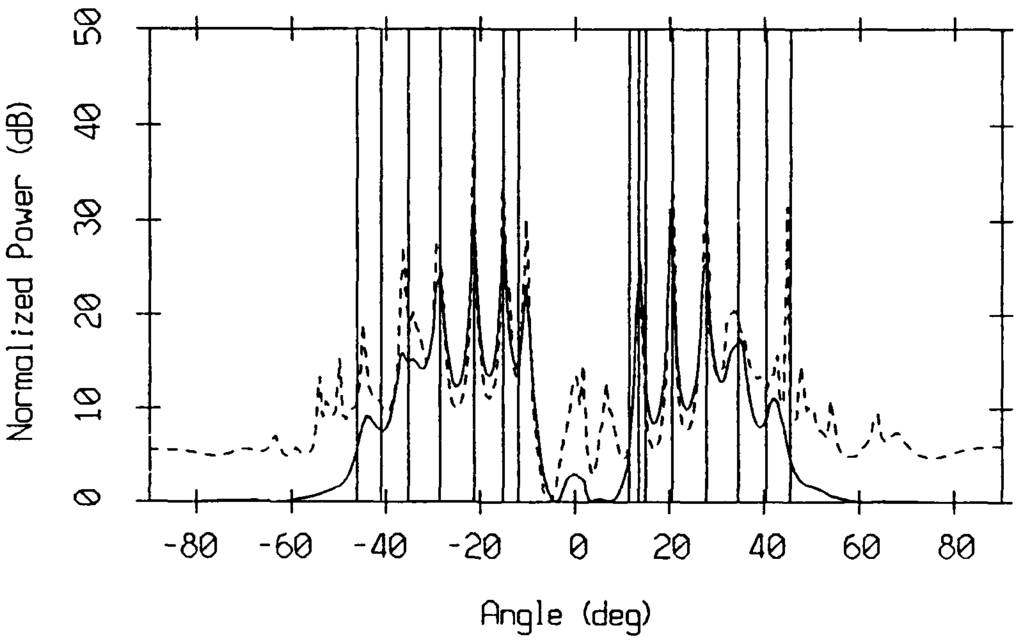

Figure 3.38: Composite MUSIC (solid line) and Minimum Norm (dotted line) "spectra" overlaid with the GSM eigenray angles at the sound axis and at 100 Hz.

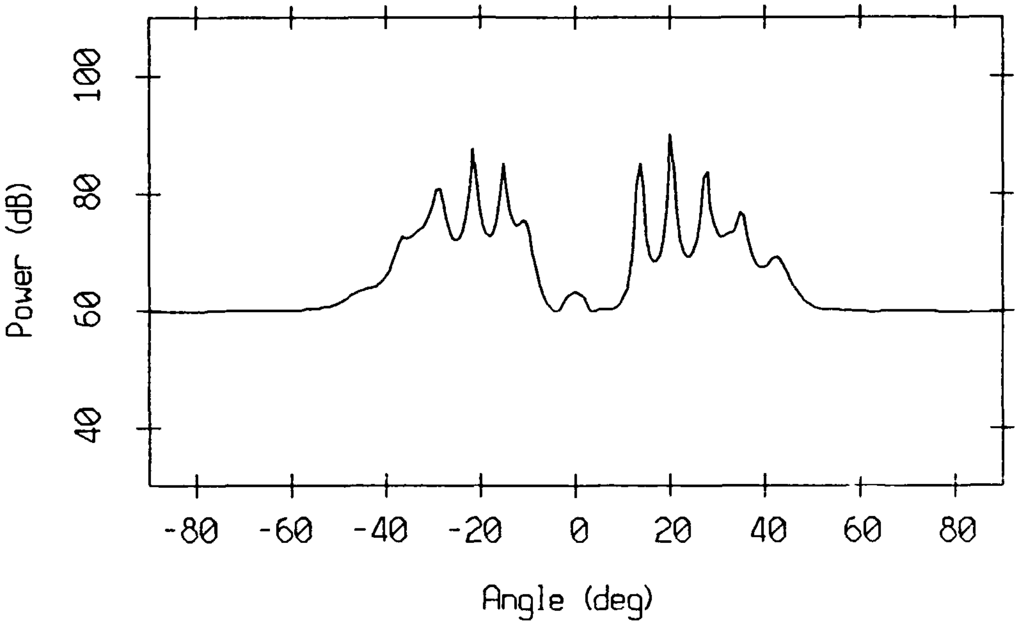

Figure 3.39: MVDR subaperture angular spectrum (averaged on 4 non-overlapping 32 sensor subarray spectra at 100 Hz). Spatial smoothing is performed with a subsegment length of 20 sensors.

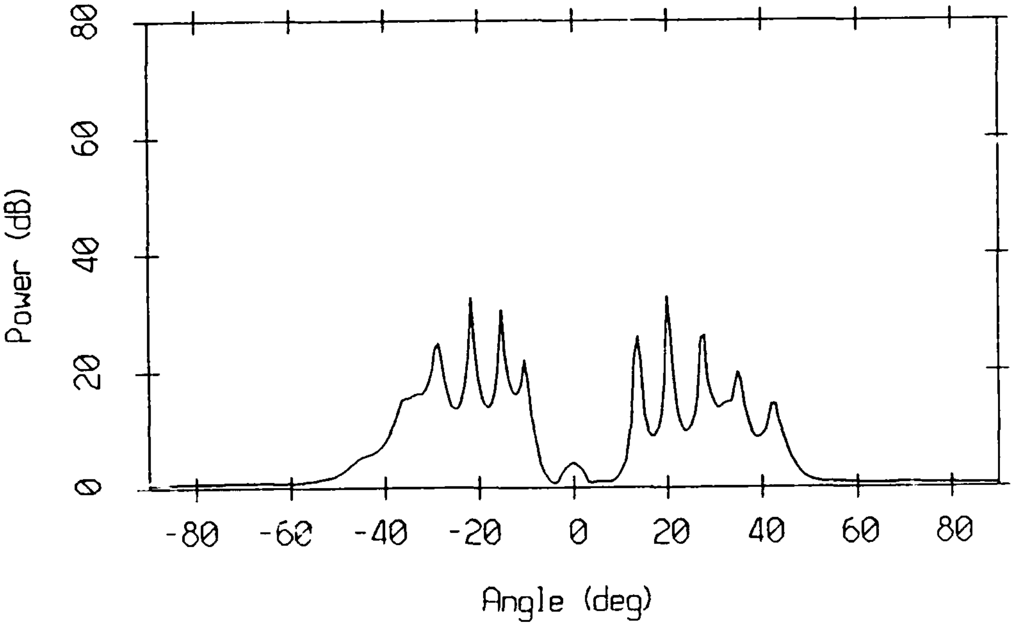

Figure 3.40: MUSIC subaperture "spectrum" (averaged on 4 non-overlapping 32 sensor subarray spectra at 100 Hz). Spatial smoothing is performed with a subsegment length of 20 sensors. The number of signals is set to 12.

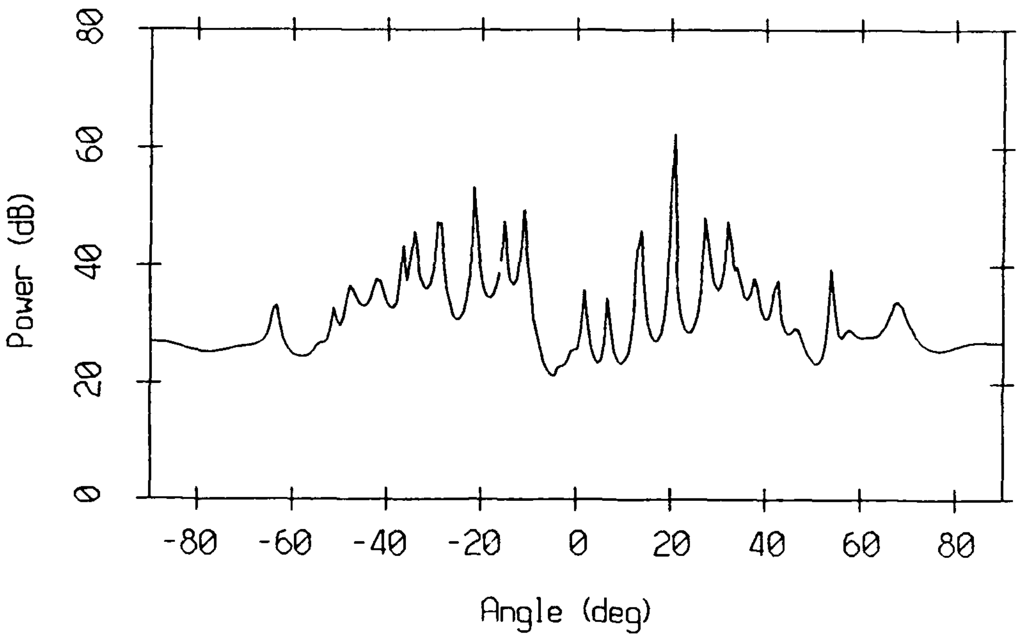

Figure 3.41: Minimum Norm subaperture "spectrum" (averages on 4 non-overlapping 32 sensor subarray spectra at 100 Hz). Spatial smoothing is performed with subsegment length of 20 sensors. The number of signals is set to 12.

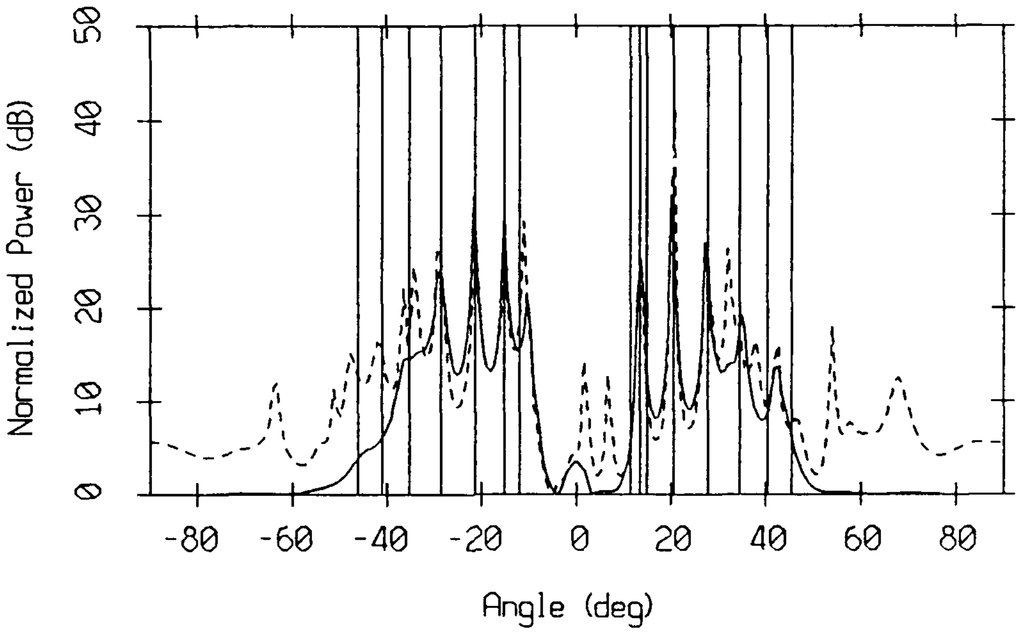

Figure 3.42: MUSIC (solid line) and Minimum Norm (dotted line) "spectra" averaged on 4 non-overlapping 32 sensor subarrays overlaid with the GSM eigenray angles at the sound axis and at 100 Hz.

BIBLIOGRAPHY

Boyles, A. C., *Acoustic Waveguides, Applications to Oceanic Sciences*, John Wiley, N.Y., 1984.

Capon, J., "High Resolution Frequency-Wavenumber Spectrum Analysis," *Proc. IEEE*, vol. 57, pp. 1408-1418, 1969.

Cornyn, J. J., *GRASS: A Digital Computer Ray Tracing and Transmission Loss Prediction System*, 1, NRL Report 7621, 21 December 1973.

Gordon, D. F. and H. P. Bucker, *Arctic Acoustic Propagation Model with Ice Scattering*, NOSC Technical Report 985, 30 September 1984.

Jensen, F. B., "Wave Theory Modeling: A Convenient Approach to CW and Pulse Propagation Modeling in Low-Frequency Acoustics," *IEEE J. Ocean. Eng.*, vol. 13, no. 4, pp. 186-197, October 1988.

Marple, S. L., *Digital Spectral Analysis with Applications*, Prentice-Hall, N.J., 1987.

Murphy, D. A. and D. R. DelBazo, "Multipath Processing for Improved Detection on a Long Vertical Array," in *Progress in Underwater Acoustics*, pp. 765-772, Plenum Press, N.Y., 1987.

Nickel, U., "Algebraic Formulation of the Kumaresan-Tufts Superresolution Method Showing Relation to ME and MUSIC Methods," *IEE Proc. Part F*, vol. 135, no. 1, pp. 7-10, 1988.

Orfanidis, S. J., *Optimum Signal Processing, An Introduction*, Macmillan, New York, 1988.

Schmidt, R. O., "Multiple Emitter Location and Signal Parameter Estimation," *Trans. Ant. Prop.*, vol. 34, no. 3, pp. 276-280, 1986 .

Sotirin, B. J. and J. A. Hildebrand, "Large Aperture Digital Acoustic Array," *IEEE J. Oceanic Eng.*, vol. 13, no. 4, pp. 271-281, October 1988.

Speiser, J. M., "Progress in Eigenvector Beamforming," *SPIE Proceedings*, vol. 564, San Diego, CA, August 22-23.

Tran, J-M. and W. S. Hodgkiss, "High Resolution Beamforming on Vertical Arrays in a Realistic Oceanic Environment," *MPL Technical Memorandum 408, MPL-U-03/89*, Marine Physical Laboratory, Scripps Institution of Oceanography, San Diego, CA, January 1989 .

Urick, R. J., *Principles of Underwater Sound*, McGraw-Hill, N.Y., 1983.

Weinberg, H., "A Continuous-Gradient Curved Fitting Technique for Acoustic-Ray Analysis," *J. Acoust. Soc. Am.*, vol. 50, no. 3 Part 2, pp. 975-984, March 1971.

Weinberg, H., *Generic Sonar Model*, NUSC Technical Document 5971-D, 6 June 1985.